NATIONAL AERONAUTICS AND SPACE ADMINISTRATION

FINAL REPORT

GRANT NUMBER NASA NSG 1150

AN ANALYSIS OF TURBULENT DIFFUSION FLAME IN AXISYMMETRIC JET

By Paul M. Chung

and Kwan H. Im

ABSTRACT

The kinetic theory of turbulent flow previously developed is employed to study the mixing-limited combustion of hydrogen in axisymmetric jet. The integro-differential equations in two-spatial and three velocity coordinates describing the combustion are reduced to a set of hyperbolic partial differential equations in the two spatial coordinates by a bimodal approximation. The MacCormick's finite difference method is then employed for solution. The flame length is longer than that predicted by the flame-sheet analysis, and is found to be in general agreement with a recent experimental result. Increase of either the turbulence energy or scale results in an enhancement of the combustion rate and, hence, in a shorter flame length. Details of the numerical method as well as of the physical findings are discussed.

NATIONAL AERONAUTICS AND SPACE ADMINISTRATION

FINAL REPORT

GRANT NUMBER NASA NSG 1150

AN ANALYSIS OF TURBULENT DIFFUSION FLAME IN AXISYMMETRIC JET

By Paul M. Chung

and Kwan H. Im

SUMMARY

Kinetic theory of turbulence developed previously was employed to analyze the turbulent diffusion flame in axisymmetric hydrogen jet. The fluid was assumed to be incompressible, and the mean flow field was considered to be given for convenience. The kinetic equations governing the chemical species and energy were transformed into a set of hyperbolic differential equations by the use of bimodal moment method which has been modified to circumvent certain difficulty encountered in earlier works. These equations were integrated by a finite difference scheme. This method of solution was shown to be flexible and applicable to many combustion problems of engineering interest. The solution was compared to the existing experimental data. Satisfactory agreements with the experimental data were obtained on the flame length and on the centerline variations of the chemical species concentrations. The maximum temperature

of the flame was substantially below that predicted by the conventional flame-sheet solution. The overall combustion rate enhances and, therefore, the flame length shortens as the turbulence energy and scale were increased. Greater turbulence energy enhances the overall combustion rate by increasing both the mixing and the turbulent dissipation-limited chemical reaction rate. On the other hand, the larger scale gave a greater overall combustion rate through increased mixing, but a maximum would be reached beyond which the combustion rate would decrease because of the reduced dissipation-limited reaction rate.

INTRODUCTION

Recognizing certain inherent limitations of the conventional method of analysis of chemically reacting flows, a kinetic theory of turbulence was developed previously. (See ref. 1-6.) This theory describes the probability density function of the fluid elements comprising turbulence field. Probability density functions of the chemical species being transported by the fluid elements are also described in similar manner.

The governing kinetic equations are integro-differential equations in both velocity and physical spaces, similar to those for the molecular kinetic theory, and present a formidable challenge to the available methods of solution. The only practical method of solution for chemically reacting flows was found to be the bimodal moment method, which was successfully employed to solve several chemically reacting flow problems of engineering interest (refs. 1-4). However, when the method was applied

to the combustion problems of initially unmixed reactants, it was found that the generated mean profiles contained certain discontinuities in the gradients which were not real. These discontinuities are direct consequences of the bimodal method of solution, as explained in ref. 5, and they do not affect the combustion rate and other pertinent description of the physical problem. Nevertheless, a method should be found which will remedy this difficulty.

The ultimate answer lies in the exact numerical integration of the kinetic equations. The equations were solved exactly at least in one velocity space for a combustion problem in ref. 7, and the solutions gave correct continuous mean profiles to all orders as expected. The numerical complexity, however, was such that the solution was confined to a relatively simple shear flow.

As an interim remedy of the difficulty with bimodal method, an additional kinetic equation was constructed in ref. 6 which governs the correlation function representing the chemical reaction. This equation circumvented the difficulty of the bimodal moment method, and the method was successfully applied to solution of the turbulent chemical laser problem in ref. 6.

Aside from the problems discussed above, there exists the difficulty of numerically integrating a set of hyperbolic partial differential equations resulting from the moment method in two physical dimensions. The MacCormick's finite difference scheme (ref. 8) was shown to be useful in the solution for simple two-dimensional flow (ref. 6). However, application of this scheme to the axisymmetric jet turned out to be a formidable task.

A substantial portion of the effort expended in the present work concerns the numerical integration of the governing moment equations by the MacCormick's method.

Text of this report begins with formulation of the kinetic equations governing the mixing-limited combustion in axisymmetric jet. The fluid was assumed to be incompressible and the mean flow field was considered to be known in terms of the existing incompressible solutions. Appropriate derivation and transformation of the moment equations are given. Solutions for the hydrogen combustion in air are then obtained and compared to the available experimental data. Because of the importance of the numerical scheme to the success of the kinetic-theory approach to turbulence, a detailed description of the numerical solution technique is included in the appendix.

SYMBOLS

a	stoichiometric coefficient for oxidant
a_1, a_2, a_3, a_4	constants for Eqs. (14), (16), and (17).
b	stoichiometric coefficient for fuel
c	mass fraction
c_i	i-th mass fraction used in appendix
c_p	specific heat
D	molecular diffusivity
d	stoichiometric coefficient for combustion product
E	$\langle U_k U_k \rangle / u_c^2$

F	function defined in Eq. (A4)
f	probability density function of fluid elements
h	$C_p\ T/\Delta h^\circ$
Δh°	heat of combustion per unit mass of product
k_f	forward reaction rate coefficient
L	nozzle diameter
M	molecular weight
Q	general function of $\vec{U}$
R	r/L
r	radial coordinate defined in Fig. 1
S	function defined in Eq. (A5)
T	absolute temperature
U	x-component of instantaneous velocity relative to the mean velocity
U_i	i-component of instantaneous velocity relative to the mean velocity
$\vec{U}$	instantaneous velocity vector relative to the mean velocity vector
u	x-component of instantaneous velocity
u_c	average center line velocity
u_i	i-component of instantaneous velocity
u_p	average velocity at the nozzle
u_∞	average free stream velocity
V	r-component of instantaneous relative velocity
v	r-component of instantaneous velocity
W	instantaneous relative velocity component normal to x-r plane

w	instantaneous velocity component normal to x-r plane
X	x/L
x	axial coordinate defined in Fig. 1
z	general mass fraction representing c_a, c_b, etc.
z_1, z_2	functions defined by Eqs.(22) - (24)
z^+, z^-	functions defined by Eq. (37)
$\langle Q \rangle$	$= \int fQ \, d\vec{U}$
γ	dissipation ratio in turbulence
ϵ	$1 - (u_\infty/u_p)$
ϵ_m	eddy diffusivity
η	similarity variable defined by Eq.(17)
λ	turbulence scale
$\hat{\lambda}$	λ/L
$\xi^\pm$	characteristic directions defined by Eq. (39)
$\zeta_i, \hat{\zeta}_i$	functions defined by Eqs.(A9) and (A10)
ρ	density
σ	constant for Eq. (17)
Φ	function defined by Eq.(32a)
ϕ^+, ϕ^-	functions defined by Eq. (36)
Ψ	functions defined by Eq. (32b)
Ω	functions defined by Eqs.(A3) and (A6)
ω	instantaneous production rate per unit mass by chemical reaction

Subscripts

a	oxidant
b	fuel
c	center line
d	product
e	chemically inert species
h	$C_h \equiv h$
i,j,k	Cartesian tensor indices
o	ensemble averaged
p	at the nozzle
∞	free stream

Superscript

$\rightarrow$,$\sim$	vectors

Note that all symbols for velocities, except u_p, u_c, and u_∞, represent dimensionless quantities after Eq. (26).

FORMULATION

Chemical Reaction

The standard axisymmetric turbulent jet shown in Fig. 1 is studied. The jet, consisting of a fuel and a chemically inert species, is surrounded by air, and the following one-step combustion is considered to take place.

$$a(\text{oxidant}) + b(\text{fuel}) \xrightarrow{k_f} d(\text{product}) \qquad (1)$$

From the law of mass action, the rates of production by chemical reaction of the three reactants are given by

$$\omega_d = k_f \frac{d\, M_d}{M_a^a\, M_b^b} \rho^{a+b-1} c_a^a c_b^b,$$

$$\omega_a = -\left(\frac{a}{d}\right)\left(\frac{M_a}{M_d}\right)\omega_d, \tag{2}$$

and

$$\omega_b = -\left(\frac{b}{d}\right)\left(\frac{M_b}{M_d}\right)\omega_d.$$

All symbols are defined in the nomenclature.

Kinetic Equations

Starting point of formulation of the governing equations is the kinetic equation (see refs. 1, 5, and 6),

$$(u_{oj} + u_j)\frac{\partial fz}{\partial x_j} = \frac{\langle U_k U_k\rangle^{1/2}}{2\lambda}\left[(1+\gamma)\frac{\partial}{\partial U_j}(fU_j z) + \frac{\langle U_k U_k\rangle}{3}\frac{\partial^2 fz}{\partial U_j \partial U_j}\right] - \frac{\langle U_k U_k\rangle^{1/2}\gamma}{2\lambda} f(z - z_o) + f\omega_z \tag{3}$$

where j and k are the Cartesian tensor indices. The symbol z stands for difinite quantity being transported by the fluid elements. For the combustion described by Eqs. (2), Eq. (3) represents the five kinetic equations respectively for

$$z = c_a,\ c_b,\ c_d,\ c_e \text{ and } h. \tag{4}$$

These equations will be solved by the bimodal moment method subsequently. As was discussed in the preceeding section, certain discontinuities in the gradients of the mean profiles are expected in the results when $k_f \to \infty$. Although these do not affect the combustion rate and other physical descriptions of the problem, the discontinuities themselves are unreal consequences of the bimodal method of solution. As was discussed in ref. 5, the bimodal method approximates the continuous distribution of a reactant concentration among the fluid elements with various instantaneous velocities by two discrete values of the concentration depending only on the sign of V. At the edge of a diffusion flame zone, therefore, concentration of one of the reactants contained in all fluid elements becomes zero simultaneously. This results in the discontinuous gradients of the mean reactant concentrations at the flame edge. Such unreal discontinuities naturally disappear as more exact method is employed for solution of the kinetic equations (refs. 5, and 7). These methods (refs. 5 and 7), however, are of such complexity that their application to practical flow problems such as the axisymmetric jet is extremely difficult.

As an interim technique to circumvent the difficulty with the bimodal method, until a more viable method of solution is found, it was suggested in ref. 6 that an additional kinetic equation be employed. This equation is constructed by letting

$$z = c_a^a\, c_b^b \tag{5}$$

in Eq. (3) as

$$(u_{oj} + U_j)\frac{\partial f c_a^a c_b^b}{\partial x_j} = \frac{\langle U_k U_k\rangle^{1/2}}{2\lambda}\left[(1+\gamma)\frac{\partial}{\partial U_j}(f U_j c_a^a c_b^b) + \frac{\langle U_k U_k\rangle}{3}\frac{\partial^2 f c_a^a c_b^b}{\partial U_j \partial U_j}\right] - \frac{\langle U_k U_k\rangle^{1/2}\gamma}{2\lambda} f(c_a^a c_b^b - c_{ao}^a c_{bo}^b)$$

$$+ f\,\omega_{ab}. \tag{6}$$

Expression for ω_{ab} is constructed such that the first moment of Eq. (6) corresponds to the conservation equation for $\langle c_a^a c_b^b\rangle$ derived from the Navier-Stokes and standard species conservation equations. When $a = b = 1$, the expression for ω_{ab} was obtained in ref. 6 as

$$\omega_{ab} = c_b\omega_a + c_a\omega_b \tag{7}$$

such that the first moment of Eq. (6) was term-wise comparable to the conservation equation for $\langle c_a c_b\rangle$ derived from the standard species conservation equations for c_a and c_b, subject to the correspondence

$$2D\left\langle \frac{\partial c_a}{\partial x_j}\frac{\partial c_b}{\partial x_j}\right\rangle = \frac{\langle U_k U_k\rangle^{1/2}\gamma}{2\lambda}(\langle c_a c_b\rangle - c_{ao}c_{bo}). \tag{8}$$

The present analysis is mainly concerned with the combustion of

hydrogen

$$O_2 + 2H_2 \xrightarrow{k_f} 2H_2O \tag{9}$$

for which $a = 1$, and $b = 2$. For these stoichiometric coefficients, it was found that

$$\omega_{ab} = c_b^2\omega_a + 2c_a c_b \omega_b \tag{10}$$

gives the term-wise compatibility of the first moment of Eq. (6) with the conservation equation for $\langle c_a c_b^2 \rangle$ derived from the conventional conservation equations for c_a and c_b, subject to the following correspondence for dissipation,

$$2D\left(\left\langle \frac{\partial c_a}{\partial x_j}\,\frac{\partial c_b^2}{\partial x_j}\right\rangle + \left\langle c_a \frac{\partial c_b}{\partial x_j}\,\frac{\partial c_b}{\partial x_j}\right\rangle\right)$$

$$= \frac{\langle U_k U_k\rangle^{1/2}\gamma}{2\lambda}\left(\langle c_a c_b^2\rangle - C_{ao}c_{bo}^2\right) . \tag{11}$$

The dissipation correspondence of Eqs. (8) and (11) are plausible hypotheses, and consistency of Eq. (6) with the original kinetic equations for c_a, c_b, etc. cannot be established. Therefore, the bimodal solutions using this additional equation must be considered interim ones until more exact solutions of the integro-differential kinetic equations can be obtained.

Mixing-Limited Reaction

When the chemical reaction rate, k_f, is sufficiently larger than the mixing and other characteristic rates of the problem, Eqs. (2) demand that

$$c_a^a c_b^b = 0 \tag{12}$$

for all $\vec{x}$ and $\vec{U}$. Each term of Eq. (6), then, vanishes except the last two terms, the dissipation and chemical reaction terms, which become with the use of Eq. (10) and Eqs. (2),

$$f\omega_a = -\frac{\langle U_k U_k \rangle^{1/2}\gamma}{2\lambda} f \frac{c_{ao} c_{bo}^2}{\left(c_b^2 + 4 \frac{M_b}{M_a} c_a c_b\right)} \cdot \tag{13}$$

As explained in ref. 1, the above shows that, in the limit of fast reaction, the reaction rate is equal to the turbulent dissipation rate.

The set of kinetic equations governing the hydrogen combustion now consists of the five equations represented by Eqs. (3) and (4), and the degenerated equation, Eq. (13). Solution of this set is discussed in the next section following the brief consideration of the flow field given below.

Flow Field

Mean flow field for incompressible turbulent jet is well known. (See refs. 9 and 10.) So that full attention can be given to describing the combustion phenomenon, the mean flow field solutions found in refs. 9 and 10 are employed in the present analysis instead of solving

for the flow field by the kinetic theory.

Recognizing the fact that exact details of the flow field have only a secondary effect on combustion, solution of ref. 9 for $u_\infty/u_p = 0$ is first modified slightly to include the influence of the finite initial jet diameter on the flow field using the information given i ref. 10. The result is then generalized so that it can be approximately used for arbitrary values of u_∞/u_p also. The mean velocity components employed are

$$\frac{u_c}{u_p} = \frac{a_1}{a_2 + 5.8} \left[1 - \varepsilon \left(1 - \frac{a_2 + 5.8}{a_2 + X}\right)\right] , \tag{14}$$

$$\frac{u_o}{u_c} = 1 - \varepsilon \left[1 - \frac{1}{(1 + \frac{1}{4}\eta^2)^2}\right] , \tag{15}$$

and

$$\frac{v_o}{u_c} = \varepsilon \frac{a_3(\eta - \frac{1}{4}\eta^3)}{(1 + \frac{1}{4}\eta^2)^2} , \tag{16}$$

where

$$\varepsilon = 1 - \left(\frac{u_\infty}{u_p}\right) ,$$

$$\eta = \sigma \frac{R}{a_2 + X} , \tag{17}$$

and

$$a_1 = 6.4, \quad a_2 = 0.6, \quad \text{and} \quad a_3 = 0.03295.$$

Having completed formulation of the problem, solution of Eq. (3), with Eq. (4), and Eq. (13) constitutes the next section.

ANALYSIS

As stated earlier, the kinetic equations governing combustion will be solved by the bimodal moment method. The method is similar to that employed in the previous work, ref 6, except the mean velocity component, v_o , is not zero in the present problem, and this requires a somewhat different approach in the division of the velocity space.

Moment Equations

The first two moments of Eq. (3) are obtained by multiplying the equation by 1 and V successively and by integrating the resulting equations term-wise with respect to the velocity space. In cylindrical coordinates, these equations are

$$\frac{\partial}{\partial x}\int (u_o + U) f\, z\, d\vec{U} + \frac{1}{r}\frac{\partial}{\partial r} r \int (v_o + V) f\, z\, d\vec{U} = \int f\, \omega_z\, d\vec{U} , \qquad (18)$$

and

$$u_o \frac{\partial}{\partial x}\int Vf\, z\, d\vec{U} + v_o \frac{\partial}{\partial r}\int Vf\, z\, d\vec{U} + \frac{\partial}{\partial r}\int V^2 f\, z\, d\vec{U}$$

$$+ \left(u_o \frac{\partial v_o}{\partial x} + v_o \frac{\partial v_o}{\partial r}\right)\int f\, z\, d\vec{U} + \frac{\partial v_o}{\partial r}\int Vf\, z\, d\vec{U}$$

$$= -\frac{\langle U_k U_k \rangle^{1/2}}{2\lambda}\,(1 + 2\gamma)\int Vf\, z\, d\vec{U} + \int Vf\, \omega_z\, d\vec{U} \quad . \qquad (19)$$

In the derivation of Eq. (19), the continuity equation resulting from setting $z = 1$ in Eq. (18), and the relationships

$$\int UVf\ z\ d\vec{U} \ll u_o \int Vf\ z\ d\vec{U}\ ,$$

and (20)

$$\int Uf\ z\ d\vec{U} \ll u_o \int f\ z\ d\vec{U}\ ,$$

have been employed.

Bimodal Approximation

For convenience, the probability density function of the fluid elements is approximated by a Maxwellian function in terms of the velocity components relative to the mean velocity. Thus,

$$f = \frac{1}{\left(\frac{2}{3}\pi \langle U_k U_k \rangle\right)^{3/2}} \exp - \frac{U^2 + V^2 + W^2}{(2\langle U_k U_k \rangle/3)} \quad . \tag{21}$$

The species mass fraction, z, is then approximated by a bimodal function as,

$$\begin{aligned} z(\vec{x},\vec{U}) &= z(x,r,V) \\ &= z_1(x,r) + z_2(x,r), \end{aligned} \tag{22}$$

where

$$z_2(x,r) = 0 \qquad \text{for} \quad V > -v_o \,,$$

and (23)

$$z_1(x,r) = 0 \qquad \text{for} \quad V < -v_o \,.$$

Note that the above relationships imply

$$z_2(x,r) = 0 \qquad \text{for} \quad v > 0 \,,$$

and (24)

$$z_1(x,r) = 0 \qquad \text{for} \quad v < 0 \,.$$

Therefore, the bimodal division is actually carried out in the absolute velocity space.

Eqs. (21) and (22) facilitate the evaluation of a moment as

$$\langle Qz \rangle = \int Qf\, z\, d\vec{U} = \int_{-v_o}^{\infty} dV \int_{-\infty}^{\infty} dW \int_{-\infty}^{\infty} dU\, Qf\, z$$

$$+ \int_{-\infty}^{-v_o} dV \int_{-\infty}^{\infty} dW \int_{-\infty}^{\infty} dU\, Qf\, z \,, \tag{25}$$

where Q denotes an arbitrary function of $\vec{U}$.

Governing Equations for Combustion

With the use of Eqs. (21), (25), and (13), and the relationship between ω_b, ω_d, and ω_a given in Eqs. (2), Eqs. (18) and (19) are reduced to a set of explicit partial differential equations in x and r for each of the z defined by Eq. (4). Then, with appropriate non-

dimensionalization and some manipulation, the following four sets of equations are obtained.

In all subsequent equations, the symbols for velocities, except u_p , u_c , and u_∞ , represent the normalized velocities with respect to u_c ,

$$u_o = u_o/u_c \,, \quad v_o = v_o/u_c \,,$$

$$U = U/u_c \,, \quad V = V/u_c \,, \quad \text{and} \quad W = W/u_c \,. \tag{26}$$

$$\Phi(c_a) = -\frac{E^{1/2}\gamma}{2\hat{\lambda}} \frac{c_{ao}c_{bo}^2}{2} \left\{\phi^+ + \phi^- \operatorname{erf}\left[\left(\frac{3}{2E}\right)^{1/2} v_o\right]\right\}, \tag{27a}$$

$$\Psi(c_a) = -\left[\left(\frac{u_o}{u_c} \frac{\partial v_o u_c}{\partial X} + v_o \frac{\partial v_o}{\partial R}\right) c_{ao} + \langle Vc_a \rangle \frac{\partial v_o}{\partial R}\right]$$

$$- \frac{E^{1/2}}{2\hat{\lambda}} (1 + 2\gamma)\langle Vc_a \rangle - \frac{E\gamma}{2\hat{\lambda}(6\pi)^{1/2}} c_{ao}c_{bo}^2 \phi^- \cdot$$

$$\exp\left(-\frac{3}{2E} v_o^2\right) \,, \tag{27b}$$

$$\Phi(c_b) = -\frac{M_b}{M_a} \frac{E^{1/2}\gamma}{\hat{\lambda}} \frac{c_{ao}c_{bo}^2}{2} \left\{\phi^+ + \phi^- \operatorname{erf}\left[\left(\frac{3}{2E}\right)^{1/2} v_o\right]\right\}, \tag{28a}$$

$$\Psi(c_b) = -\left[\left(\frac{u_o}{u_c} \frac{\partial v_o u_c}{\partial X} + v_o \frac{\partial v_o}{\partial R}\right) c_{bo} + \langle Vc_b \rangle \frac{\partial v_o}{\partial R}\right]$$

$$- \frac{E^{1/2}}{2\hat{\lambda}} (1 + 2\gamma)\langle Vc_b \rangle - \frac{M_b}{M_a} \frac{E\gamma}{\hat{\lambda}(6\pi)^{1/2}} \cdot$$

$$c_{ao} c_{bo}^2 \phi^- \exp\left(- \frac{3}{2E} v_o^2\right) , \qquad (28b)$$

$$\Phi(c_d) = \frac{M_d}{M_a} \frac{E^{1/2}\gamma}{\hat{\lambda}} \frac{c_{ao} c_{bo}^2}{2} \left\{ \phi^+ + \phi^- \operatorname{erf}\left[\left(\frac{3}{2E}\right)^{1/2} v_o\right]\right\}, \qquad (29a)$$

$$\Psi(c_d) = -\left[\left(\frac{u_o}{u_c} \frac{\partial v_o u_c}{\partial X} + v_o \frac{\partial v_o}{\partial R}\right) c_{do} + \langle Vc_d \rangle \frac{\partial v_o}{\partial R}\right]$$

$$- \frac{E^{1/2}}{2\hat{\lambda}} (1 + 2\gamma)\langle Vc_d \rangle + \frac{M_d}{M_a} \frac{E\gamma}{\hat{\lambda}(6\pi)^{1/2}} \cdot$$

$$c_{ao} c_{bo}^2 \phi^- \exp\left(- \frac{3}{2E} v_o^2\right) , \qquad (29b)$$

$$\Phi(h) = \frac{M_d}{M_a} \frac{E^{1/2}\gamma}{\hat{\lambda}} \frac{c_{ao} c_{bo}^2}{2} \left\{ \phi^+ + \phi^- \operatorname{erf}\left[\left(\frac{3}{2E}\right)^{1/2} v_o\right]\right\}, \qquad (30a)$$

$$\Psi(h) = - \left[\left(\frac{u_o}{u_c} \frac{\partial v_o u_c}{\partial X} + v_o \frac{\partial v_o}{\partial R}\right) h_o + \langle Vh \rangle \frac{\partial v_o}{\partial R}\right]$$

$$- \frac{E^{1/2}}{2\hat{\lambda}} (1 + 2\gamma)\langle Vh \rangle + \frac{M_d}{M_a} \frac{E\gamma}{\hat{\lambda}(6\pi)^{1/2}} \cdot$$

$$c_{ao} c_{bo}^2 \phi^- \exp\left(- \frac{3}{2E} v_o^2\right) . \qquad (30b)$$

The functions governing the chemically inert species are obtained from those of the other chemical species as

$$f\, c_{e1}\, d\vec{U} = f\left[1 - (C_{a1} + c_{b1} + c_{d1})\right]\, d\vec{U}\,,$$

$$f\, c_{e2}\, d\vec{U} = f\left[1 - (c_{a2} + c_{b2} + c_{d2})\right]\, d\vec{U}\,. \tag{31}$$

The operators Φ and Ψ are defined by

$$\Phi(z) = u_o \frac{\partial z_o}{\partial X} + v_o \frac{\partial z_o}{\partial R} + \frac{1}{R}\frac{\partial}{\partial R}\left(R\langle Vz\rangle\right)\,, \tag{32a}$$

and

$$\Psi(z) = \frac{u_o}{u_c}\frac{\partial u_c\langle Vz\rangle}{\partial X} + v_o \frac{\partial\langle Vz\rangle}{\partial R} + \frac{\partial}{\partial R}\langle V^2 z\rangle\,. \tag{32b}$$

Various ensemble averaged quantities appearing in Eqs. (27) - (32) are given by

$$z_o = \langle z\rangle = \frac{1}{2}(z_1 + z_2) + \frac{1}{2}(z_1 - z_2)\,\mathrm{erf}\left[\left(\frac{3}{2E}\right)^{1/2} v_o\right]\,, \tag{33}$$

$$\langle Vz\rangle = (z_1 - z_2)\left(\frac{E}{6\pi}\right)^{1/2}\exp\left(-\frac{3}{2E}v_o^2\right)\,, \tag{34}$$

$$\langle V^2 z\rangle = \frac{E}{6}(z_1 + z_2) + (z_1 - z_2)\left\{\frac{E}{6}\,\mathrm{erf}\left[\left(\frac{3}{2E}\right)^{1/2} v_o\right]\right.$$

$$-\left(\frac{E}{6\pi}\right)^{1/2} v_o \exp\left(-\frac{3}{2E} v_o^2\right)\Bigg\} \ . \qquad (35)$$

Functions ϕ^+ and ϕ^- arising from Eq. (13) are defined as

$$\phi^{\pm} = \frac{1}{\left(\frac{c_b^+ + c_b^-}{2}\right)^2 + \frac{M_b}{M_a}(c_a^+ + c_a^-)(c_b^+ + c_b^-)}$$

$$\pm \frac{1}{\left(\frac{c_b^+ - c_b^-}{2}\right)^2 + \frac{M_b}{M_a}(c_a^+ - c_a^-)(c_b^+ - c_b^-)} \ , \qquad (36)$$

where

$$z^+ = z_1 + z_2 \ , \quad \text{and} \quad z^- = z_1 - z_2 \ . \qquad (37)$$

With the velocity profiles given by Eqs. (14) - (17), and the turbulence properties, E and $\hat{\lambda}$, considered to be known in the present analysis, as will be discussed subsequently, Eqs. (27a) through (31) constitute ten equations for the equal number of unknown functions, c_{a1}, c_{a2}, c_{b1}, c_{b2}, c_{d1}, c_{d2}, c_{e1}, c_{e2}, h_1, and h_2 .* Solution of these equations and discussion of the results comprise the remainder of this report.

---

*One may alternatively consider c_a^+, c_a^-, c_b^+, c_b^-, etc., as the unknown functions via Eqs. (37).

Wave Behavior of Equations and Boundary Conditions

As was stated earlier, the governing equations, Eqs. (27a) - (31), are hyperbolic. These equations will be solved by a finite difference scheme; however, it will be useful before the solution to study their behavior on the characteristic plane. Such a study, among other things, will clarify the boundary conditions to be applied.

The sets of two equations, (27a) and (27b), (28a) and (28b), etc., are all similar. Equations (27a) and (27b), therefore, are used in the following discussion of the general behavior of the governing equations.

The terms $\phi^- \operatorname{erf}\left(\frac{3}{2E}\right)^{1/2} v_o$ in Eq. (27a) and $\left[(u_o/u_c)(\partial v_o u_c/\partial X) + v_o(\partial v_o/\partial R)\right] c_{ao}$ in Eq. (27b) do not affect the basic behavior of the equations. Neglecting these terms for the present discussion, Eqs. (27a) and (27b) can be transformed into the following set of characteristic equations.

$$\frac{d}{d\xi^{\pm}}\left[c_a^+ \mp \left(\frac{2}{\pi}\right)^{1/2} c_a^-\right] = -\left\{u_o^2 + \left[v_o \mp \left(\frac{E}{3}\right)^{1/2}\right]^2\right\}^{-1/2}\left\{\frac{E^{1/2}\gamma}{16\hat{\lambda}} c_a^+ (c_b^+)^2 \phi^+ + \left(\frac{2E}{3\pi}\right)^{1/2} \frac{1}{R} c_a^- \mp \left[\frac{1}{8(2\pi)^{1/2}} \frac{E^{1/2}\gamma}{\hat{\lambda}} c_a^+ (c_b^+)^2 \phi^- + \left(\frac{E}{2\pi}\right)^{1/2} \frac{(1+2\gamma)}{\hat{\lambda}} c_a^- + \left(\frac{2}{\pi}\right)^{1/2} c_a^- u_o \frac{d\,\ell n\, u_c}{dX}\right]\right\}, \tag{38}$$

$$\left(\frac{dR}{dX}\right)_{\xi}^{\pm} = \frac{v_o}{u_o} \mp \left(\frac{E}{3u_o^2}\right)^{1/2} . \tag{39}$$

For the axisymmetric jet shown on Fig. 1, the characteristic directions defined by Eq. (39) are sketched in Fig. 2. The two waves consisting of $[c_a^+ - (2/\pi)^{1/2} c_a^-]$ and $[c_a^+ + (2/\pi)^{1/2} c_a^-]$ propagate along the two characteristic directions ξ^+ and ξ^- respectively according to Eq. (38). These waves dissipate by the quantities contained in the last curly bracket of Eq. (38). These quantities represent three physical phenomena. The first and third terms involving ϕ^+ and ϕ^- denote the chemical reaction, the second and the last terms signify the turbulent mixing, and the term next to last represent turbulent dissipation. These physical phenomena combine to dissipate the waves as they travel along the characteristics. The wave behavior will be discussed further following the numerical solution later.

As seen from Eq. (39) and Fig. 2, the R-axis is "space-like" whereas the X-axis is "time-like" (see ref. 11). Therefore, two boundary conditions are required along the R-axis and one along the x-axis. These requirements can be satisfied by the conditions that,

for $x = 0$ and all $R \geq 0$,

$$c_a^+ = (c_a^+)_{x=0} \quad , \tag{40}$$

and

$$c_a^- = (c_a^-)_{x=0} \quad . \tag{41}$$

For $R = 0$ and all $x \geq 0$,

$$c_a^- = 0 \quad . \tag{42}$$

By the use of Eq. (33), Eq. (40) can be replaced by the mean mass fraction profile, $(c_{ao})_{x=0}$. The boundary condition of Eq. (42) arises from the reflective wave condition,

$$c_a^+ - \left(\frac{2}{\pi}\right)^{1/2} c_a^- = c_a^+ + \left(\frac{2}{\pi}\right)^{1/2} c_a^- \quad , \tag{43}$$

which can be satisfied only by Eq. (42).

SOLUTION

As was stated previously, the governing equations, Eqs. (27a) through (31), are solved by the MacCormick's finite difference method (ref. 8). Details of the numerical method and the computer program are given in the Appendix. The turbulence properties and the boundary conditions corresponding to Eqs. (40) - (42) employed are discussed in this section.

Turbulence Properties

Turbulence energy and scale are needed to render the governing equations self-contained. Here, these quantities are chosen such that they will give the conventional eddy diffusivity (ref. 9) in the limit of the statistically near-equilibrium turbulence field (refs. 5, 6). As was done for discussion of the wave properties of the governing equations in the preceeding section, Eqs. (27a) and (27b), with the term $[(u_o/u_c)(\partial v_o u_c/\partial X)$

$+ v_o(\partial v_o/\partial R)]c_{ao}$ neglected, are used for demonstration. General behavior of all sets of the two equations, (27a) and (27b), (28a) and (28b), etc., is the same.

Equilibrium turbulence field is approached as

$$\frac{E^{1/2}}{\hat{\lambda}} \longrightarrow \infty \quad . \tag{44}$$

In this limit, Eqs. (27b), (34), and (36) show that

$$\begin{aligned} \langle Vc_a \rangle &\longrightarrow 0 \ , \\ c_a^- &\longrightarrow 0 \ , \\ \text{and} \qquad \phi^- &\longrightarrow 0 \ . \end{aligned} \tag{45}$$

Eq. (27b) then reduces to the conventional, gradient driven diffusion relationship,

$$\langle Vc_a \rangle = - \frac{2}{3(1 + 2\gamma)} \hat{\lambda} E^{1/2} \frac{\partial c_{ao}}{\partial R} \quad . \tag{46}$$

The eddy diffusivity is defined by the above equation as

$$\frac{\epsilon_m}{u_c L} = \frac{2}{3(1 + 2\gamma)} \hat{\lambda} E^{1/2} \quad . \tag{47}$$

A substitution of Eq. (46) into Eq. (27a) results in the conventional, parabolic conservation equation (refs. 9, 10) with the same flame-sheet reaction (ref. 12),

$$u_c u_o \frac{\partial c_{ao}}{\partial x} + u_c v_o \frac{\partial c_{ao}}{ar} = \frac{1}{r} \frac{\partial}{\partial r} \left(r \varepsilon_m \frac{\partial c_{ao}}{\partial r} \right) + \omega_{ao} \delta(r - r^*) \quad , \qquad (48)$$

where r^* denotes the position of flame sheet.

The turbulence scale and energy, $\hat{\lambda}$ and E, are chosen to satisfy Eq. (47) with the conventional value of eddy diffusivity, ε_m. The mean velocity profiles to be employed, Eqs. (14) - (17), have been obtained from ref. 9 for the axisymmetric jet with $u_\infty/u_p = 0$. The same reference gives

$$\sigma = 15.17 \, ,$$

and (49)

$$\varepsilon_m = 0.01388 \, L \, u_p \, .$$

Implicit in the conventional similarity analysis of ref. 9 is that all length scales vary as $1/(a_2 + X)$ according to the variable η given in Eqs. (17). Therefore, the present turbulence scale $\hat{\lambda}$ should be a constant fraction of the jet radius, and should vary with respect to X such that η is a constant. Denoting this constant by a_4, Eqs. (17) give the relationship

$$\hat{\lambda} = a_4 \left(\frac{X + a_2}{\sigma} \right) . \qquad (50)$$

A substitution of Eqs. (14), (49), and (50) into Eq. (47) results in

$$a_4 = \frac{0.0493 \, (1 + 2\gamma)}{E^{1/2}} \quad . \qquad (51)$$

The turbulence dissipation ratio, γ, is set to 1/3 as was done in the previous work, ref. 6.

Eq. (51) shows that E must be a constant value in order to produce the conventional conservation set, Eqs. (47) and (48), in the limit of near-equilibrium turbulence field. Existing literature (see, for instance, refs. 10 and 13) shows that E is of order 0.1. The values of E employed in the present computation are,

$$E = 0.05 \text{ to } 0.2. \tag{52}$$

The corresponding values of a_4 are determined from Eq. (51). Note that $a_4 = 0.26$ when $E = 0.1$. Since the jet boundary corresponds to $\eta \approx 2.5$, the turbulence scale represented by $a_4 = 0.26$ is about one tenth of the jet radius which is of the order of the mixing length as expected. Solutions for $E = 0.1$ and $a_4 = 0.26$ will be used for comparison with the experimental data subsequently.

Boundary Conditions

The boundary conditions for Eqs. (27a) - (30b) are the same as Eqs. (40) - (42) for each of the variables, c_a^+, c_a^-, c_b^+, c_b^-, etc. The conditions of Eqs. (40) and (41), however, also imply that each of the variables is specified at $R \to \infty$ for all X.

Before the boundary conditions are explicitly specified, a consideration should be given to the following. The similarity velocity profiles given by Eqs. (14) - (16) are valid for $X \gtrsim 5.8$ (see ref. 10). In fact, ususally, the flow is not fully turbulent for $X < 5.8$ and there the present turbulence

analysis does not apply. Since the present interest lies with the combustion description for large X's where influence of the initial condition is negligible, the initial conditions are specified at $X = 5.8$.

Solutions of Eqs. (27a) - (30b) are obtained for the following initial and boundary conditions.

At $X = 5.8$,

$$c_{ao} = \tilde{c}_{ao}(R) , \qquad \bar{c}_a = \bar{c}_a(R) , \tag{53}$$

$$c_{bo} = c_{bo}(R) , \qquad \bar{c}_b = \bar{c}_b(R) , \tag{54}$$

$$c_{do} = 0 , \qquad \bar{c}_d = 0 , \tag{55}$$

$$h_o = h_o(R) , \qquad \bar{h} = \bar{h}(R) . \tag{56}$$

For $R \to \infty$ and $X > 5.8$,

$$c_{ao} = 0.22 , \qquad \bar{c}_a = 0 , \tag{57}$$

$$c_{bo} = 0 , \qquad \bar{c}_b = 0 , \tag{58}$$

$$c_{do} = 0 , \qquad \bar{c}_d = 0 , \tag{59}$$

$$h_o = 0.1 , \qquad \bar{h} = 0 . \tag{60}$$

At $R = 0$,

$$\bar{c}_a = \bar{c}_b = \bar{c}_d = \bar{h} = 0 . \tag{61}$$

The initial profiles for c_{ao} and c_{bo} shown on Fig. 3 are specified for Eqs. (53) and (54). The profile for c_{bo} is chosen such that it corresponds to the pure hydrogen jet issuing from a circular nozzle of radius $L/2$ as seen in Fig. 3; that is

$$\frac{\pi L^2}{4} = 2\pi\left(\int_o^\infty c_{bo}u_o r\, dr\right)_{X = 5.8} \tag{62}$$

The c_{ao} profile of Fig. 3 is chosen arbitrarily with only two conditions in mind. The mixing with hydrogen begins at $X = 5.8$, and that c_{ao} profile is continuous with Eqs. (57) satisfied. Any overt discontinuities will tend to propagate along the characteristics and may cuase numerical difficulty.

An arbitrarily continuous profield for h_o is specified at $X = 5.8$ for Eqs. (56) to satisfy Eqs. (60).

The simplest value for c_a^-, c_b^-, and h^- to be assigned at $X = 5.8$ is zero. It was found, however, that numerical stability of the solution is improved by specifying a small but non-vanishing function for each to satisfy Eqs. (57), (58), and (60). Both c_{do} and c_d^- are specified to be zero for all R initially.

As was stated earlier, the present interest lies with the combustion description for large values of X and with the overall combustion phenomena for the entire jet. Details of the initial conditions have very little effect on these.

Solutions of the governing equations, (27a) through (31), satisfying the boundary conditions, Eqs. (53) - (61), are obtained by the MacCormick's (ref. 8) finitie difference method. Details of application of the method are found in the Appendix. Results of the solution are discussed in the next section.

DISCUSSION OF RESULTS

Figs. 4, 5, and 6 show the mean reactant mass fraction and temperature profiles for the three different axial locations of $X = 21.81$, 61.82, and 105.81 respectively. These are the solutions for $E = .1$ and $a_4 = 0.26$ which together comprise the eddy diffusivity given in ref. 9 in the limit of an equilibrium turbulence field (see the preceding section). Therefore, these solutions are considered as the more representative ones for the standard jet issuing into a stationary air.

Solutions were found to be insensitive to u_∞/u_p when it is smaller than 0.2. On the other hand, the numerical difficulty increased rapidly with decreasing u_∞/u_p. Therefore, the solutions discussed in this section were obtained for $u_\infty/u_p = 0.2$.

The general shapes of the mean profiles are same as those found in the experimental works of refs. 14 - 17. Note that the present results, c_{ao} and c_{bo}, are in mass fractions whereas those given in refs. 14 and 15 are in mole fractions. Mean profiles of the combustion product are similar to those of temperature, and are not shown in the figures.

The temperature peak is located at a point away from the jet axis for small values of X (see Fig. 4). The peak point is slightly on the fuel-rich side from the stoichiometric location, where the fuel-to-oxygen mass ratio is $1/8$, in agreement with the finding of ref. 14. Location of the temperature peak moves to the jet axis as X is increased.

At the larger X's (Figs. 5 and 6), oxygen survives through the combustion zone and appears in the jet axis. The flame comprising a shell

in the jet (Fig. 4) for smaller X's pervades throughout the inner core of the jet (Figs. 5 and 6) for larger values of X . The flame thickness is of the order of one-tenth of the jet axial distance, X , and comprises about one-half of the jet cross section.

Distribution with respect to R of the combustion rate is shown in Fig. 7. Note that the maximum burning point does not correspond to the peak temperature position; particularly for X = 61.82 and 105.81 . For all X's , the maximum combustion point is slightly on the fuel-rich side of the stoichiometric position. For X = 21.81 , the maximum burning takes place at a point between the temperature peak and the point of stoichiometry.

Comparison of Figs. 8, 5, and 9 shows the effects of varying turbulence energy on the mean profiles. Other than the substantial change in the burning rate evident from the level of c_{bo} , E does not basically change the mean profiles. The combustion rates will be elaborated upon subsequently in conjunction with another figure. Thickness of the flame is seen to be insensitive to the turbulence energy variation.

Figs. 10, 5, and 11 show that the flame thickness is substantially affected by the turbulence scale represented by a_4 (see Eq. (50). Greater the scale (size of the energy containing eddies), greater is the flame thickness. This was expected from the previous studies (refs. 1 and 6).

The flame is thick in contrast to the infinitesimally thin flame sheet predicted by the conventional theory (see ref. 12). Therefore, the flame shape and length for the jet flow cannot be precisely defined. However, loci of the stochiometric locations may be used for comparison of the flame shapes and lengths. Fig. 12 shows the stoichiometric positions

for the four of the computed cases. Both increased turbulence energy and scale result in the shorter flame lengths.

Shorter flame lengths, of course, are caused by the enhanced burning rates, and this is seen in Figs. 13 and 14. These figures show the total integrated burning rates across the jet cross-section as functions of X. Stoichiometric lengths of the flames for $E = 0.1$ and 0.2 with $a_4 = 0.26$ found in Fig. 12 are also shown in Fig. 13. Because of the very thick nature of the flame zone, the combustion rate does not become zero at the stoichiometric end of the flow (Fig. 13), but it asymptotically approaches zero.

Both larger turbulence energy and scale result in enhanced combustion rates (Figs. 13 and 14), and, hence, in the shorter flame lengths (Fig. 12). Increased turbulence energy enhances both mixing and the chemical reaction rate which is controlled by the turbulent dissipation (Eq. 13). This is evident in the characteristic equations, Eqs. (38) and (39). Larger turbulence energy implies, according to Eq. (39), the greater slopes of the characteristics which cause a faster mixing between the fuel and the surrounding air. The increased turbulence energy also enlarges the dissipation-limited chemical reaction terms of Eq. (38), which are the terms involving ϕ^+ and ϕ^-. Therefore, turbulence energy has a substantial influence on the combustion rate and flame length. This is in agreement with the previous findings (ref. 6) in plane mixing layer of infinite domain. It was found in ref. 6 that the combustion rate increased with $\sqrt{E}$. Although the present jet problem is quite different from the plane mixing layer

problem analyzed in the reference, it is interesting to note that the two jet combustion rates respectively for $E = 0.1$ and 0.2, as represented by reciprocals of the two stoichiometric lengths of the flames (see Fig. 12), scale very closely as $\sqrt{E}$.

Larger turbulence scale, $\hat{\lambda}$, enhances the combustion rate through increased mixing which is brought about in a manner quite different from that for the larger E discussed above. The characteristic directions are independent of the turbulence scale (Eq. (39)). Increased scale actually reduces the turbulence dissipation-limited chemical reaction rate as seen in Eq. (38). In fact, magnitudes of all the terms on the right-hand side of Eq. (38) are reduced by the increased $\hat{\lambda}$ except the mixing terms which are the second and last terms in the second curly bracket. However, as explained in the sentences following Eqs. (38) and (39), this right-hand side constitutes the wave dissipation.* With the dissipation action on the wave diminished, the wave propagates further and for a longer period of time. For instance, the wave consisting of the fuel properties propagates into the oxygen-rich territory until the chemical reaction, the dissipative action on the wave, completes its task. Therefore, increased $\hat{\lambda}$ simply stretches the reaction zone as seen in Figs. 10, 5, and 11, and in so doing, brings the reaction zone into the oxygen-rich region.

---

*Note that the word "wave dissipation" is employed to mean the standard dissipative action on the wave. This should not be confused with the "turbulence dissipation" which refers to the viscous dissipation of the turbulent fluctuations.

This implies an enhanced mixing and, consequently, an enhanced combustion rate. This is in agreement with the findings of ref. 6 for the plane mixing layer. As was found in that reference, however, it is expected that continuous increase of the scale will eventually result in the reduced combustion rate. This is because a point must be reached with increasing $\hat{\lambda}$ beyond which no amount of efficient mixing can overcome the inefficiency of the turbulence dissipation-limited reaction rate caused by the large scale.

Typical variations of the reactant mass fractions and temperature along the jet centerline are shown in Figs. 15 - 17. As explained earlier, the temperature peak occurs away from the centerline for small values of X. The maximum temperature is also indicated in the figures when it does not correspond to the centerline value. When the conventional flame-sheet solution is obtained, the temperature peak exists at the sheet which is located away from the centerline until the end of the flame. Also, this temperature is constant until the flame ends and it can be readily computed. This flame sheet temperature is shown in the figures for comparison. Because the chemical reaction is spread across a thick flame zone, the peak temperature computed in the present study is substantially below the hypothetical flame sheet temperature. This difference is greater than the difference found in the experimental work of ref. 14. As was stated previously, variation the combustion product is similar to that of the temperature. Since concentration of the combustion product was measured in ref. 15, but not the temperature, as well as in ref. 14 for pure hydrogen jet combustion, the present computed values of the combustion product is compared with those

of refs. 14 and 15 in Fig. 18. The present values of the H_2O concentration agree rather closely with the experimental values of Hawthorne, et al, (ref. 15) but are considerably below those of Kent (ref. 14).

Fig. 18 shows that the computed concentrations of H_2 and O_2 agree satisfactorily with the experimental data of both refs. 14 and 15. Note that the O_2 centerline concentration was found to be practically zero in ref. 15 up to X of about 66, which is in agreement with the present results.

Finally, the computed stoichiometric contour of the flame is compared with that measured in ref. 14 in Fig. 19. No detailed agreement in these contours was expected since the present solution was based on an incompressible flow assumption. However, it is rather surprising to see the close agreement on the flame length, that is, on the overall combustion rate. Hawthorne, et al, (ref. 15) measured the "luminous" flame lengths for various jet flow conditions and found them to be between about $X \approx 128 \rightarrow 146$. These values also agree closely with the computed results. The computed contour for the hydrogen mass fraction of 0.003 is also shown in Fig. 19. This shows that the flame is thick and the combustion continues for a substantial distance following the stoichiometric end of the flame, though at diminishing rates, as explained earlier.

CONCLUDING REMARKS

The kinetic theory of turbulent flow was employed to analyze the mixing-limited combustion in axisymmetric jet. The bimodal moment method of solution of the kinetic equations was modified to circumvent certain

difficulty encountered previously. In the absence of a more direct numerical capability for solution of the original kinetic equations, this modification enables one to obtain satisfactory solutions of the turbulent combustion problems. It is noted that a direct numerical technique is being tried elsewhere (see ref. 7) with some success, and such a method should eventually replace the present method.

The modified bimodal method was employed to transform the kinetic equations governing the combustion energetics into a set of hyperbolic differential equations. Assuming, for convenience, that the incompressible mean flow field is given, this set of the equations was integrated by the MacCormick's finite difference scheme for combustion of hydrogen.

Detailed structure of the flame as well as the overall combustion rate of the hydrogen jet were computed. The centerline variations of the reactant concentrations and the flame length obtained were compared with the available experimental data which showed a satisfactory agreement. A full discussion is found in the preceeding section.

One of the contributions of this report is the successful application of the finite difference scheme to solution of the governing equations for combustion based on the kinetic theory. This numerical technique—together with the modified moment method—should provide a considerable flexibility for analysis of the various combustion problems of engineering interest. Details of the application of the numerical method are given in the appendix.

ACKNOWLEDGEMENT

The authors are indebted to Dr. John Evans of NASA, Langley Research Center for his continued encouragement and support during the course of this research.

APPENDIX

INTEGRATION OF THE GOVERNING EQUATIONS

Numerical Analysis

Eqs. (27a) - (30b) are transformed into a first order vector differential equation. Numerical solutions are obtained for the variables c_i^+ and c_i^- where

$$c_1^+ = c_a^+, \quad c_3^+ = c_b^+, \quad c_5^+ = c_d^+, \quad c_7^+ = c_h^+,$$

$$c_2^- = c_a^-, \quad c_4^- = c_b^-, \quad c_6^- = c_d^-, \quad c_8^- = c_h^- . \tag{A1}$$

The vector differential equation is

$$\frac{\partial \tilde{\Omega}}{\partial X} + \frac{\partial}{\partial R} \tilde{F}(\tilde{\Omega}) = \tilde{S}(\tilde{\Omega}) . \tag{A2}$$

Components of the vectors are given as follows.

For i = odd;

$$\Omega_i = c_i^+ , \tag{A3}$$

$$F_i(\tilde{\Omega}) = \frac{2v_o}{u_o} c_{io} + \frac{2}{u_o} \langle Vc_i \rangle - \sqrt{\pi} \frac{v_o}{u_o} \exp\left(\frac{3}{2E} v_o^2\right) c_{io} , \tag{A4}$$

$$S_i(\tilde{\Omega}) = -\left[\frac{\sqrt{\pi}}{u_o}\left(1 + \frac{3}{E} v_o^2\right) \exp\left(\frac{3}{2E} v_o^2\right) \frac{\partial v_o}{\partial X}\right.$$

$$+ \sqrt{\pi}\, v_o \exp\left(\frac{3}{2E} v_o^2\right) \frac{\partial}{\partial R}\left(\frac{1}{u_o}\right) - 2 \frac{\partial}{\partial R}\left(\frac{v_o}{u_o}\right)\Bigg] c_{io}$$

$$+ \Bigg[- \frac{3\sqrt{\pi}}{E} v_o \exp\left(\frac{3}{2E} v_o^2\right)\left(\frac{1}{u_o} \frac{\partial v_o}{\partial R} - \frac{1}{u_c} \frac{\partial u_c}{\partial X}\right)$$

$$- \frac{3}{E}\sqrt{\frac{3}{2E}}\, v_o \frac{\partial v_o}{\partial X} \exp\left(\frac{3}{2E} v_o^2\right)$$

$$+ 2\left(\frac{\partial}{\partial R}\left(\frac{1}{u_o}\right) - \frac{1}{u_o R}\right)$$

$$- \sqrt{\pi}\, v_o^2 \frac{\partial v_o}{\partial X} \exp\left(\frac{3}{2E} v_o^2\right)\Bigg] \langle Vc_1 \rangle$$

$$+ \frac{2}{u_o} \zeta_1 - \frac{3}{E}\sqrt{\pi} \frac{v_o}{u_o} \exp\left(\frac{3}{2E} v_o^2\right) \hat{\zeta}_1 \quad , \tag{A5}$$

and for i = even;

$$\Omega_i = c_i^- \quad , \tag{A6}$$

$$F_i(\tilde{\Omega}) = \sqrt{\frac{2\pi E}{3}} \exp\left(\frac{3}{2E} v_o^2\right) \frac{c_{io}}{u_o} \quad , \tag{A7}$$

$$S_i(\tilde{\Omega}) = \exp\left(\frac{3}{2E} v_o^2\right)\left[\sqrt{\frac{6\pi}{E}} \frac{v_o}{u_o} \frac{\partial v_o}{\partial X} + \sqrt{\frac{2\pi E}{3}} \frac{\partial}{\partial R}\left(\frac{1}{u_o}\right)\right] c_{io}$$

$$+ \left[\left(\frac{1}{u_o}\frac{\partial v_o}{\partial R} - \frac{1}{u_c}\frac{\partial u_c}{\partial X}\right)\sqrt{\frac{6\pi}{E}}\right.$$

$$\left. + \sqrt{\frac{2\pi E}{3}}\, v_o \frac{\partial v_o}{\partial X}\right] \exp\left(\frac{3}{2E} v_o^2\right) \langle Vc_1 \rangle$$

$$+ \sqrt{\frac{6\pi}{E}} \exp\left(\frac{3}{2E} v_o^2\right) \frac{\hat{\zeta}_1}{u_o} \quad , \tag{A8}$$

where

$$\zeta_1 = \text{Right hand side of Eq. (27a), (28a), (29a), or (30a)} \tag{A9}$$

and

$$\hat{\zeta}_1 = \text{Right hand side of Eq. (27b), (28b), (29b), or (30b)} - \frac{\partial v_o}{\partial R} \langle VC_1 \rangle \, . \tag{A10}$$

The undifferentiated term $\tilde{S}(\tilde{\Omega})$ is treated as source term.

The numerical method employed is based on the two-step explicit procedure developed by Lax and Wendroff (ref. 18) and, more recently, by MacCormick (ref. 8). The intermediate state, $\tilde{\Omega}_j^*$, is computed as

$$\tilde{\Omega}_j^* = \tilde{\Omega}_j - \frac{\Delta X}{\Delta R}\left[\tilde{F}(\tilde{\Omega}_{j+1}^n) - \tilde{F}(\tilde{\Omega}_j^n)\right] + \Delta X\, \tilde{S}(\tilde{\Omega}_j^n) \, . \tag{A11}$$

The final state is then determined by

$$\tilde{\Omega}_j^{n+1} = 0.5\left\{\tilde{\Omega}_j^n + \tilde{\Omega}_j^* - \frac{\Delta X}{\Delta R}\left[\tilde{F}(\tilde{\Omega}_j^*) - \tilde{F}(\tilde{\Omega}^*_{j-1})\right]\right.$$

$$+ \Delta X \, \tilde{S}(\tilde{\Omega}_j^*) \Big\} \quad . \tag{A12}$$

Thus, for a given vector $\tilde{\Omega}^n$ at $X = n\Delta X$, the subsequent state vector is computed forward in the X-direction. The two-step explicit procedure provides a solution with second order accuracy in the finite difference increment. This method has an advantage in which no maxtrix inversion and iteration are required. It has, however, the disadvantage of being conditionally stable.

Stability condition of the difference equations requires that the Courant condition be satisfied at each axial position X as,

$$\Delta X \leq \min\left(\sqrt{\frac{3}{2\pi E}} \exp\left(-\frac{3}{2E} v_o^2\right) u_o \, \Delta R, \; 0.5 \frac{u_o}{v_o} \Delta R\right) . \tag{A13}$$

For the jet problem, the non-dimensional velocity u_o varies from one at the center to zero at the jet boundary. Therefore, it is difficult to satisfy the stability condition. This, however, can be ameliorated by specifying a small but non-zero value of u_o at the jet boundary.

There exists another difficulty associated with the small u_o for $R \to \infty$. The difficulty arises because the gradiant of the flux function, $\partial \tilde{F}/\partial R$, is small while the source function, $\tilde{S}$, does not vanish due to the terms containing $1/u_o$. This causes an inaccuracy near the jet boundary which then propagates inward. This difficulty, of course, can be remedied by demanding a higher degree of accuracy for $\tilde{\Omega}$ by reducing the grid size, ΔR. However, the required computer time rapidly increases with the reduction

of ΔR . For instance, halving of the ΔR results in quadrupling of the computer time. The problem was resolved by the combination of reduction of ΔR to a practically feasible value and imposition of the condition,

$$c_i^+ = \min \left[c_i^+ , \; c_i^+ (R \to \infty) \right] , \tag{A14}$$

on the oxidant which diffuses from jet boundary to the core region. With the above stability and accuracy considerations, solution of the governing equations is obtained by the two-step Lax-Wendroff procedure.

One additional point should be made. The dependent variables of Eqs. (27a) - (30b) are c_{io} , $\langle Vc_i \rangle$, and $\langle V^2 c_i \rangle$. These are functions of z_1 , and z_2 , as defined in Eqs. (33) - (35), which are, in turn, functions of z^+ and z^- via Eq. (37). It was found that the stability and accuracy criteria were best satisfied by employing c_i^+ and c_i^- as the dependent variables of the equations rather than c_{io} , $\langle Vc_i \rangle$, etc.

Computer Program

The computer program is written in PL/I language. A brief description of the procedures (subroutines in FORTRAN language) used in the code is given. The program structure is implicit so that numerous variables are implicitly passed through the procedures.

1. Procedures

JETFLAME — This is the main procedure which calls the necessary procedures and controls the step-size DX . The standard step-size DX_SAVE

is first tried, and if $c_{ao} < 0$ at any point in R the step-size is reduced by 80 percent.

SOLVE — This procedure performs the solution by the two-step Lax-Wendroff numerical scheme.

SOURCE — This is the procedure in which $\tilde{F}(\tilde{\Omega})$ and $\tilde{S}(\tilde{\Omega})$ are computed and the procedure SOLVE calls SOURCE.

BOUNDRY — The boundary values for c_a^+, c_b^+, c_d^+, c_h^+, c_a^-, c_b^-, c_d^-, and c_h^- are specified at $X = X_o$.

ERRFCTN — This procedure computes the error function with the polynomial fit,

$$\text{erf}\,(x) = \sum_{n=1}^{5} a_n t^n , \tag{A15}$$

where

$$t = \frac{1}{1 + 0.32759\,X} . \tag{A16}$$

REACTION_RATE — The overall effective reaction rate,

$$\int_o^\infty \langle\hat{\omega}\rangle\, R\, d\, R , \tag{A17}$$

is computed where

$$\langle\hat{\omega}\rangle = \frac{u_c}{2} \frac{\sqrt{E}}{\gamma\hat{\lambda}}\, c_{ao} c_{bo}^2 \left[\phi^+ + \text{erf}\left(\sqrt{\frac{3}{2E}}\, v_o\right) \phi^-\right] . \tag{A18}$$

TRAPEZO — Integration is performed by a trapezoidal scheme.

2. Inputs to the Code

It consists of the procedure INPUT and a file INPUT 1. The variables for the input are as follows.

E	$\epsilon = 1 - (u_\infty/u_p)$
ETAMAX	maximum value of η
XSTART	X-value at which the initial values are specified
XSTOP	maximum value of X
XOUT	output control parameter; prints for every XOUT
DR	grid size in R
E_HAT	E
MB_OVER_MA	M_b/M_a
MD_OVER_MA	M_d/M_a
A1	a_1
A2	a_2
A3	a_3
A4	a_4
D	γ
SIGMA	σ

SPECIES(I,J) i-th species at j-th grid point where

$$
\begin{aligned}
i = 1 &\rightarrow c_a^+ , \quad 5 \rightarrow c_d^+ , \\
2 &\rightarrow c_a^- , \quad 6 \rightarrow c_d^- , \\
3 &\rightarrow c_b^+ , \quad 7 \rightarrow c_h^+ , \\
4 &\rightarrow c_b^- , \quad 8 \rightarrow c_h^- .
\end{aligned}
\tag{A19}
$$

The variables listed--except SPECIES(*, 1) and SPECIES(*, MAXG)--are given in the procedure INPUTS. However, they are overridden and replaced by the values in the file INPUT 1. The values of c_a^+, c_b^+, c_d^+, and c_h^+ at the jet center and at $R \rightarrow \infty$ must be given in the file INPUT 1.

3. Outputs from the Code

The final outputs are the average mass fractions, the turbulent diffusion fluxes, and the local chemical reaction rate, $\langle\hat{\omega}\rangle$.

A list of the other program symbols is given below.

CZO	z_o
<V*cz>	$\langle Vz \rangle$
<WP>	$\int_o^\infty \langle\hat{\omega}\rangle R \, d \, R$
WP(R)	$\langle\hat{\omega}\rangle$, (Eq. (A18))
ETA	η

4. Program Listing

COMPUTER PROGRAM

(PL/I LANGUAGE)

```
FLAME:PROC OPTIONS(MAIN);
DCL(SPECIES(*,*), F(*,*), S(*,*), SPT(*,*)) CTL FLOAT DEC(16);
DCL (CHEM_REACTION(*), SPECIES_SAVE(*,*) ) CTL FLOAT DEC(16);
DCL(AA,  BB, A1, A2, A3, A4,
    X, X2, DX, DX_SAVE, XOUT, ETAMAX,
    XSTART, XSTOP,
    R, DR, RMAX, E,
    A, D, E_HAT, LAMDA, SIGMA, REF_CB0,
    MB_OVER_MA, MD_OVER_MA, SQRTE ) FLOAT DEC(16);
DCL (SET_PROFILE, YES INIT('Y'), NO INIT('N')) CHAR(1);
DCL(GRID, MAXG, MAXR, INCREMENT, ITR, ITR_MAX) FIXED BIN(15);
DCL(EXP, MAX, MIN, SQRT, FLOAT, ABS, FIXED) BUILTIN;
DCL(I,J) FIXED BIN(15);
DCL INPUT1 FILE;
/*  SPECIES(I)= C_ VECTOR
    WHERE 1=CA0
          2=<V*CA>,
          3= CB0,
          4=<V*CB>,
          5= CD0,
          6=<V*CD>,
          7= H0,
          8=<V*H>                    */
CALL INPUTS;
AA=SQRT(1.5/E_HAT);
BB=SQRT(E_HAT/18.848);
DX_SAVE=0.70*(1.-E)*DR;
INCREMENT=FIXED(0.1/DR);
IF INCREMENT=0 THEN INCREMENT=1;
X2,X=XSTART;
SQRTE=SQRT(E_HAT);
CALL BOUNDRY(SPECIES);
SPT=SPECIES;
MAXR=MAXG-2;
```

```
41.          LAMDA=A4*(X+A2)/SIGMA;
42.          SET_PROFILE=YES;
43.          DX=DX_SAVE;
44.          MAXR=FIXED(20.*(X+A2)/(SIGMA*DR));
45.          CALL OUT1;
46.          LLL:DO J=1 TO 15;
47.              CALL SOLVE(SPECIES,F,S,RETRY);
48.              END LLL;
49.          SET_PROFILE=NO;
50.          CALL OUT1;
51.          MAIN:DO WHILE(X<XSTOP);
52.               DX=DX_SAVE;
53.          RETRY:X=X+DX;
54.               IF DX<1.E-09*DX_SAVE THEN
55.                              DO;
56.                              PUT SKIP(4) EDIT('SPECIES(1) IS NEGATIVE' )
57.                                  (COL(4),A);
58.                              GO TO FINISH;
59.                              END;
60.               LL2:DO J=10 TO MAXG;
61.                   MAXR=J;
62.                   IF SPECIES(1,J)>0.9998*SPECIES(1,MAXG) THEN GO TO OP2;
63.                   END;
64.               OP2:LAMDA=A4*(X+A2)/SIGMA;
65.               MAXR=MAXR+8;
66.               CALL SOLVE(SPECIES,F,S,RETRY);
67.               IF SPECIES(3,1)<0.005 THEN GO TO FINISH;
68.          IF X>=X2 THEN DO;
69.          X2=X2+XOUT;
70.          CALL OUT1;
71.          END;
72.          IF SPECIES(3,1)<0.005 THEN GO TO FINISH;
73.          END MAIN;
74.     0
75.     0
76.     0
```

```
77.      0    SOLVE:PROC(SPECIES,F,S,RETRY);
78.           DCL(SPECIES(*,*),F(*,*),S(*,*), SIGN,SLOPE) FLOAT DEC(16),
79.              (I,GRID,IX) FIXED BIN(15);
80.           DCL J FIXED BIN(15);
81.           DCL RETRY LABEL;
82.           CALL SOURCE(SPECIES,F,S);
83.           FIRST:DO GRID=2 TO MAXR-1;
84.           SPEC1:DO I=1 TO 8;
85.                 IF ABS(F(I,GRID))>1.E-30 THEN
86.                 SPT(I,GRID)=SPECIES(I,GRID)-(F(I,GRID+1)
87.                                /F(I,GRID)-1.)* F(I,GRID)*DX/DR
88.                               +DX*S(I,GRID) ;
89.                 ELSE
90.                      SPT(I,GRID)=SPECIES(I,GRID)
91.                            -(F(I,GRID+1)-F(I,GRID))*DX/DR +DX*S(I,GRID) ;
92.                 IF SET_PROFILE=NO  THEN
93.                 CHECK1:DO;
94.                        SPT(4,GRID)=MAX(0.0,SPT(4,GRID));
95.                        IF SPT(1,GRID)<0.0 THEN
96.                                DO;
97.                                X=X-DX;
98.                                DX=0.2*DX;
99.                                IF ABS(SPT(1,GRID))>1.E-06 THEN GO TO RETRY;
100.                               ELSE SPT(1,GRID)=0.0;
101.                               END;
102.                      END CHECK1;
103.                ELSE  SPT(1,GRID)=MAX(0.0,SPT(1,GRID));
104.                IF ABS(SPT(I,GRID))<1.E-12 THEN SPT(I,GRID)=0.0;
105.                END SPEC1;
106.                END FIRST;
107.          DO I=1 TO 4;
108.          SPT(2*I-1,1)=SPT(2*I-1,2);
109.          END;
110.          CALL SOURCE(SPT,F,S);
111.          SECOND:DO GRID=2 TO MAXR-1;
```

```
112.            SPEC2:DO I=1 TO 8;
113.                  IF ABS(F(I,GRID-1))>1.E-30 THEN
114.                  SPECIES(I,GRID)=0.5*(SPT(I,GRID)+SPECIES(I,GRID)
115.                        -(F(I,GRID)/F(I,GRID-1)-1.)*F(I,GRID-1)*DX/DR
116.                              +DX*S(I,GRID)) ;
117.                  ELSE
118.                  SPECIES(I,GRID)=0.5*(SPT(I,GRID)+SPECIES(I,GRID)
119.                              -(F(I,GRID)-F(I,GRID-1))*DX/DR
120.                              +DX*S(I,GRID)) ;
121.                  IF ABS(SPECIES(I,GRID))<1.E-12 THEN SPECIES(I,GRID)=0.0;
122.                  END SPEC2;
123.                  END SECOND;
124.             DO I=1 TO 4;
125.             SPECIES(2*I-1,1)=SPECIES(2*I-1,2);
126.             END;
127.           END SOLVE;
128.     0
129.     0
130.     0
131.     0     SOURCE:PROC(SPECIES,F,S);
132.           DCL(SPECIES(*,*), F(*,*), S(*,*),
133.               ETA, V0, U0, V0_OVER_U0,ERF, R,
134.               G1, G2, G3,  VA,
135.               F5, UC,
136.                CHEM1, CHEM2, STCHMTRY,
137.               TERM1, TERM2, TERM4, TERM6,
138.               VSP(4), W1, W2,
139.               DERI_V0, DERI_V0_X, DERI_V0_R,DERI_U0_R,DERI_LOGUC,
140.               PHI_PLUS, PHI_MINUS ) FLOAT DEC(16);
141.           DCL SPECI(*,*) CTL FLOAT DEC(16);
142.           DCL (I,J) FIXED BIN(15);
143.           ALLOCATE SPECI(8,MAXR);
144.           BOUNDRY:DO I=1 TO 4;
145.                    F(2*I,1)=1.447202*SQRTE*SPECIES(2*I-1,1)/2.;
146.                    END BOUNDRY;
```

```
147.                IF SET_PROFILE=YES THEN
148.                 LL:DO I=2 TO MAXR;
149.                    IF SPECIES(1,I)<0.0 THEN SPECIES(1,I)=0.0;
150.                    IF SPECIES(2,I)>0.0 THEN SPECIES(2,I)=SPECIES(2,I-1);
151.                    END LL;
152.             L8:DO I=1 TO 8;
153.                L6:DO J=1 TO MAXR;
154.                   IF ABS(SPECIES(I,J))<1.E-12 THEN SPECIES(I,J)=0.0;
155.                   END L6;
156.                END L8;
157.             R=0.0;
158.          L1:DO J=2 TO MAXR-1;
159.             R=R+DR;
160.             ETA=SIGMA*R/(X+A2);
161.             F5=1./(1.+0.25*ETA*ETA);
162.             UC=A1/(A2+5.8) - E*(A1/(A2+5.8) - A1/(A2+X) );
163.             U0=1.-E*(1.-F5**2);
164.             V0=E*A3*(ETA-0.25*ETA**3)*F5**2;
165.             DERI_U0_R=-E*ETA*F5**3*SIGMA/(X+A2);
166.             DERI_V0=E*A3*(1.-0.75*ETA*ETA)*F5*F5-V0*ETA*F5;
167.             DERI_V0_R=DERI_V0*SIGMA/(X+A2);
168.             DERI_V0_X=-DERI_V0*ETA/(X+A2);
169.             DERI_LOGUC=-E*A1/((X+A2)**2*UC);
170.             VA=AA*V0;
171.             IF ABS(VA)>0.09 THEN CALL ERRFCTN(VA, G1);
172.             ELSE G1=VA;
173.             G2=EXP(-VA*VA);
174.             G3=1./G2;
175.             CONTROL_AT_LARGE_ETA:
176.                      IF ETA>2.45 THEN
177.                          SPECIES(2,J)=-ABS(SPECIES(2,J));
178.                      SPECIES(1,J)=MIN(SPECIES(1,J),SPECIES(1,MAXG));
179.             L9:DO I=1 TO 4;
180.                SPECI(2*I-1,J)=0.5*(SPECIES(2*I-1,J)+1.2247448/SQRTE
181.                                  *V0*SPECIES(2*I,J));
```

```
182.              SPECI(2*I,J)=0.2303294*SQRTE*G2*SPECIES(2*I,J);
183.              END L9;
184.
185.              L3:DO I=1 TO 4;
186.                 F(2*I-1,J)=2.*V0/U0*SPECI(2*I-1,J)+2.*SPECI(2*I,J)/U0
187.                            -1.773245385*V0*G3*SPECI(2*I-1,J)/U0;
188.                 F(2*I,J) =1.4472025*SQRTE*G3*SPECI(2*I-1,J)/U0;
189.                 END L3;
190.           IF SPECI(1,J)=0.0 THEN SPECI(2,J)=0.0;
191.           IF SPECI(1,J)<5.0E-03  THEN
192.              DO;
193.              CHEM1=SQRTE*D/LAMDA*SPECI(1,J) ;
194.              CHEM2=0.0;
195.              CHEM_REACTION(J)=CHEM1;
196.              GO TO OPT;
197.              END;
198.           ELSE IF SPECI(3,J)<5.0E-03  THEN
199.                 DO;
200.                 CHEM1=0.25*SQRTE*D/LAMDA*SPECI(3,J)/MB_OVER_MA ;
201.                 CHEM2=0.0;
202.                 CHEM_REACTION(J)=CHEM1;
203.                 GO TO OPT;
204.                 END;
205.           ELSE L7:DO;
206.           TERM1=(0.25*(SPECIES(3,J)+SPECIES(4,J))**2
207.                 +MB_OVER_MA*(SPECIES(1,J)+SPECIES(2,J))
208.                       *(SPECIES(3,J)+SPECIES(4,J))) ;
209.           TERM2=(0.25*(SPECIES(3,J)-SPECIES(4,J))**2
210.                 +MB_OVER_MA*(SPECIES(1,J)-SPECIES(2,J))
211.                       *(SPECIES(3,J)-SPECIES(4,J))) ;
212.           IF ABS(TERM1-TERM2)<1.E-06 THEN
213.                  DO;
214.                  PHI_PLUS=2./TERM1;
215.                  PHI_MINUS=0.0;
216.                  END;
```

```
217.              ELSE DO;
218.                      PHI_PLUS=1./TERM1 + 1./TERM2 ;
219.                      PHI_MINUS=1./TERM1 - 1./TERM2;
220.                      END;
221.           CHEM1=MAX(0.,0.5*SQRTE*D/LAMDA*SPECI(1,J)*SPECI(3,J)**2
222.                                          *(PHI_PLUS+G1*PHI_MINUS))   ;
223.           CHEM2=MAX(0.,0.2303292*E_HAT*D/LAMDA*SPECI(1,J)*SPECI(3,J)**2
224.                                           *G2*PHI_MINUS);
225.           CHEM_REACTION(J)=0.5*SQRTE*D/LAMDA*SPECI(1,J)*SPECI(3,J)**2
226.                                          *(PHI_PLUS+G1*PHI_MINUS)  ;
227.           END L7;
228.        OPT:TERM4=(U0*DERI_V0_X + V0*DERI_V0_R +V0*U0*DERI_LOGUC);
229.           TERM6=SQRTE/LAMDA*(1.+2.*D)/2.0;
230.        /* SOURCE TERMS FOR ORIGINAL EQUATIONS   PSI'S  */
231.           S(1,J)=-0.5*CHEM1;
232.           S(2,J)=-(TERM4*SPECI(1,J)+TERM6*SPECI(2,J)+0.5*CHEM2);
233.           S(3,J)=-MB_OVER_MA*CHEM1 ;
234.           S(4,J)=-(TERM4*SPECI(3,J)+TERM6*SPECI(4,J)
235.                    +MB_OVER_MA*CHEM2) ;
236.           S(5,J)=MD_OVER_MA*CHEM1;
237.           S(6,J)=-(TERM4*SPECI(5,J)+SPECI(6,J)*TERM6)
238.                                          +MD_OVER_MA*CHEM2 ;
239.           S(7,J)=MD_OVER_MA*CHEM1;
240.           S(8,J)=-(TERM4*SPECI(7,J)+SPECI(8,J)*TERM6)
241.                                          +MD_OVER_MA*CHEM2 ;
242.           L4:DO I=1 TO 4;
243.              S(2*I-1,J)=(-1.77245385*(1.+3.*V0*V0/E_HAT)*G3*DERI_V0_X/U0
244.                    +1.77245385*V0*G3*DERI_U0_R/U0**2
245.                      +2.*(DERI_V0_R/U0-DERI_U0_R*V0/U0**2))
246.                     *SPECI(2*I-1,J) + (-5.31736155/E_HAT*G3
247.                     *(DERI_V0_X-V0*DERI_LOGUC) -2.*DERI_U0_R/U0**2
248.                     -2./(U0*R) -15.9520846/E_HAT**2*V0*V0*G3*DERI_V0_X)
249.                      *SPECI(2*I,J) +2.*S(2*I-1,J)/U0
250.                     -5.317361553*G3*V0*S(2*I,J)/(E_HAT*U0);
251.              S(2*I,J)=(4.34160752/SQRTE*V0/U0*DERI_V0_X
```

```
252.                      -1.4472025*SQRTE*G3*DERI_U0_R/U0**2)*SPECI(2*I-1,J)
253.                      +(-4.34160752*G3/SQRTE*DERI_LOGUC
254.                     +13.024822/(SQRTE*E_HAT)*V0*G3*DERI_V0_X)*SPECI(2*I,J)

255.                       +4.34160752/SQRTE*G3*S(2*I,J)/U0;
256.              END L4;
257.           END L1;
258.           FREE SPECI;
259.        END SOURCE;
260.     ●
261.     ●
262.     ●
263.     ●  BOUNDRY:PROC(SPECIES);
264.        DCL( SPECIES(*,*), ETA, R, TERM, V0_OVER_U0 ,U0) FLOAT DEC(16);
265.        DCL(EXP1, EXP2) FLOAT DEC(16);
266.        DCL (I, J)  FIXED BIN(15);
267.        R=0.0;
268.        L1:DO I=2 TO MAXG;
269.           R=R+DR;
270.           ETA=SIGMA*R/(X+A2);
271.           TERM=1./(1.+0.25*ETA*ETA)**2;
272.           SPECIES(1,I)=SPECIES(1,MAXG)*(1.-TERM);
273.           SPECIES(3,I)=SPECIES(3,1)*TERM;
274.           EXP1=1.-EXP(-0.0005*R**6);
275.           EXP2=EXP(-1.5*ETA);
276.           IF EXP1<1.E-12 THEN EXP1=0.0;
277.           IF EXP2<1.E-12 THEN EXP2=0.0;
278.           IF ETA<13. THEN SPECIES(1,I)=SPECIES(1,I)*EXP1;
279.           IF ETA>7.5 THEN SPECIES(3,I)=SPECIES(3,I)*EXP2;
280.           SPECIES(5,I)=(SPECIES(5,1)-SPECIES(5,MAXG))*TERM
281.                                      +SPECIES(5,MAXG);
282.           SPECIES(7,I)=(SPECIES(7,1)-SPECIES(7,MAXG))*TERM
283.                                     +SPECIES(7,MAXG);
284.           END L1;
285.        F(4,1)=1.4472025*SQRTE*SPECIES(3,1)/2.;
286.        F(6,1)=1.4472025*SQRTE*SPECIES(5,1)/2.;
```

```
287.          F(8,1)=1.4472025*SQRTE*SPECIES(7,1)/2.;
288.          END BOUNDRY;
289.    ●
290.    ●
291.    ●
292.    ●
293.    ●     ERRFCTN:PROC(YY,ERF);
294.          DCL(YY, Y, ERF, P, T, EXPY2 ) FLOAT DEC(16);
295.          DCL  A(5) FLOAT DEC(16) INIT(0.254829592, -0.284496736,
296.                                       1.421413741, -1.453152027,
297.                                       1.061405429 ) ;
298.          DCL I FIXED BIN(15);
299.          Y=ABS(YY);
300.          IF Y<0.01 THEN
301.              DO;
302.              ERF=0.0;
303.              RETURN;
304.              END;
305.          IF Y>4.0 THEN DO;
306.                        ERF=1.0;
307.                        GO TO RTN;
308.                        END;
309.          P=0.32759;
310.          T=1./(1.+P*Y);
311.          ERF=0.0;
312.             DO I=1 TO 5;
313.             ERF=ERF+A(I)*T**I;
314.             END;
315.          EXPY2=EXP(-Y*Y);
316.          IF EXPY2<1.0E-08 THEN EXPY2=0.0;
317.          ERF=1.-ERF*EXPY2;
318.          RTN:IF YY<0.0 THEN ERF=-ERF;
319.          END ERRFCTN;
320.    ●
321.    ●
```

```
322.      0
323.      0    REACTION_RATE:PROC(WP);
324.           DCL(UC,WP,RESULT,ETA,R,F5,FCTN(*) CTL) FLOAT DEC(16);
325.           DCL J FIXED BIN(15);
326.           ALLOCATE FCTN(MAXR);
327.              R=0.0;
328.              FCTN(1)=0.0;
329.           L1:DO J=2 TO MAXR-1;
330.              R=R+DR;
331.              UC=A1/(A2+5.8) - E*(A1/(A2+5.8) - A1/(A2+X) );
332.              FCTN(J)=UC*CHEM_REACTION(J)*R;
333.              END L1;
334.           CALL TRAPEZO(FCTN,DR,MAXR,RESULT);
335.           WP=RESULT;
336.           FREE FCTN;
337.           END REACTION_RATE;
338.      0
339.      0
340.      0    TRAPEZO:PROC(FCTN,DR,MAXR,RESULT);
341.           DCL(FCTN(*),DR,RESULT) FLOAT DEC(16);
342.           DCL(I,MAXR) FIXED BIN(15);
343.           RESULT=0.0;
344.           LL:DO I=1 TO MAXR-2;
345.              RESULT=RESULT+(FCTN(I)+FCTN(I+1))*DR;
346.              END LL;
347.           END TRAPEZO;
348.      0
349.      0
350.      0
351.      0    INPUTS:PROC;
352.           DCL AAAA CHAR(1), BBBB CHAR(1);
353.           E=0.80;
354.           ETAMAX=8.0;
355.           XSTART=5.8;
356.           XSTOP=100.;
```

```
357.          DR=0.20;
358.          D=0.333333333;
359.          E_HAT=0.10;
360.          MB_OVER_MA=2./32.;
361.          MD_OVER_MA=18./32.;
362.          A1=6.4;
363.          A2=0.6;
364.          A3=0.03295;
365.          A4=0.10;
366.          SIGMA=16.;
367.          GET DATA(
368.                    E
369.                   ,ETAMAX
370.                   ,XSTART
371.                   ,XSTOP
372.                   ,DR
373.                   ,XOUT
374.                   ,E_HAT
375.                   ,MB_OVER_MA
376.                   ,MD_OVER_MA
377.                   ,A4
378.                        ) FILE(INPUT1) COPY(SYSPRINT);
379.          MAXG=FIXED(ETAMAX*(XSTOP+A2)/(SIGMA*DR));
380.          ALLOCATE SPECIES(8,MAXG),
381.                   SPT(8,MAXG),
382.                   F(8,MAXG),
383.                   CHEM_REACTION(MAXG),
384.                   S(8,MAXG);
385.          SPECIES, SPT, F, S=0.0; CHEM_REACTION =0.0;
386.          GET LIST(AAAA,  BBBB
387.                   ,SPECIES(1,1), SPECIES(1,MAXG)
388.                   ,SPECIES(3,1), SPECIES(3,MAXG)
389.                   ,SPECIES(5,1), SPECIES(5,MAXG)
390.                   ,SPECIES(7,1), SPECIES(7,MAXG)
391.                                  ) FILE(INPUT1) COPY(SYSPRINT);
```

```
392.          END INPUTS;
393.     0
394.     0
395.     0
396.     0    OUT1:PROC;
397.          DCL ( R,  WP, WPR, UC, CD, ETA, F5, V0, G2) FLOAT DEC(16);
398.          DCL SPECI(*,*) CTL FLOAT DEC(16);
399.          DCL (J,I) FIXED BIN(15);
400.          ALLOCATE SPECI(8,MAXR);
401.          PUT PAGE FILE(SYSPRINT) EDIT('X=',X) (COL(3),A,COL(6),F(9,5));
402.          CALL REACTION_RATE(WP);
403.          PUT SKIP FILE(SYSPRINT) EDIT('<WP>=',WP)(COL(3),A,E(10,3));
404.          PUT FILE(SYSPRINT) EDIT('R','CA0','<V*CA>','CB0','<V*CB>',
405.               'CD0','<V*CD>','  H0','<V*H>','CE0','WP(R)','ETA')
406.               (COL(3),A, COL(9),A, COL(19),A, COL(29),A, COL(39),A,
407.                COL(49),A, COL(59),A, COL(69),A, COL(79),A,COL(91),A,
408.                COL(102),A,COL(113),A);
409.          R=0.0;
410.          DO I=1 TO MAXR BY INCREMENT;
411.             ETA=SIGMA*R/(X+A2);
412.             F5=1./(1.+0.25*ETA*ETA);
413.             V0=E*A3*(ETA-0.25*ETA**3)*F5**2;
414.             G2=EXP(-1.5*V0**2/E_HAT);
415.           LL3:DO J=1 TO 4;
416.                SPECI(2*J-1,I)=0.5*(SPECIES(2*J-1,I)
417.                                    +1.2247448/SQRTE*V0*SPECIES(2*J,I));
418.                SPECI(2*J,I)=0.2303294*SQRTE*G2*SPECIES(2*J,I);
419.                END LL3;
420.          CD=MAX(0.0,1.-SPECI(1,I)-SPECI(3,I)-SPECI(5,I));
421.          UC=A1/(A2+5.8) - E*(A1/(A2+5.8) - A1/(A2+X) );
422.          WPR=UC*CHEM_REACTION(I);
423.          PUT FILE(SYSPRINT) EDIT(R, SPECI(1,I), SPECI(2,I),
424.          SPECI(3,I), SPECI(4,I), SPECI(5,I), SPECI(6,I),
425.          SPECI(7,I), SPECI(8,I),CD,WPR,ETA )
426.          (COL(1),F(5,2), COL(7),E(9,2), COL(17),E(9,2), COL(27),E(9,2),
```

```
427.            COL(37),E(9,2), COL(47),E(9,2), COL(57),E(9,2), COL(67),E(9,2),
428.            COL(77),E(9,2),COL(88),E(9,2),COL(99),E(9,2),COL(110),F(7,3));
429.          R=R+INCREMENT*DR;
430.          END;
431.          FREE SPECI;
432.          END OUT1;
433.     0
434.     0
435.     0    FINISH:CALL OUT1;
436.          END FLAME;
```

```
//GO.INPUT1 DD *
     E=0.80
     ETAMAX=8.0
     XSTOP=60.
     DR=0.20
     XOUT=10.
     A4=0.26
     E_HAT=0.10;
    'CENTER'  'INFINITY'
     0.00      0.44
     1.80      0.00
     0.005     0.00
     0.40      0.20
```

REFERENCES

1. Chung, Paul M.: Diffusion Flame in Homologous Turbulent Shear Flows. Physics of Fluids, vol. 15, 1972, pp. 1735-1746.

2. Chung, Paul M.: Chemical Reaction in a Turbulent Flow Field with Uniform Velocity Gradient. Physics of Fluids, vol. 13, 1970, pp. 1153-1165.

3. Chung, Paul M., and Shu, Ho T.: HF Chemical Laser Amplification Properties of a Uniform Turbulent Mixing Layer. Acta Astronautica, vol. 1, 1974, pp. 835-862.

4. Hong, Z.C.: Turbulent Chemically Reacting Flow According to a Kinetic Theory. Ph.D. Thesis, Department of Energy Engineering, University of Illinois at Chicago Circle, 1975.

5. Chung, Paul M.: A Kinetic-Theory Approach to Turbulent Chemically Reacting Flows. Combustion Science and Technology, vol. 13, 1976, pp. 123-153.

6. Hayday, A.A., and Chung, P.M.: Turbulent Flow and Pumping in the Cavity of a Chemical Laser. Gas Flow and Chemical Lasers, J.F. Wendt, ed., Hemisphere Publ. Corp., 1979, pp. 171-179.

7. Bywater, Ronald J.: The Calculation of a Turbulent Diffusion Flame in a Free Shear Flow with a Statistical Turbulence Model. AIAA preprint No. 80-0139.

8. MacCormick, R.W., and Paullay, A.J.: Computational Efficiency Achieved by Time Splitting of Finite Difference Operations. AIAA paper No. 72-154, AIAA 10th Aerospace Science Meeting, 1972.

9. Schlichting, H.: Boundary Layer Theory. Chapter XXIII, McGraw-Hill Co., Inc., 1955.

10. Hinze, J.O.: Turbulence. Chapter 6, McGraw-Hill Co., Inc., 1959.

11. Courant, R., and Friedrichs, K.O.: Supersonic Flow and Shock Waves. Chapter III, Interscience Publishers, Inc., 1948.

12. Libby, P.A.: Theoretical Analysis of Turbulent Mixing of Reactive Gases with Application to Supersonic Combustion of Hydrogen. Journal of American Rocket Soc., vol. 32, 1962, pp. 388-395.

13. Guenther, R., and Simon, H.: Turbulence Intensity, Spectral Density Functions, and Eulerian Scales of Emission in Turbulent Diffusion Flames. 12th International Symposium on Combustion, 1969, pp. 1069-1079.

14. Kent, J.H.: Turbulent Jet Diffusion Flames. Ph.D. Thesis, Department of Mechanical Engineering, University of Sydney, Sydney, Australia, 1972.

15. Hawthorne, W.R., Weddell, D.S., and Hottel, H.C.: Mixing and Combustion in Turbulent Gas Jets. Third Symposium on Combustion, Flame, and Explosion Phenomena, 1949, pp. 266-288.

16. Cohen, L.S., and Guile, R.N.: Investigation of the Mixing and Combustion of Turbulent Compressible Free Jets. NASA CR-1473, 1969.

17. Beach, H.L., Jr.: A Study of Reacting Free and Ducted Hydrogen/Air Jets. NASA TM X-72678.

18. Richtmyer, R.D., and Morton, K.W.: Difference Methods for Initial Value Problems. Interscience Publishers, Inc., 1967.

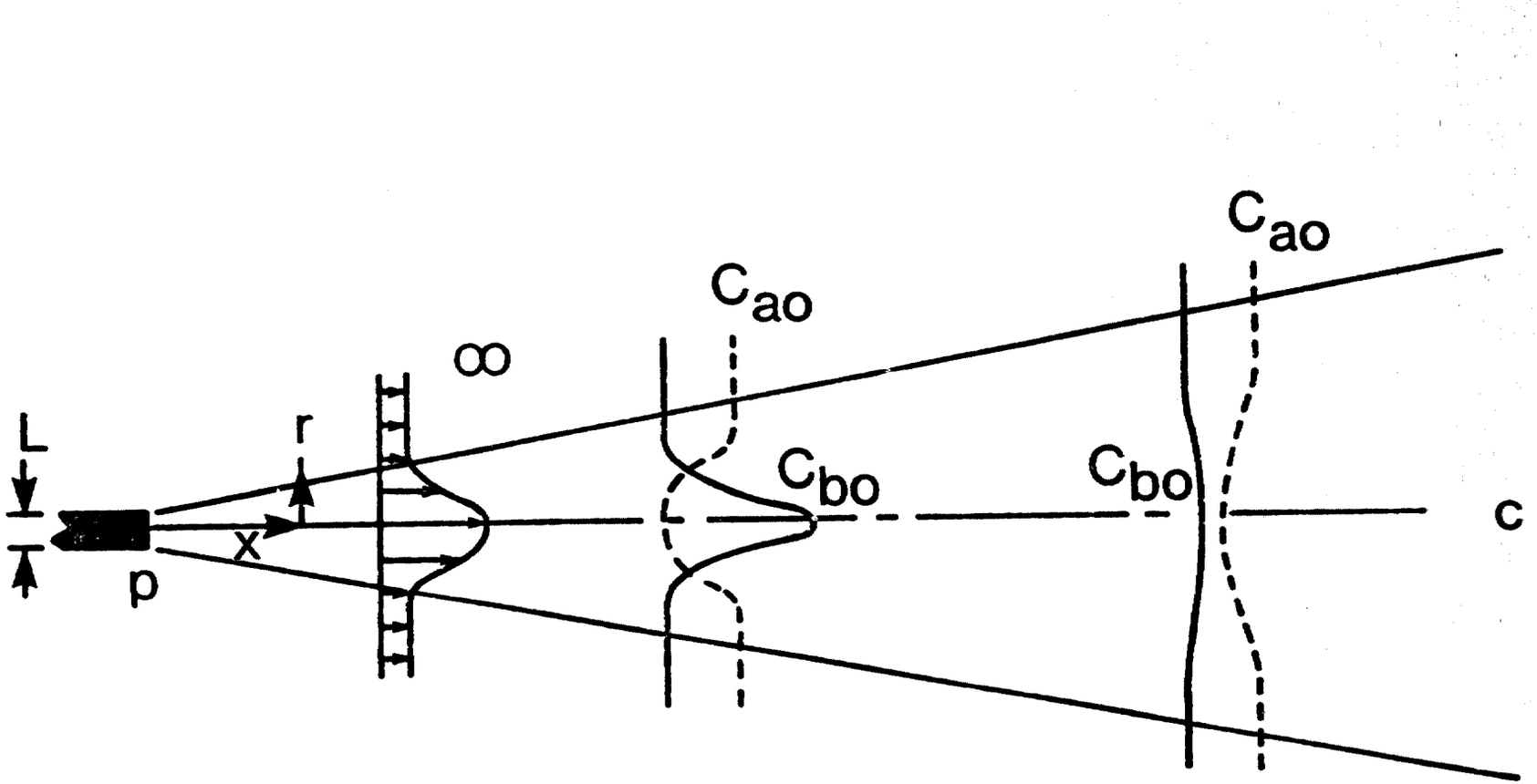

Figure 1.- Axisymmetric turbulent jet.

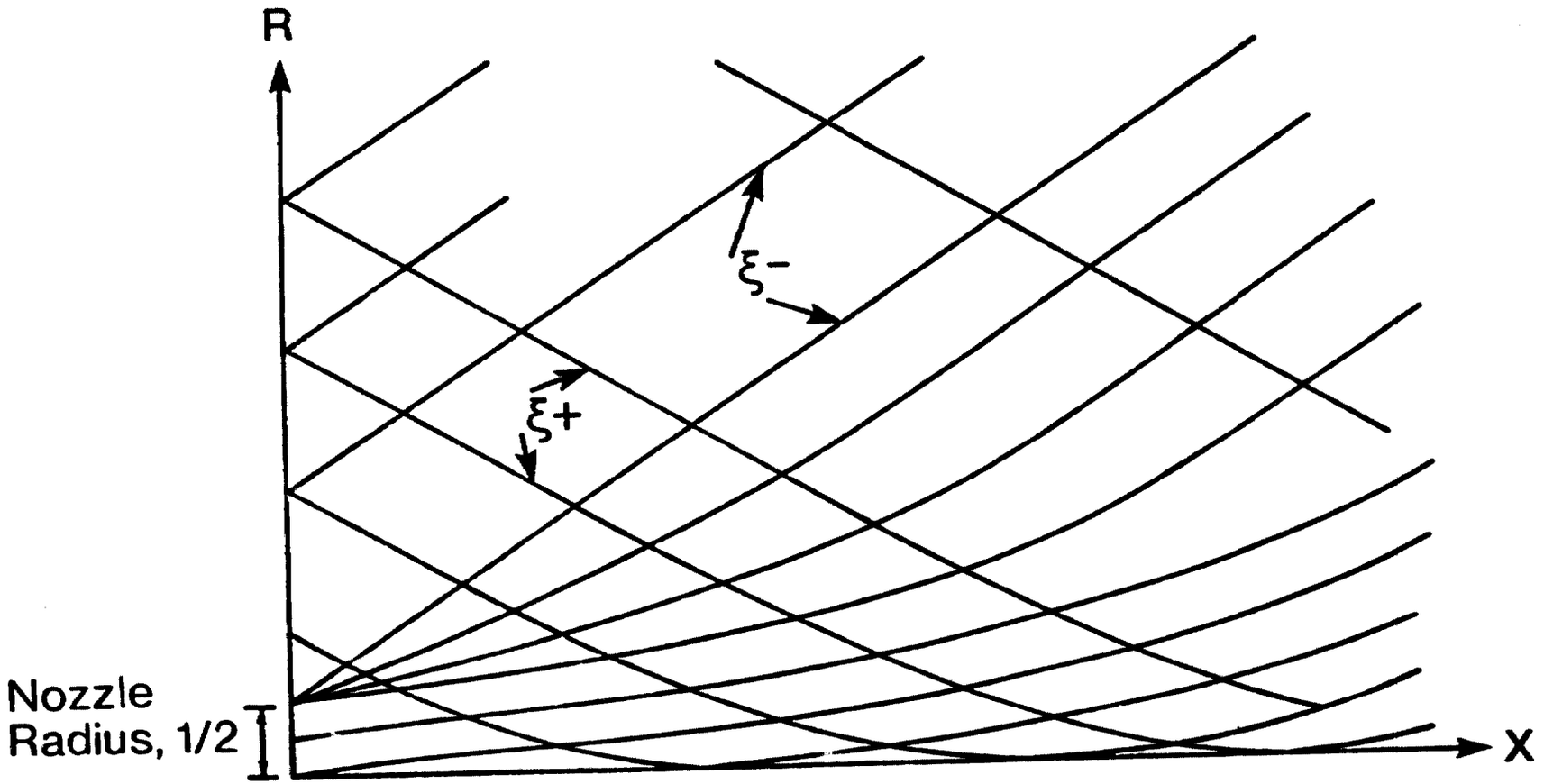

Figure 2.- Sketch of characteristics.

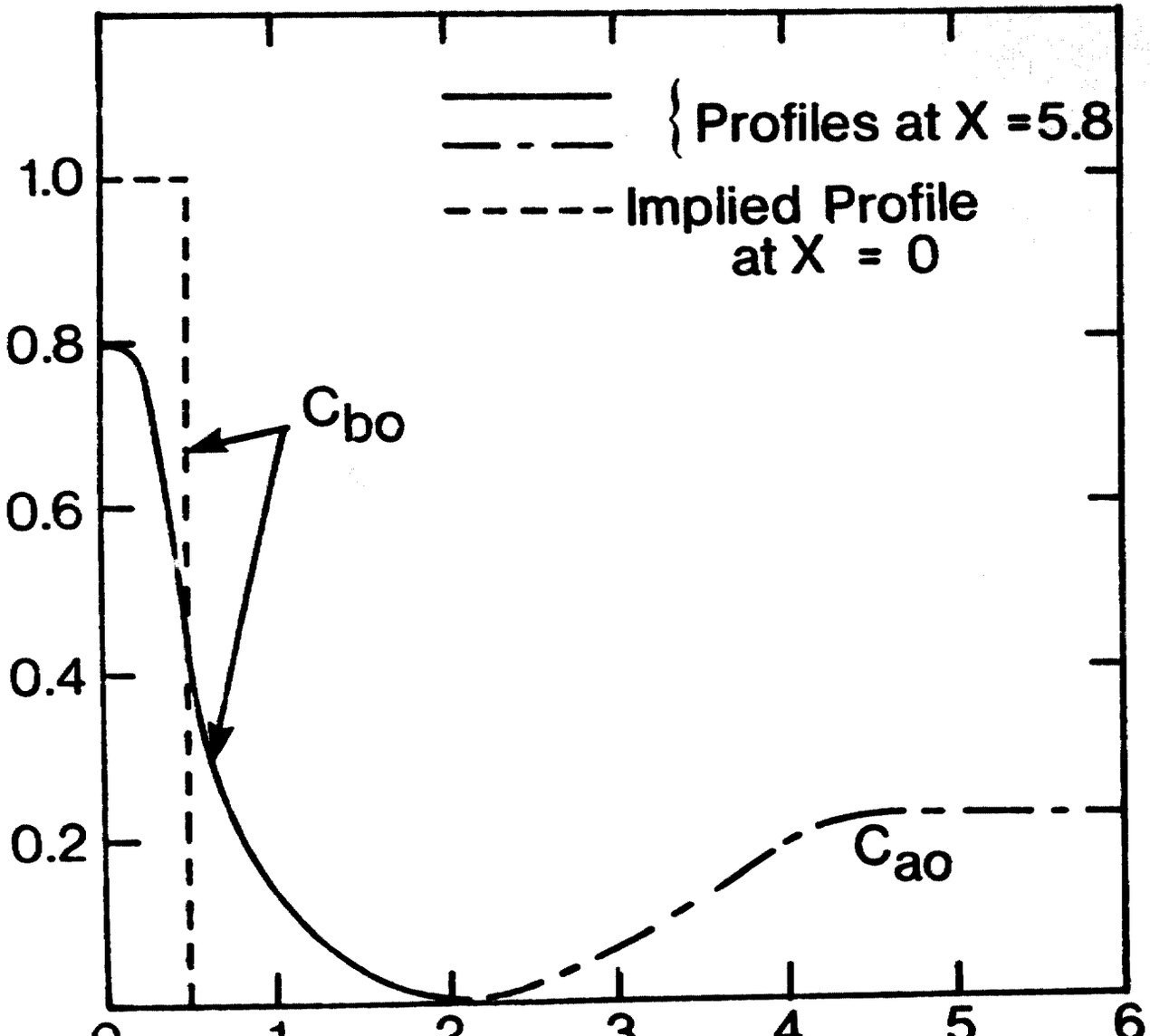

Figure 3.- Initial profiles specified.

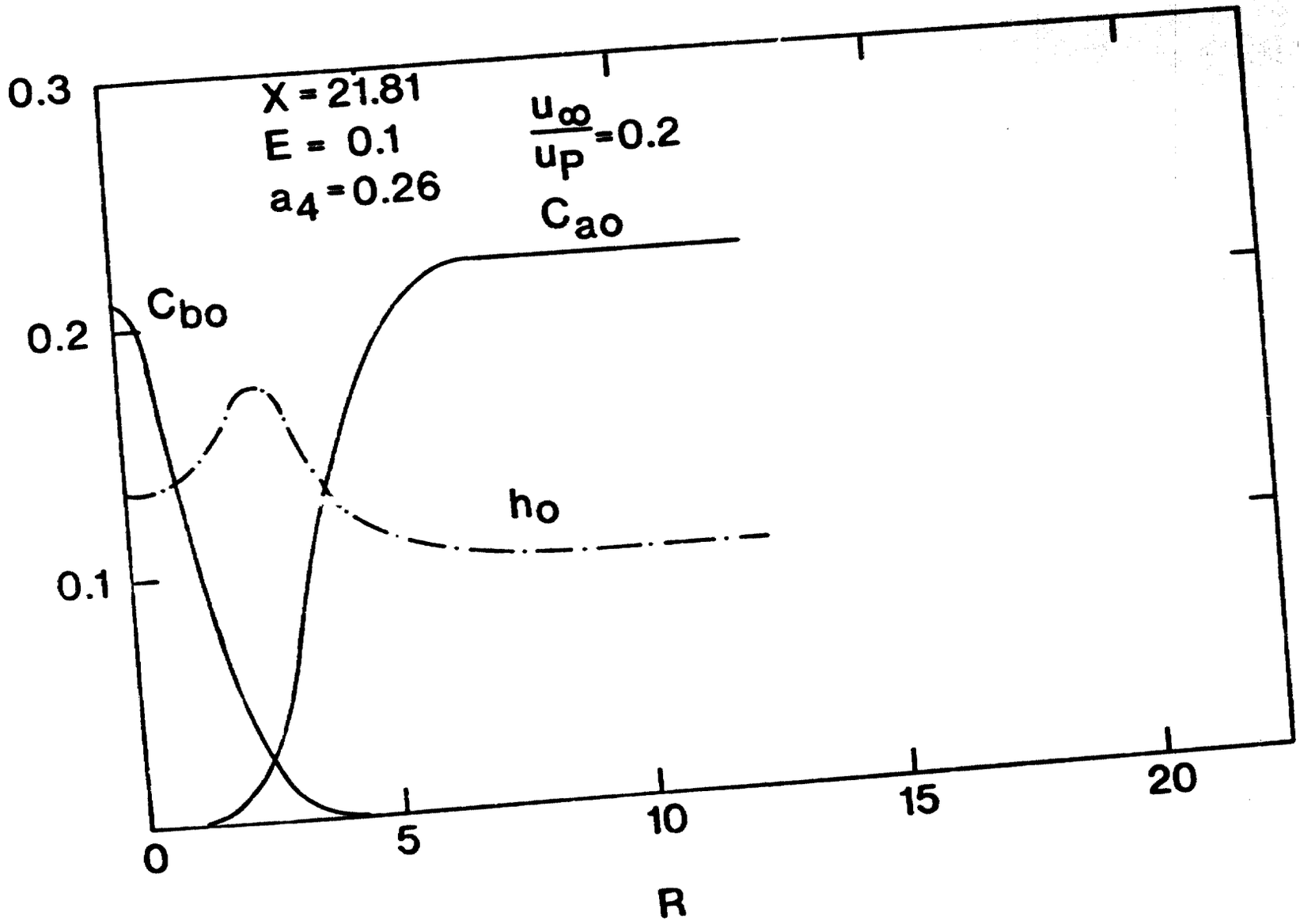

Figure 4.- Mean mass fraction and temperature profiles.

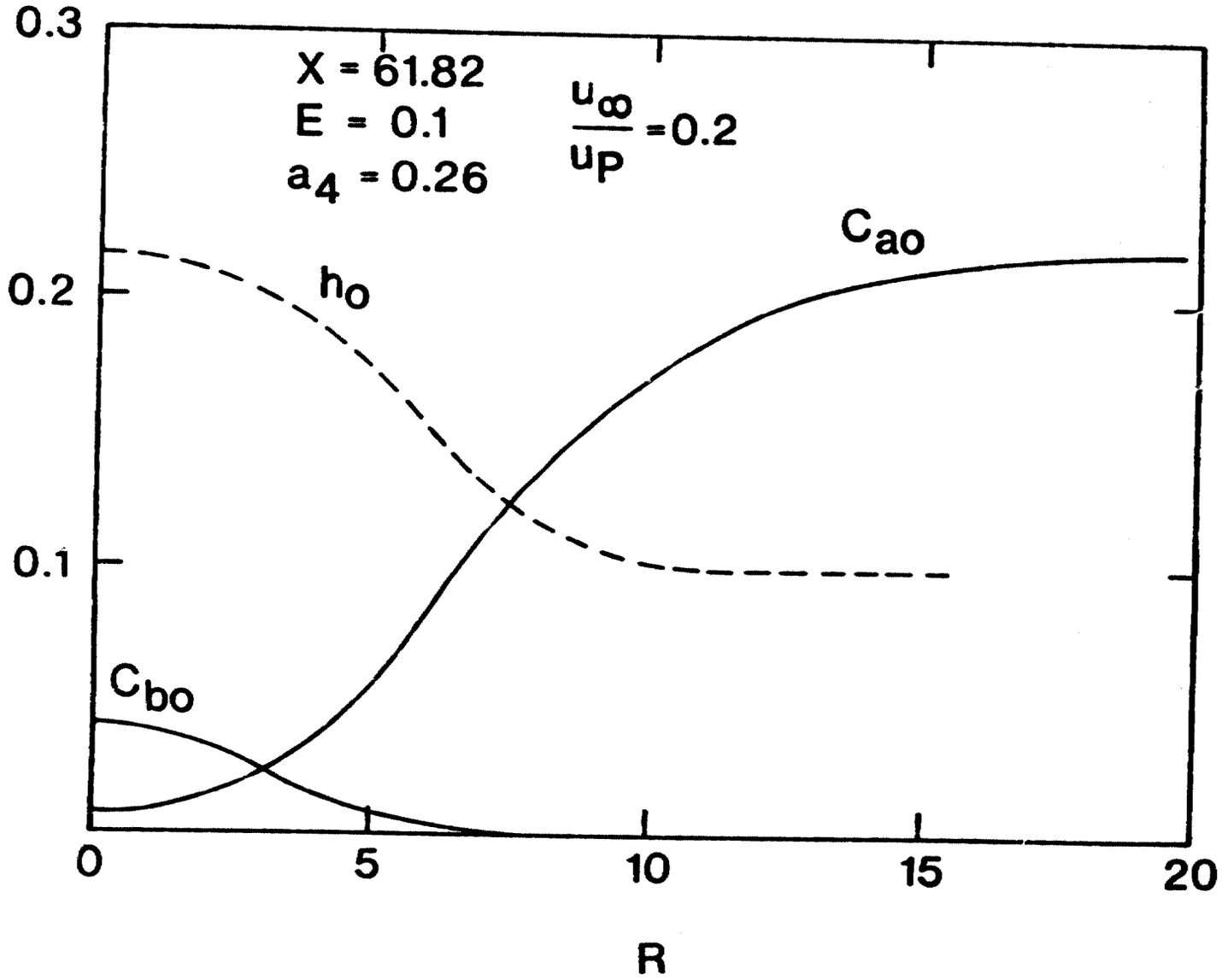

Figure 5.- Mean mass fraction and temperature profiles.

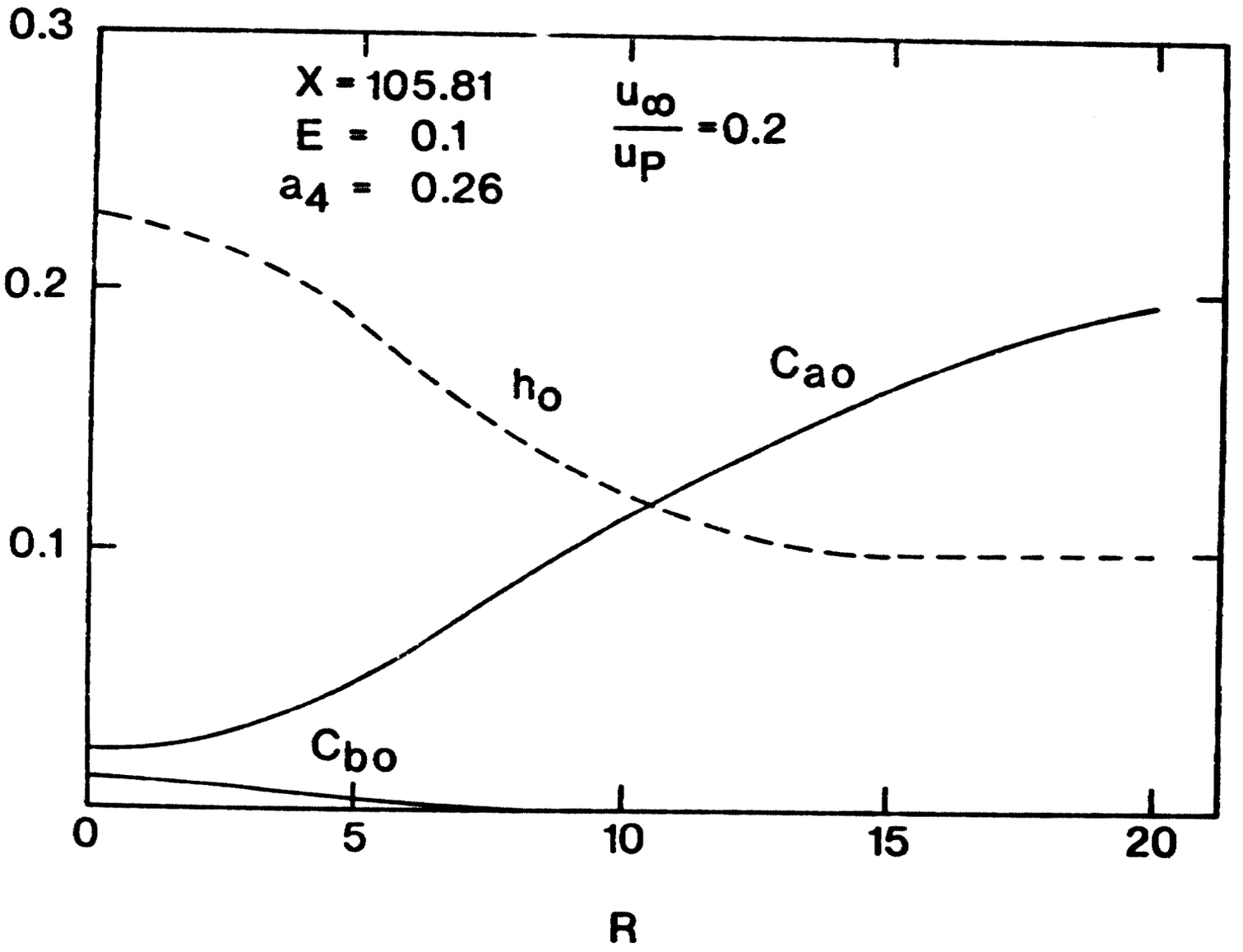

Figure 6.- Mean mass fraction and temperature profiles.

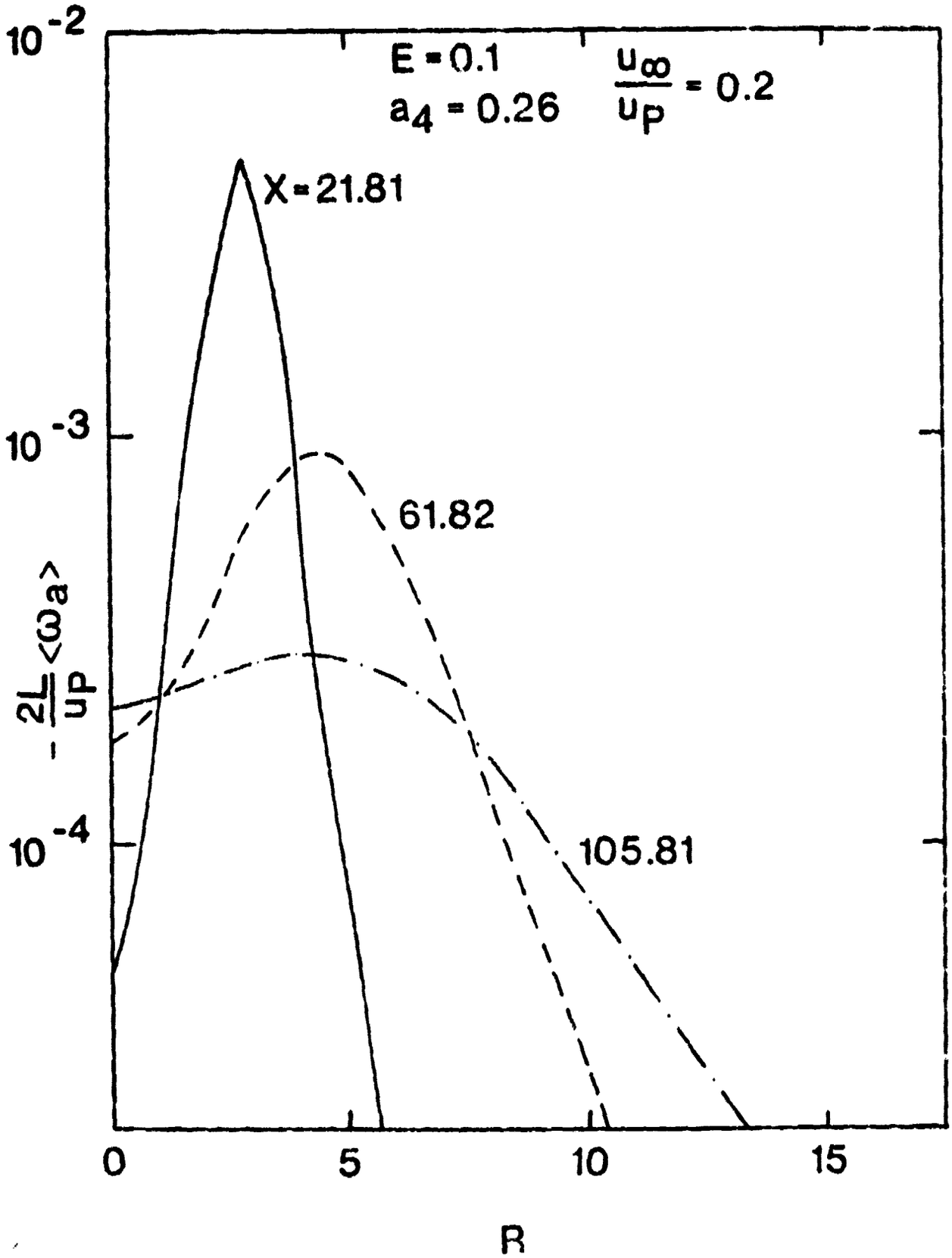

Figure 7.- Distribution of combustion rate across the jet.

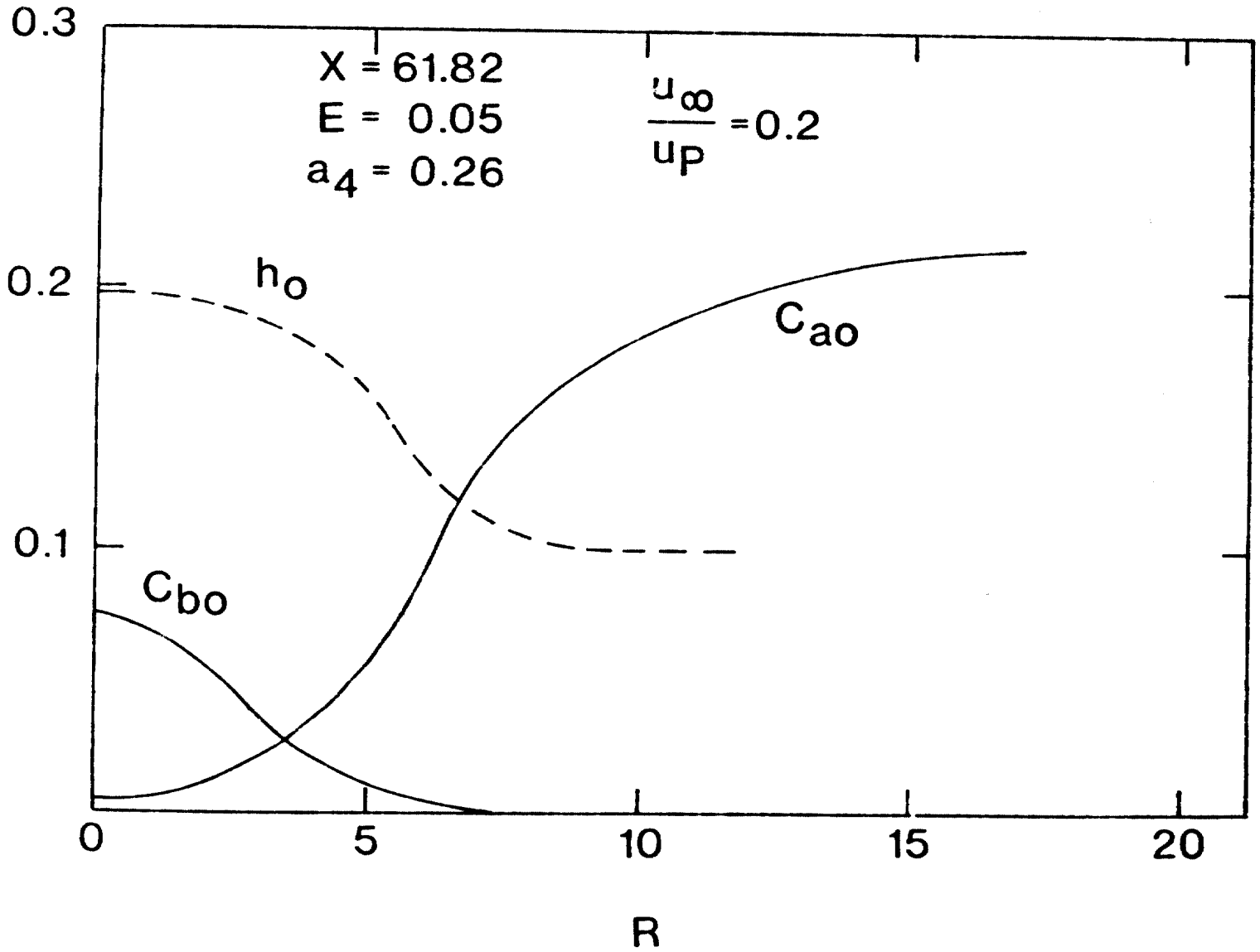

Figure 8.- Mean mass fraction and temperature profiles.

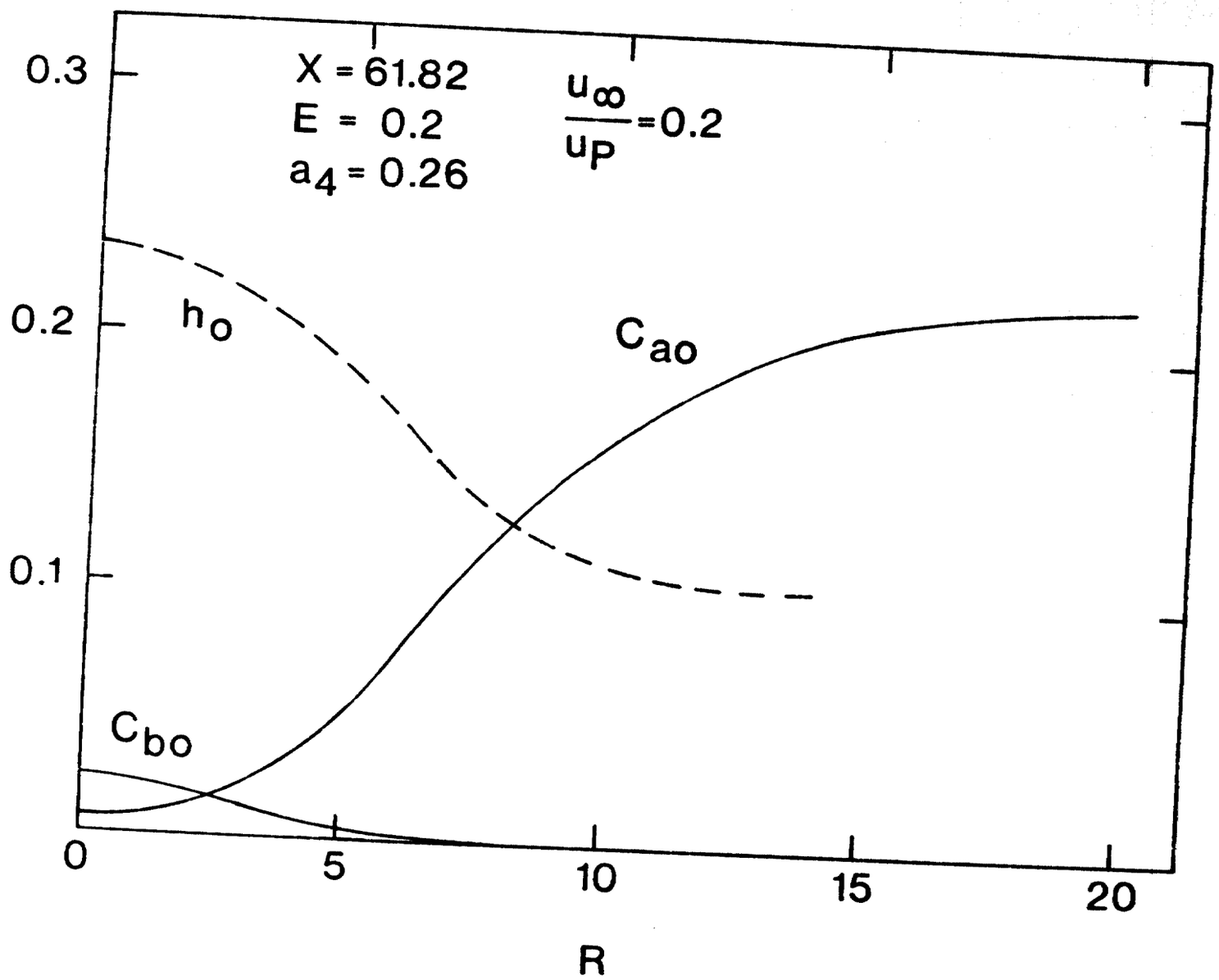

Figure 9.- Mean mass fraction and temperature profiles.

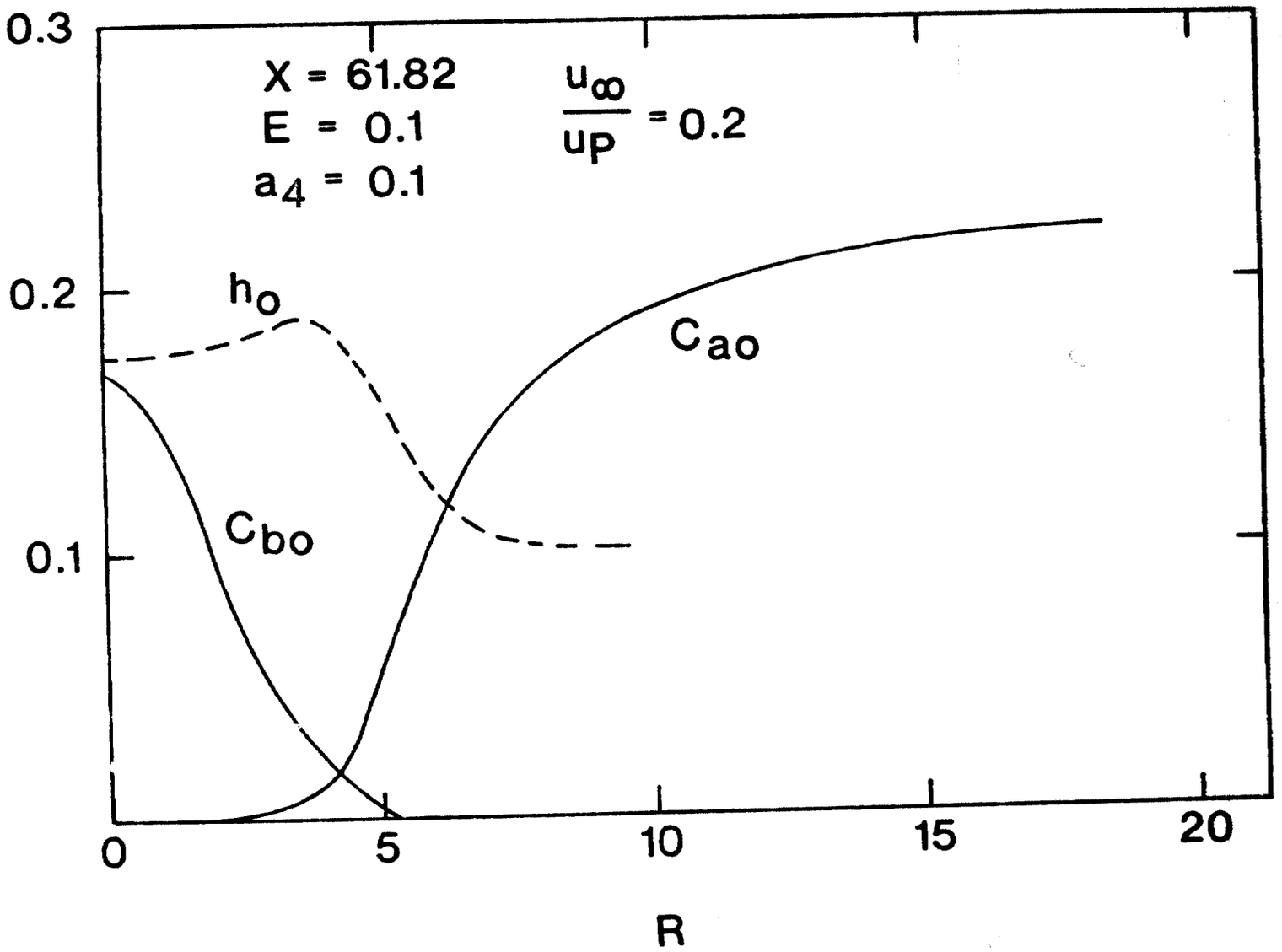

Figure 10.- Mean mass fraction and temperature profiles.

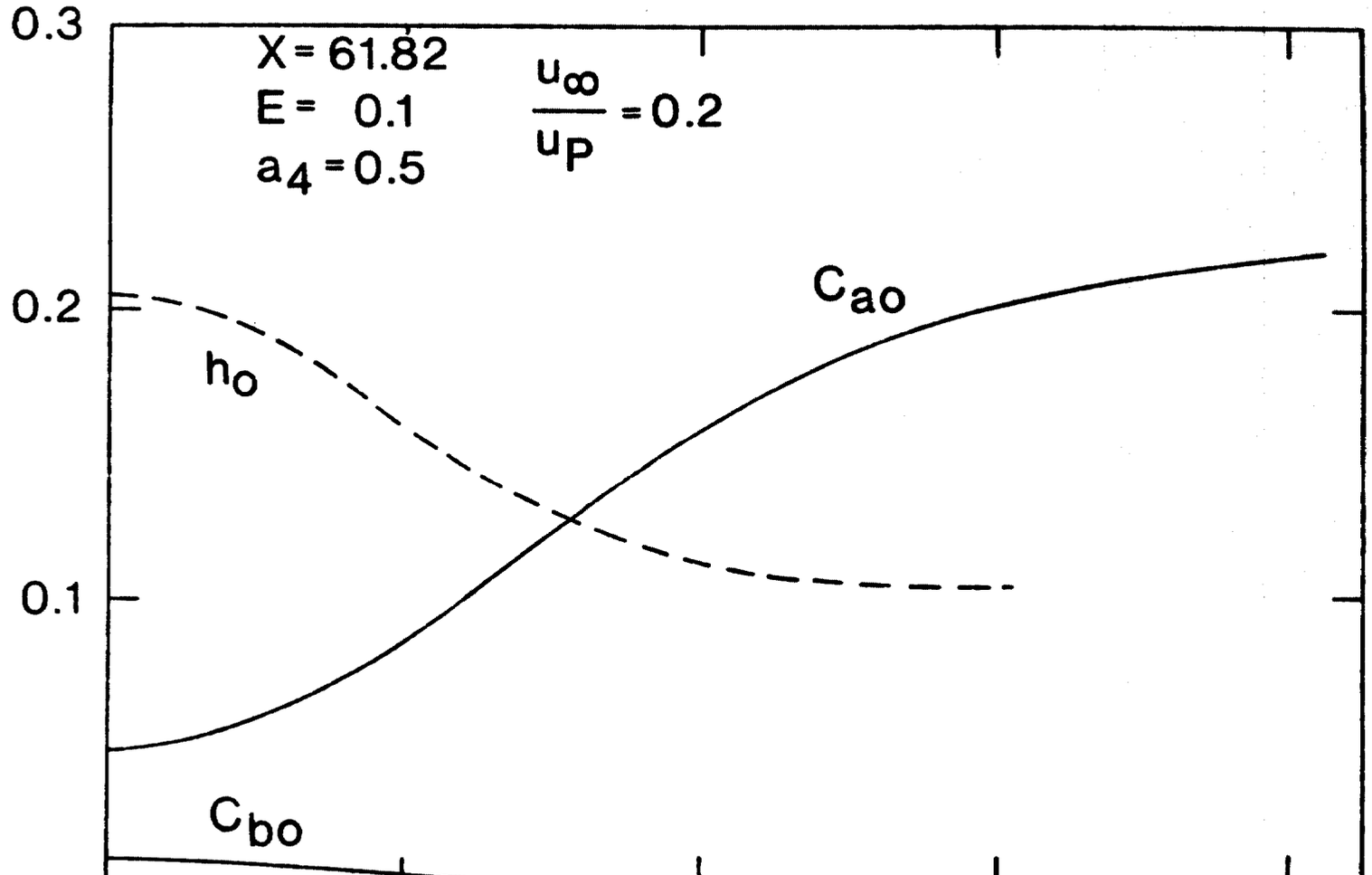

Figure 11.- Mean mass fraction and temperature profiles.

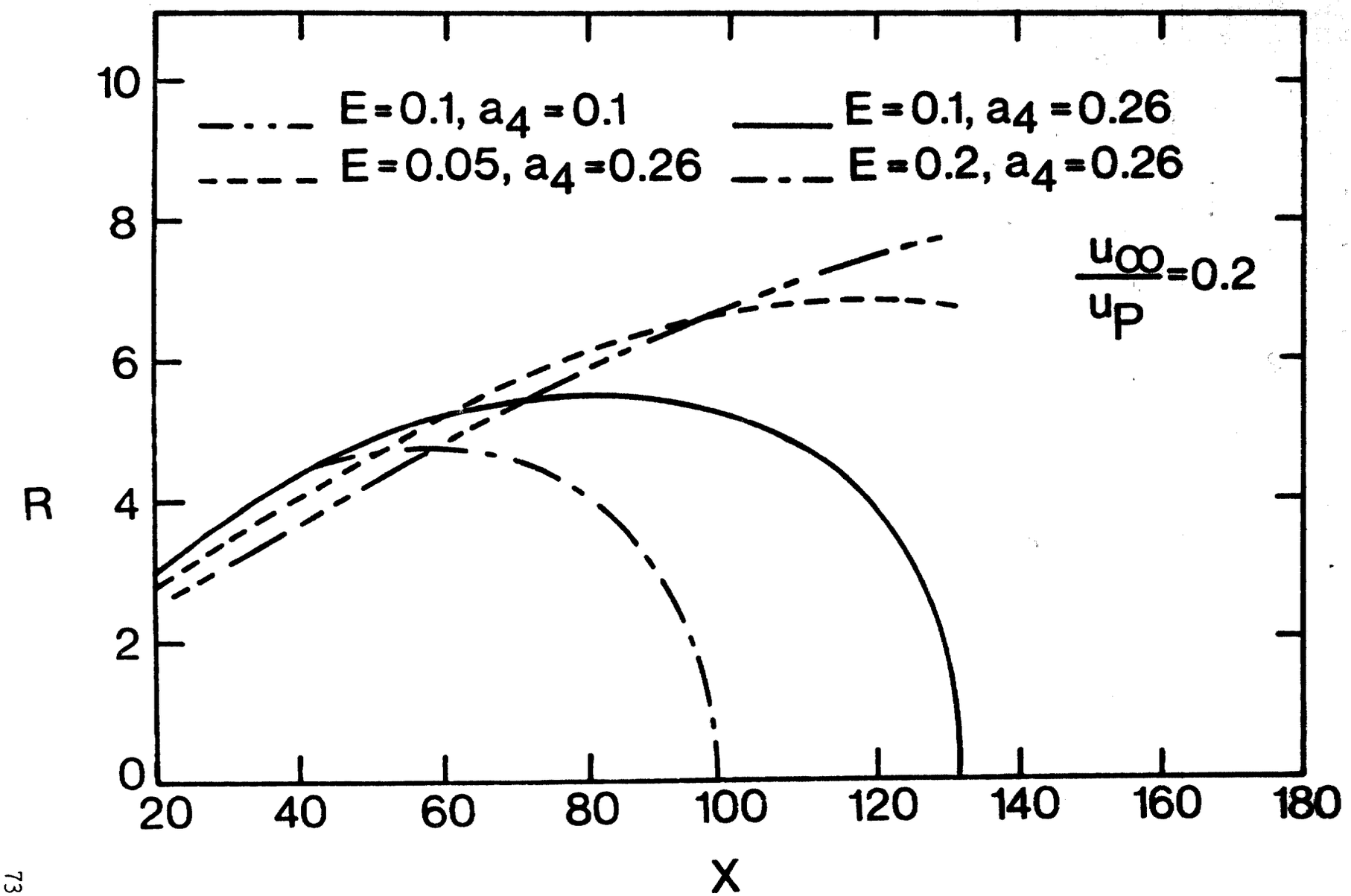

Figure 12.- Loci of flame stoichiometry.

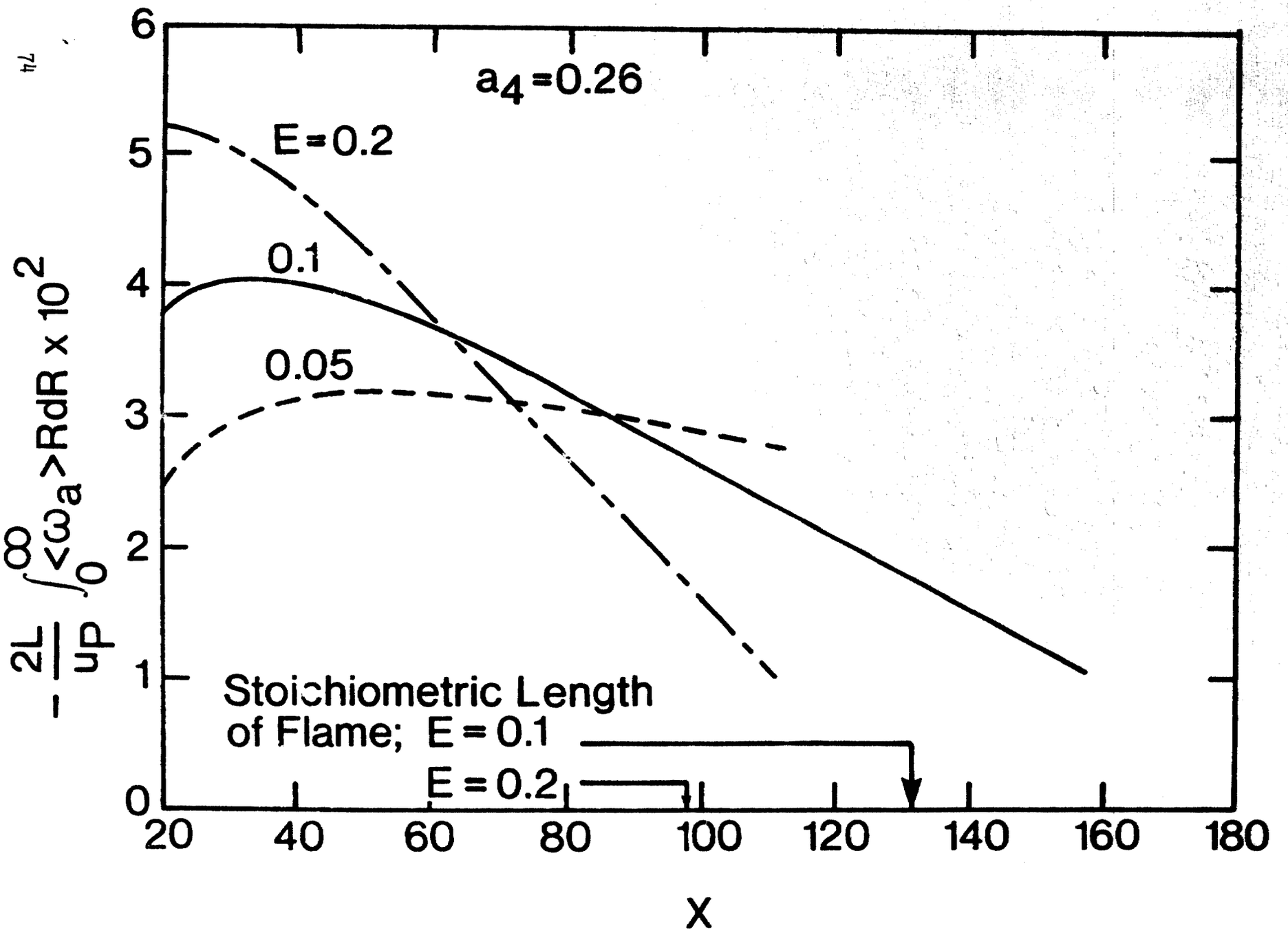

Figure 13. Axial variations of combustion rate.

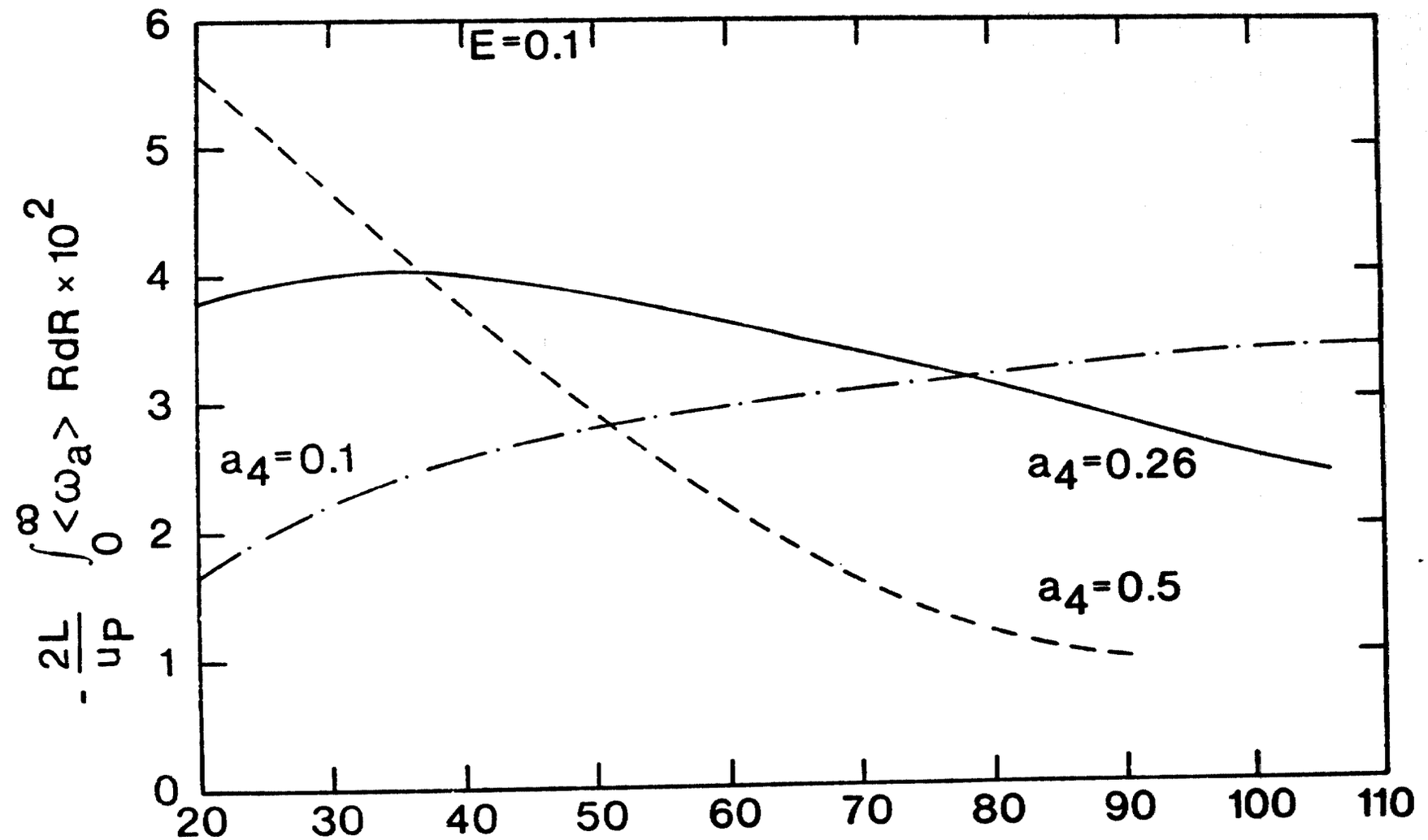

Figure 14.- Axial variations of combustion rate.

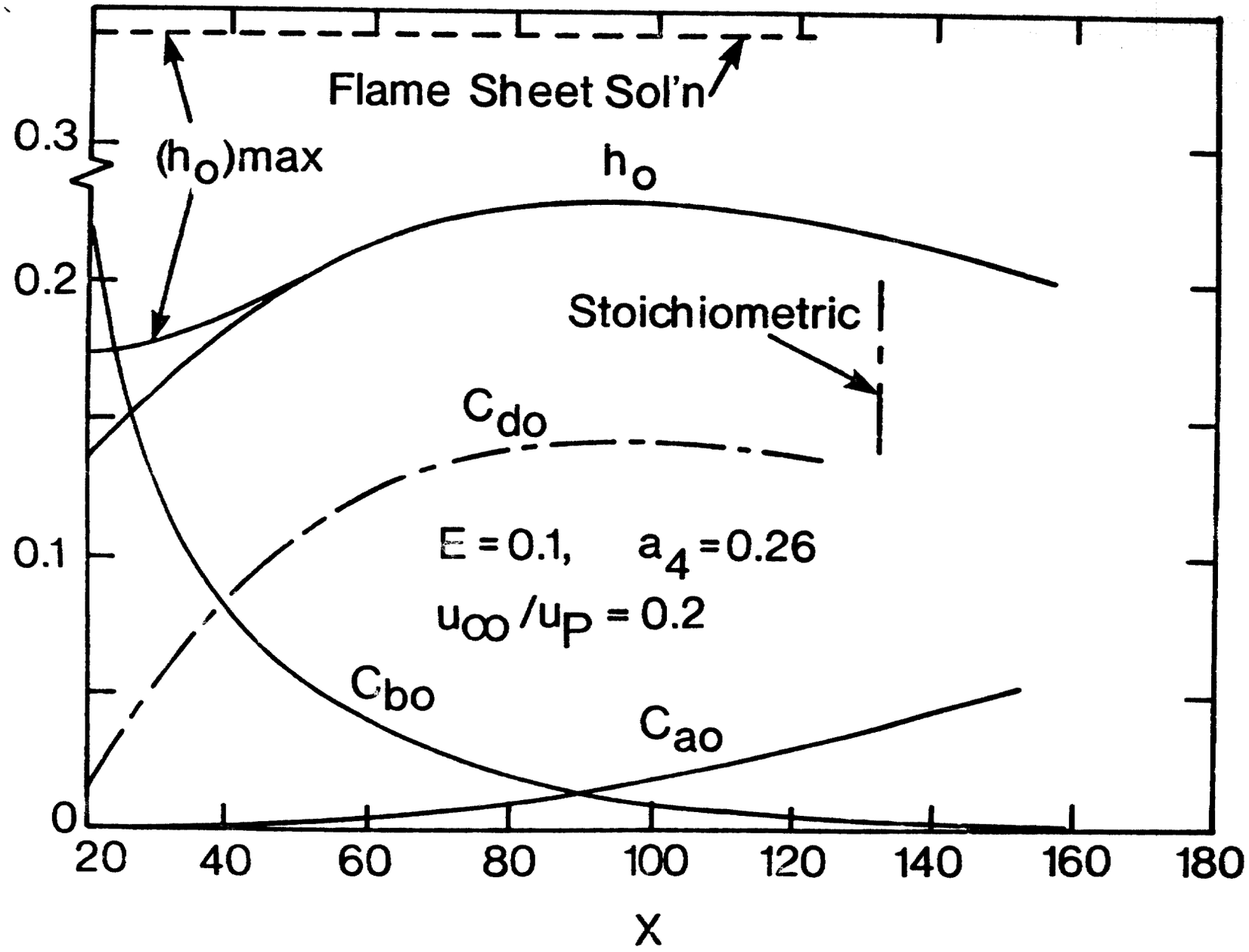

Figure 15.- Center line variations of mean mass fractions and temperature.

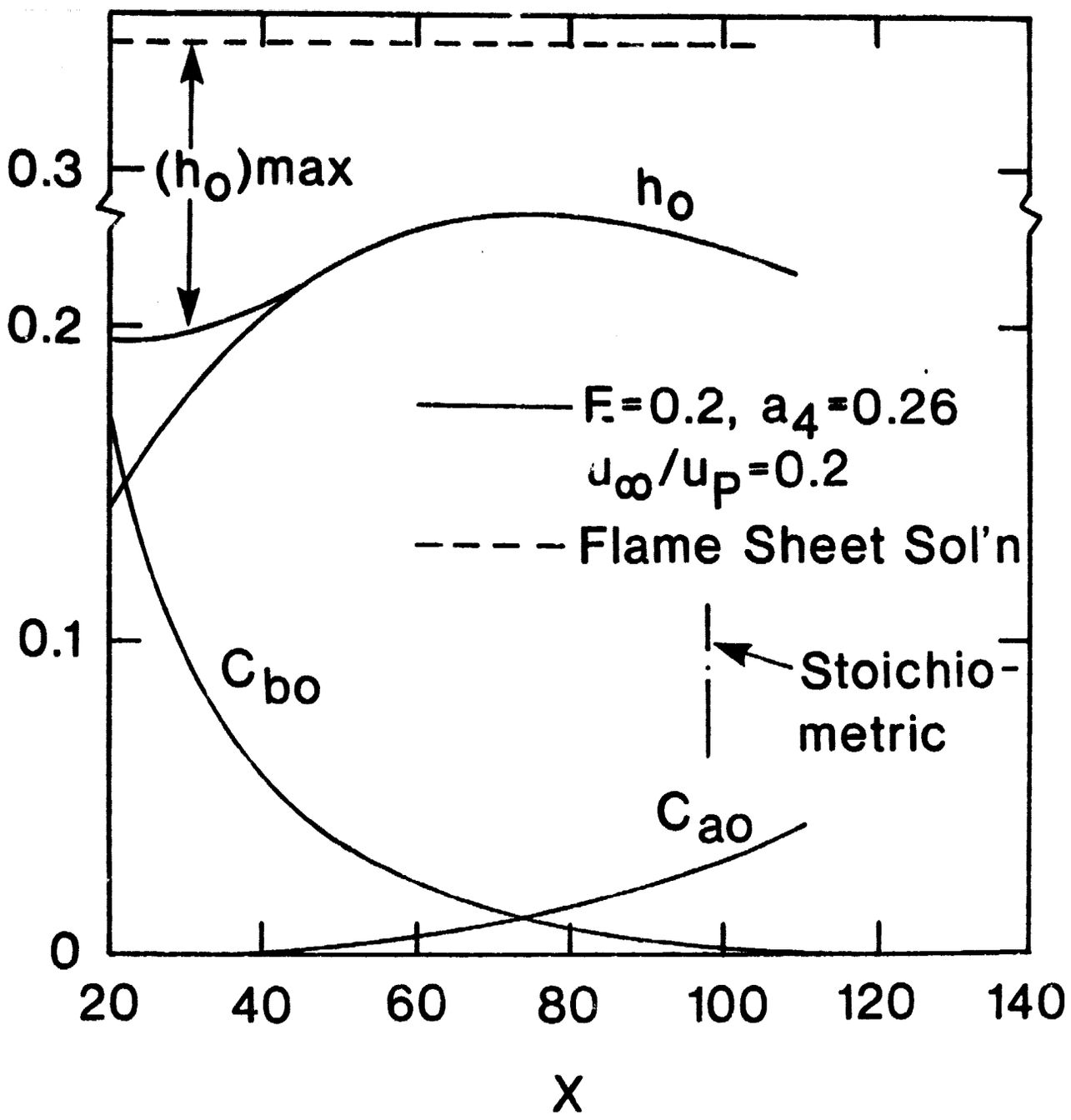

Figure 16.- Center line variations of mean mass fractions and temperature.

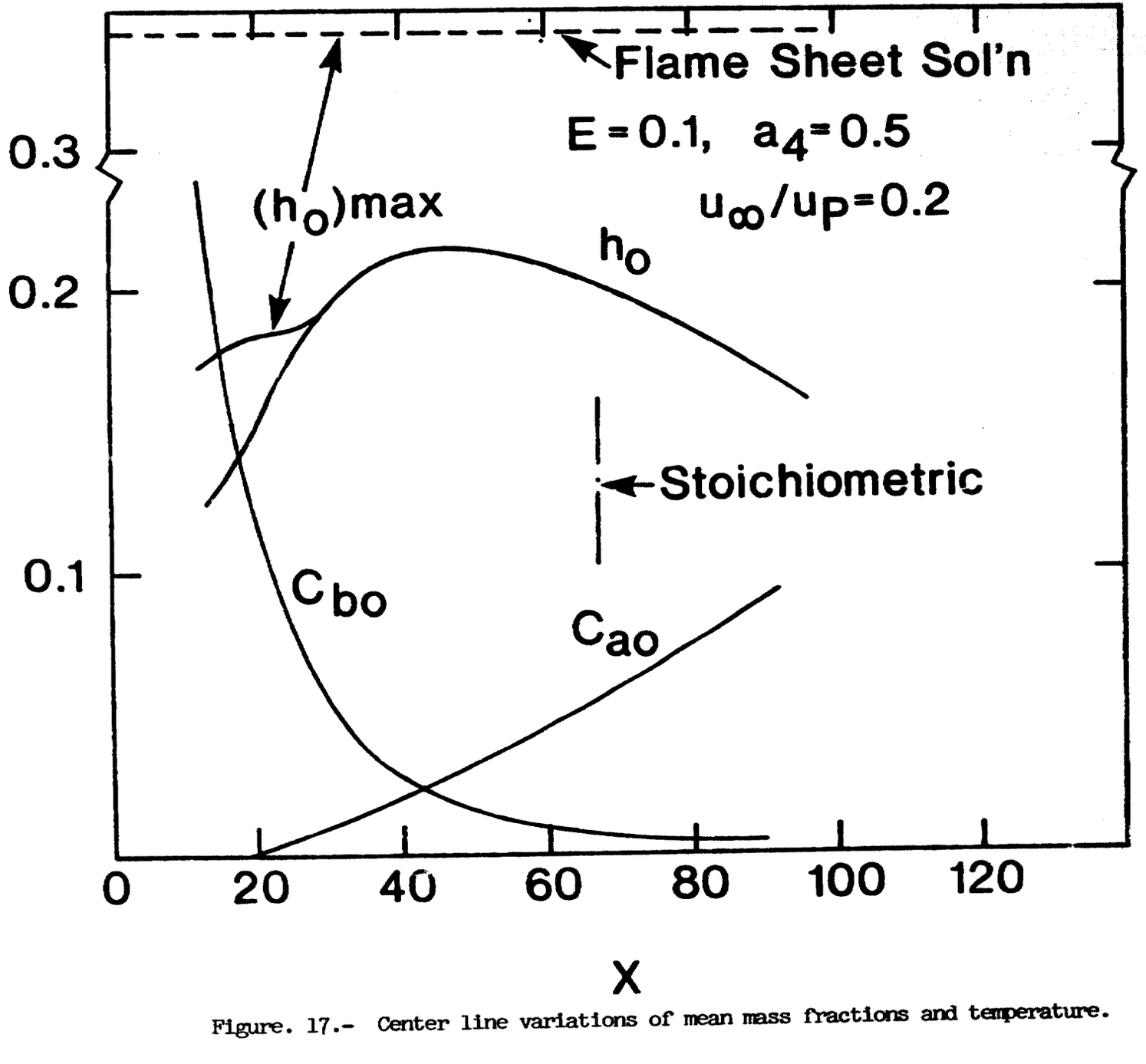

Figure. 17.- Center line variations of mean mass fractions and temperature.

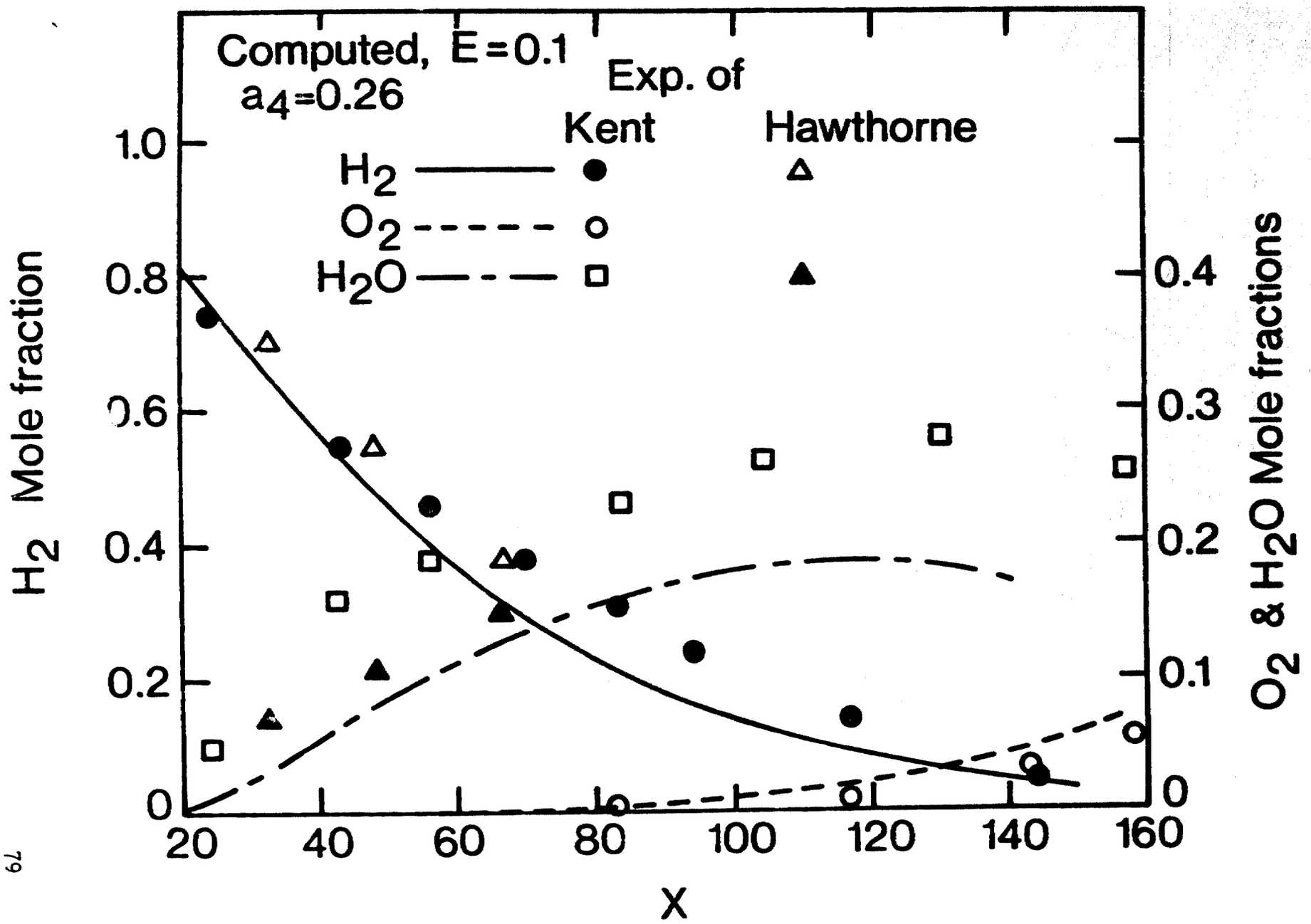

Figure 18.- Comparison of the computed values with the experimental results for the center line concentrations of chemical species.

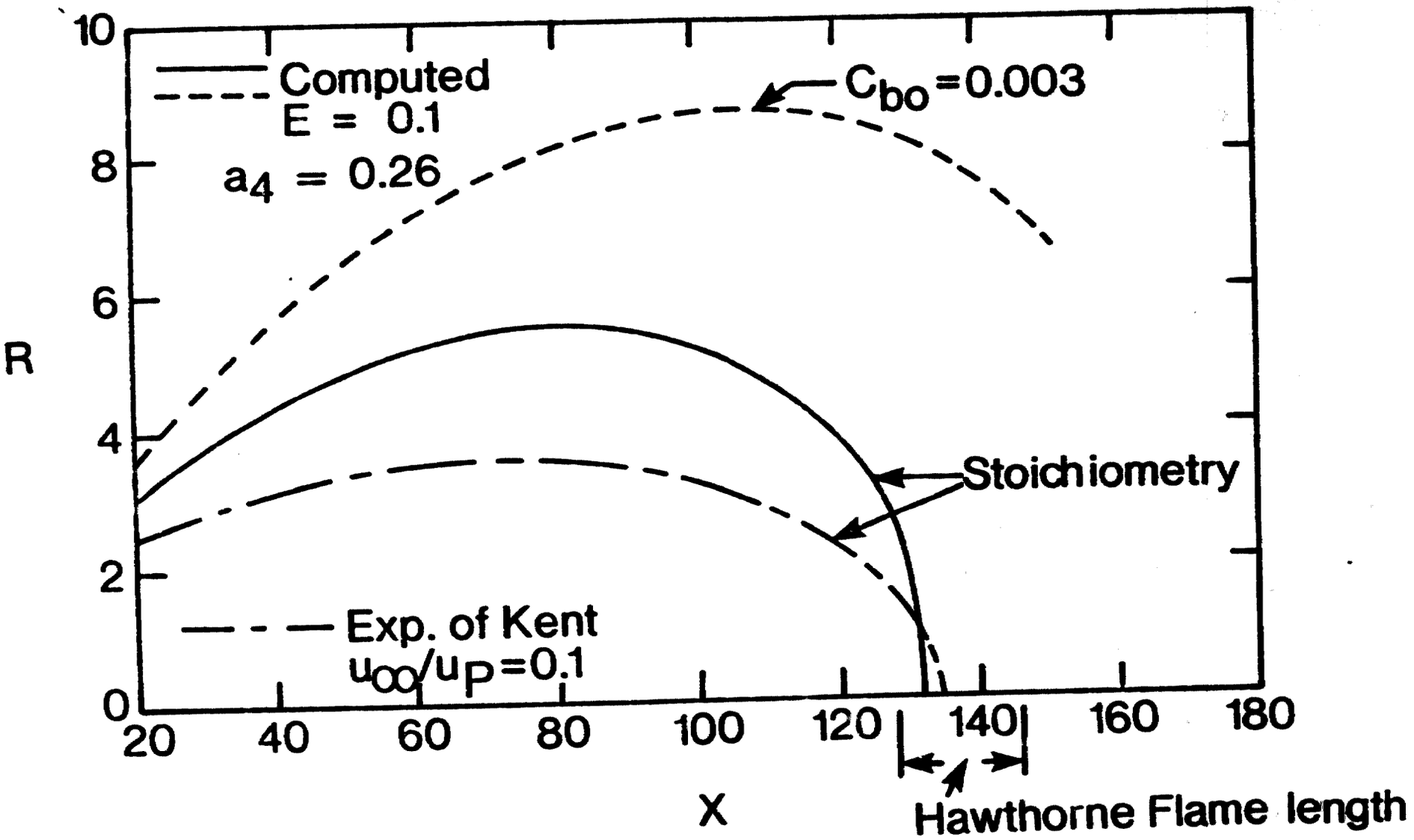

Figure 19.- Comparison of the computed values with the experimental results for the locus of flame stoichiometry and stoichiometric flame length.

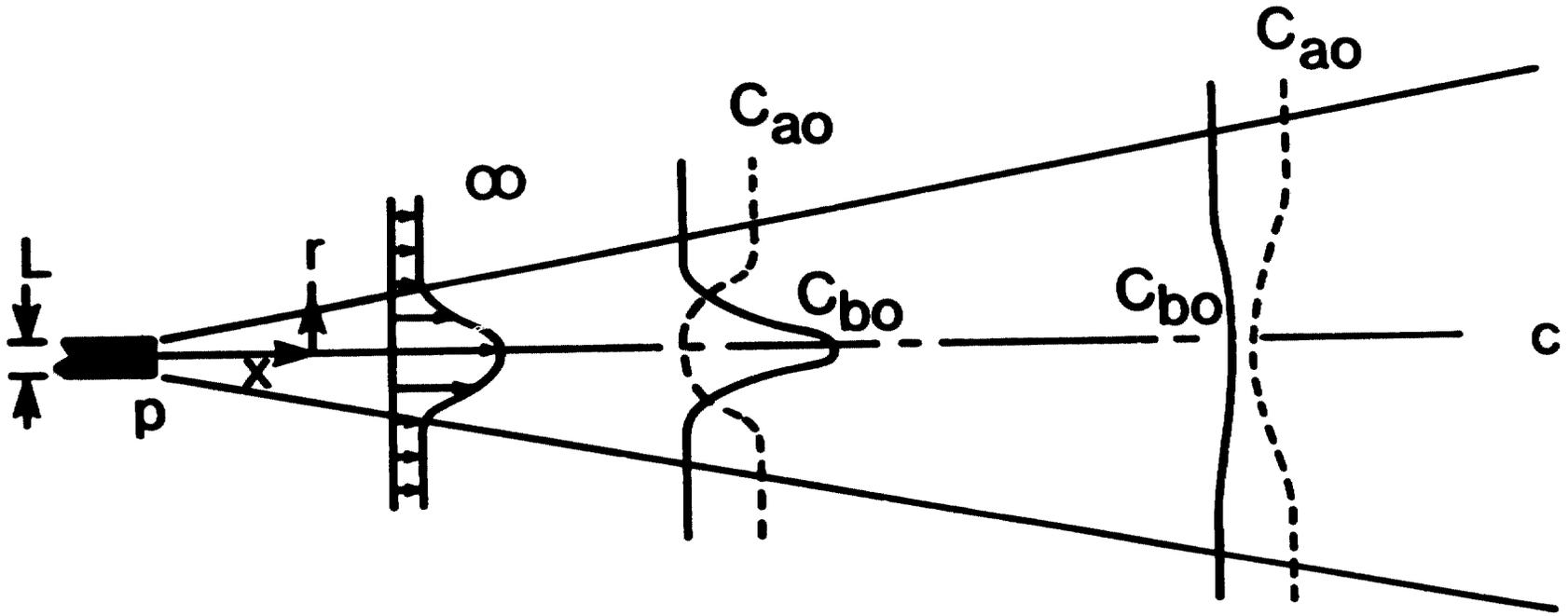
L
r
∞
C_{ao}
C_{ao}
C_{bo}
C_{bo}
c
x
p

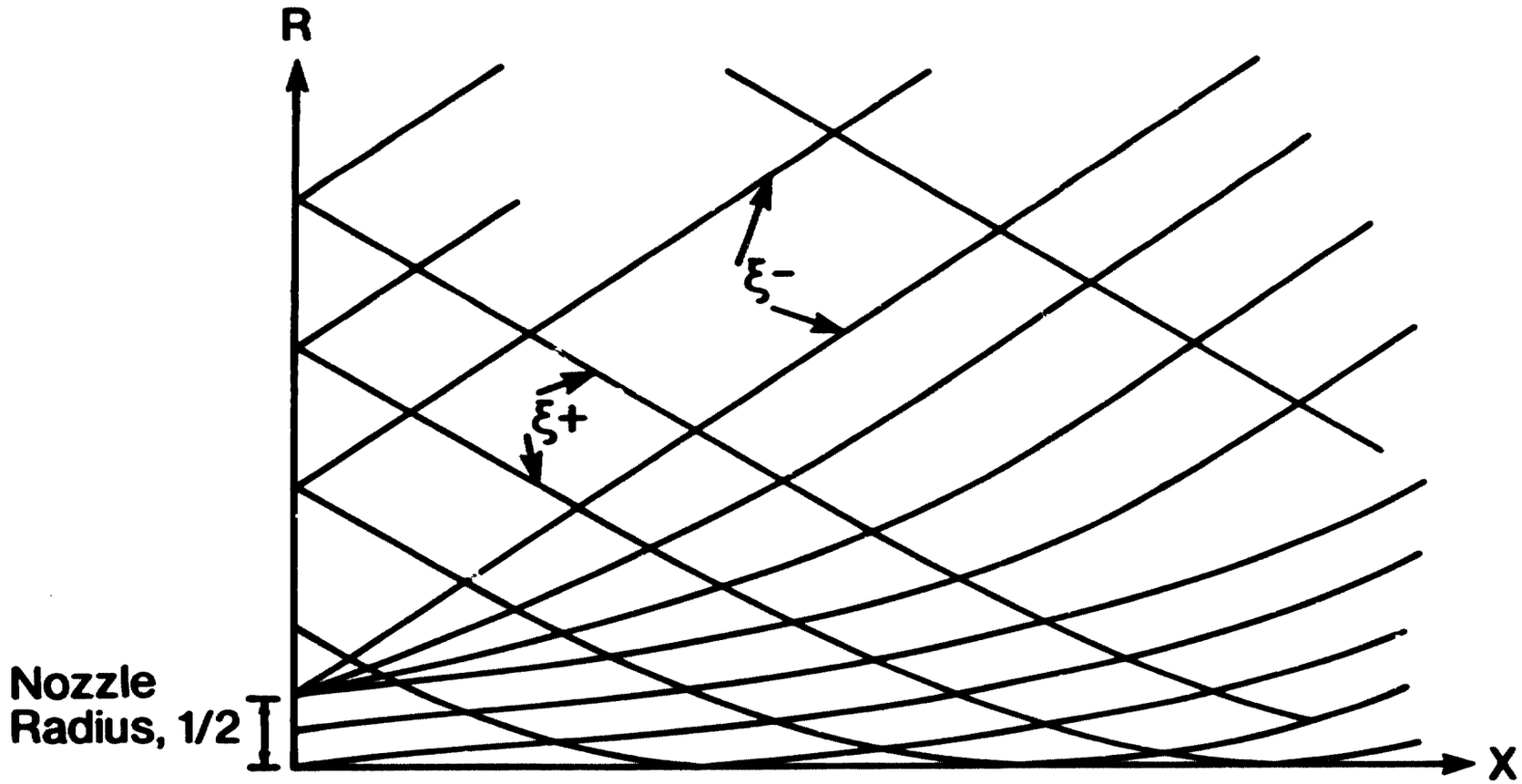
R
ξ-
ξ+
Nozzle
Radius, 1/2
X

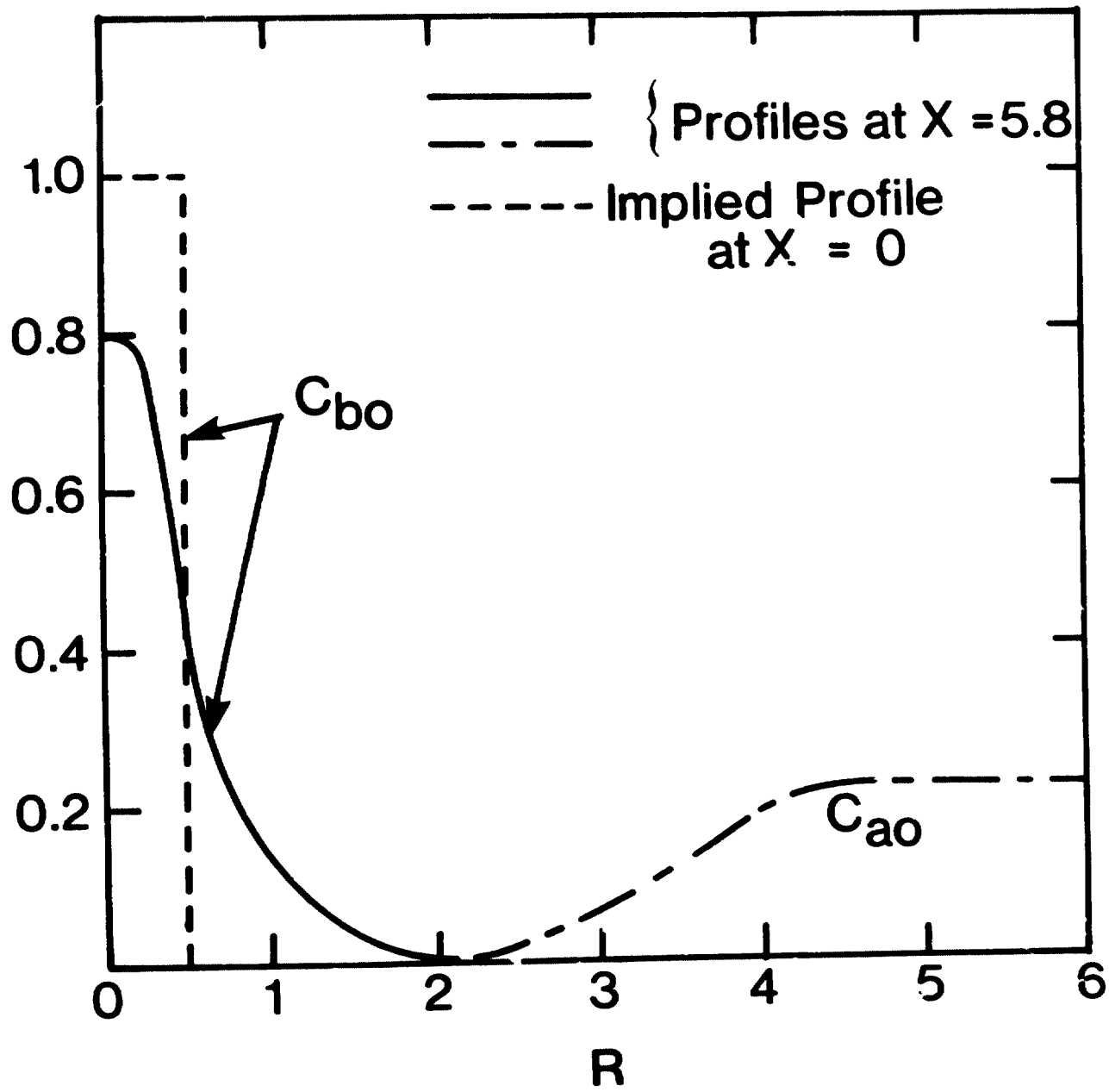
Profiles at X =5.8
Implied Profile at X = 0
1.0
0.8
0.6
0.4
0.2
C_{bo}
C_{ao}
0
1
2
3
4
5
6
R

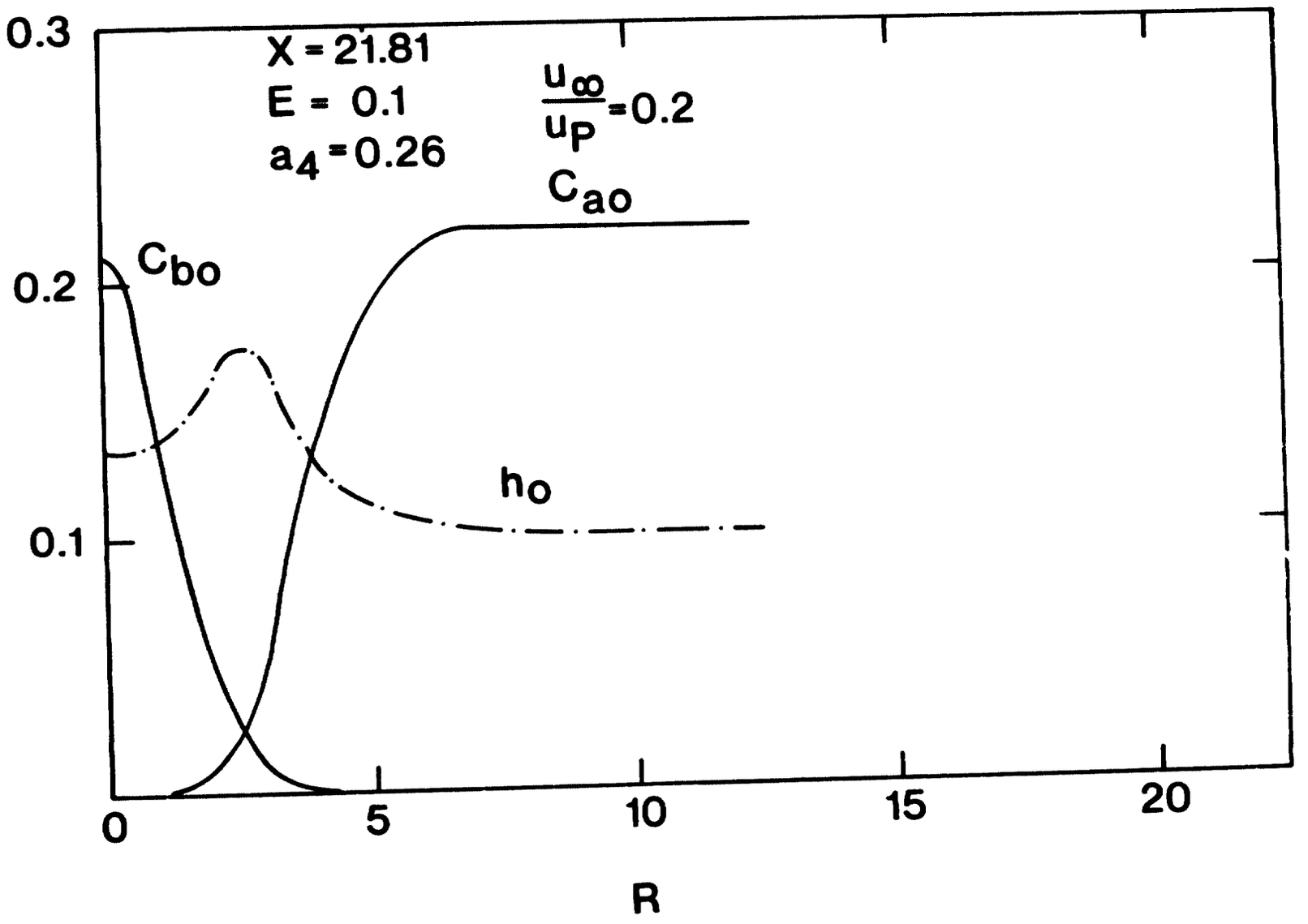
0.3
0.2
0.1
X = 21.81
E = 0.1
a_4 = 0.26
$\frac{u_\infty}{u_P}$ = 0.2
C_{ao}
C_{bo}
h_o
0
5
10
15
20
R

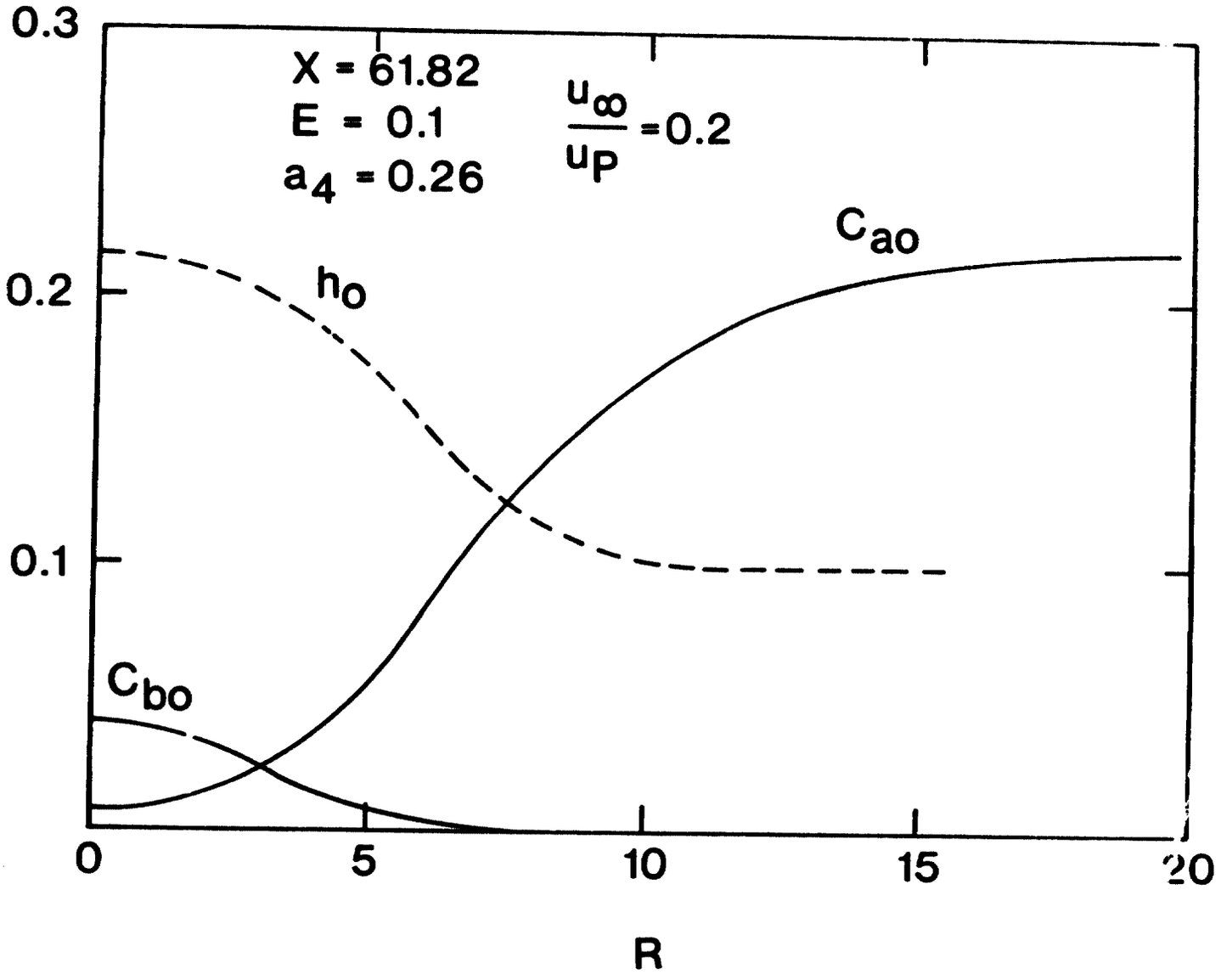
0.3
0.2
0.1
X = 61.82
E = 0.1
a_4 = 0.26
$\frac{u_\infty}{u_P}$ = 0.2
h_o
C_{ao}
C_{bo}
0
5
10
15
20
R

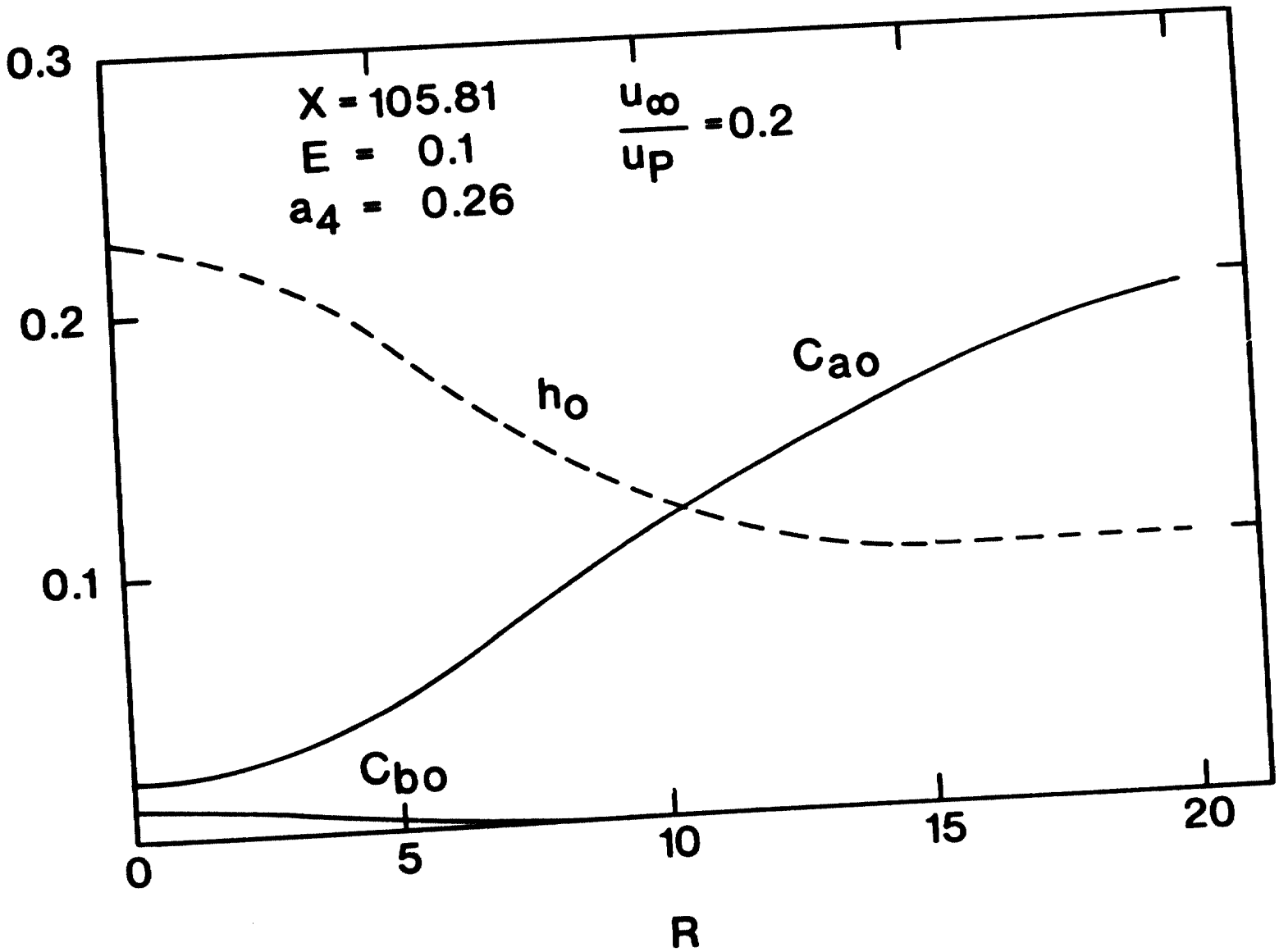
0.3
0.2
0.1
X = 105.81
E = 0.1
a_4 = 0.26
$\frac{u_\infty}{u_P}$ = 0.2
h_o
C_{ao}
C_{bo}
0
5
10
15
20
R

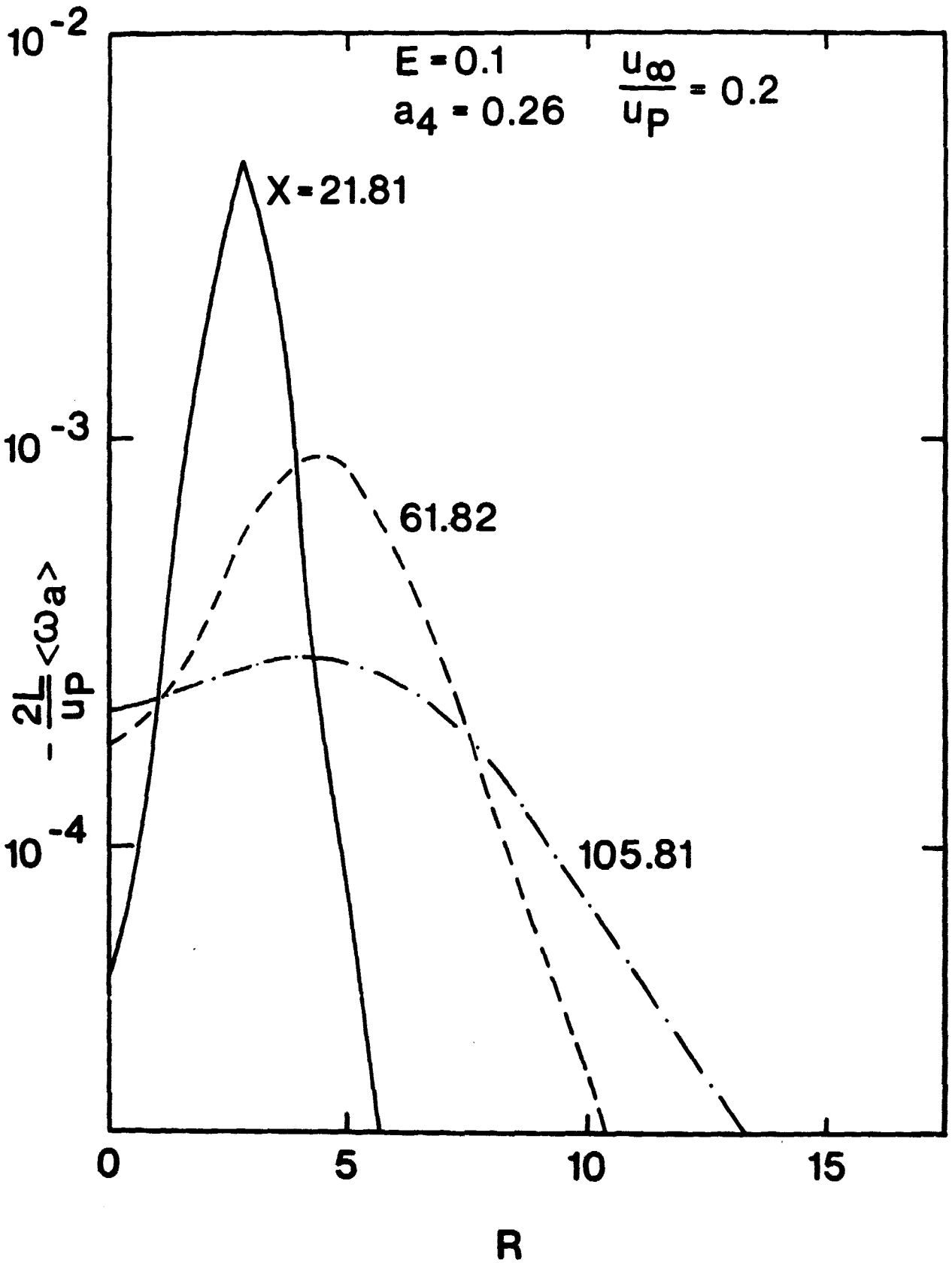
E = 0.1
a_4 = 0.26
$\frac{u_\infty}{u_P}$ = 0.2
X = 21.81
61.82
105.81
10^{-2}
10^{-3}
10^{-4}
$-\frac{2L}{u_P}\langle\omega a\rangle$
0
5
10
15
R

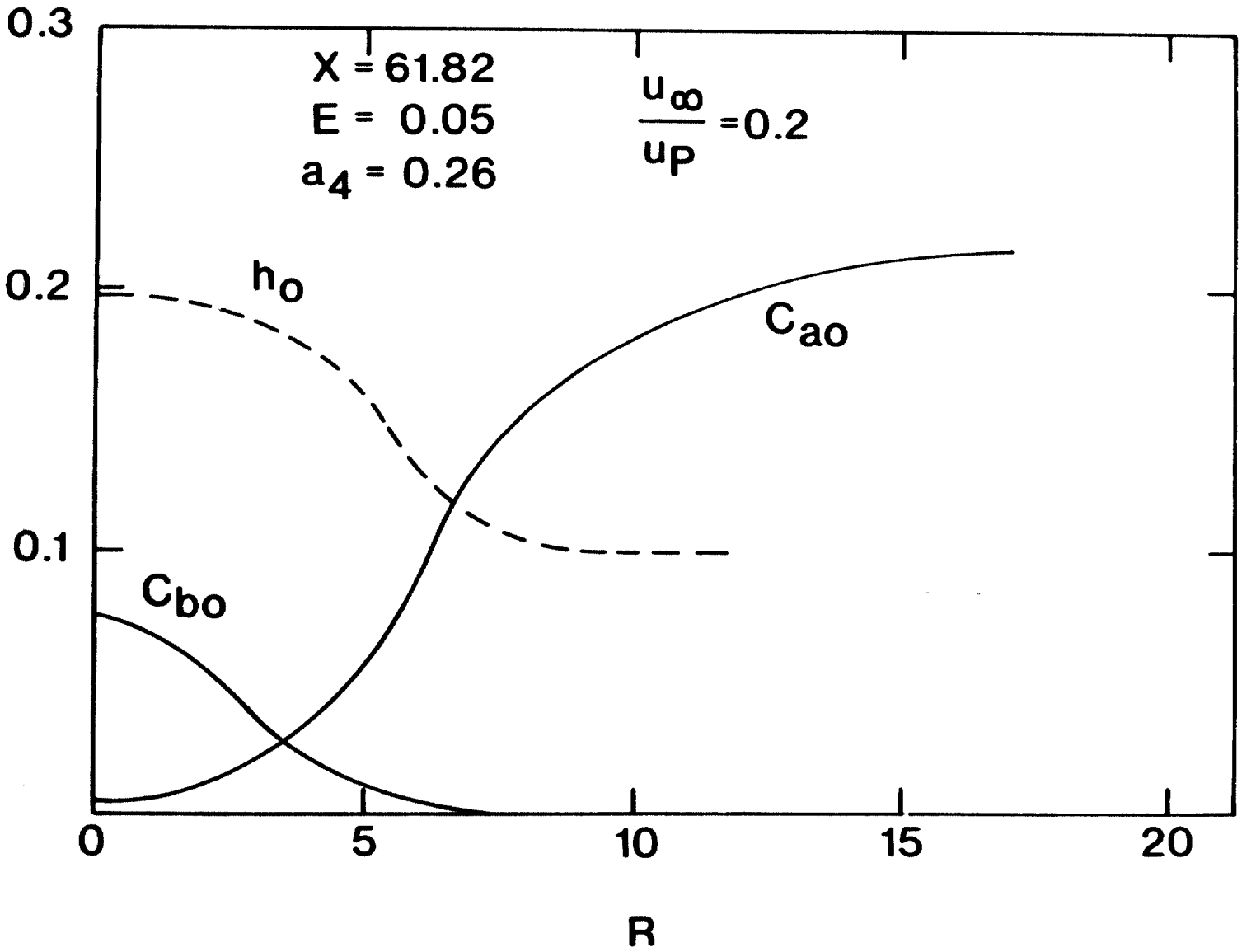
0.3
0.2
0.1
X = 61.82
E = 0.05
a_4 = 0.26
$\frac{u_\infty}{u_P}$ =0.2
h_o
C_{ao}
C_{bo}
0
5
10
15
20
R

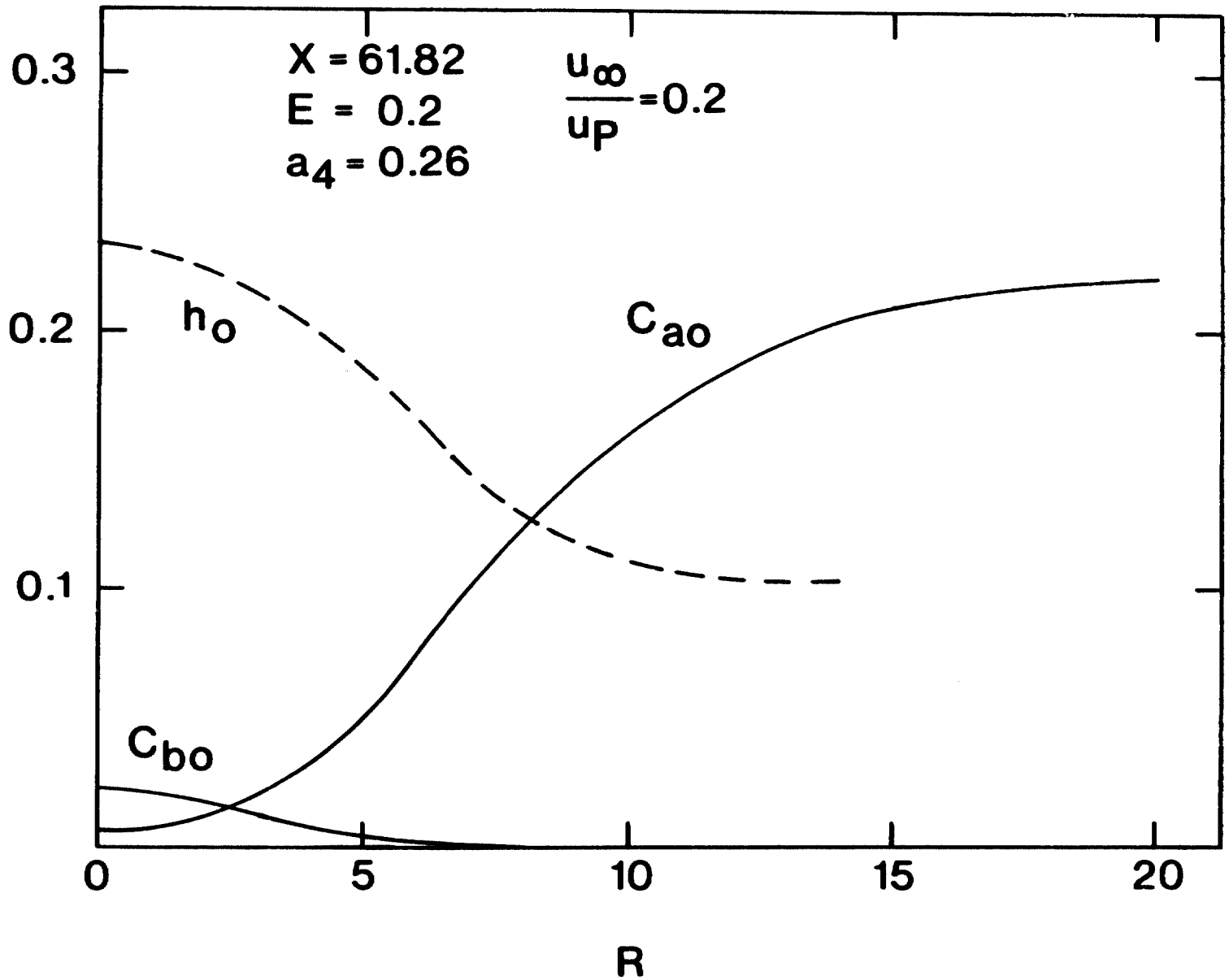
X = 61.82
E = 0.2
a_4 = 0.26
$\frac{u_\infty}{u_P}$=0.2
h_o
C_{ao}
C_{bo}
0.3
0.2
0.1
0
5
10
15
20
R

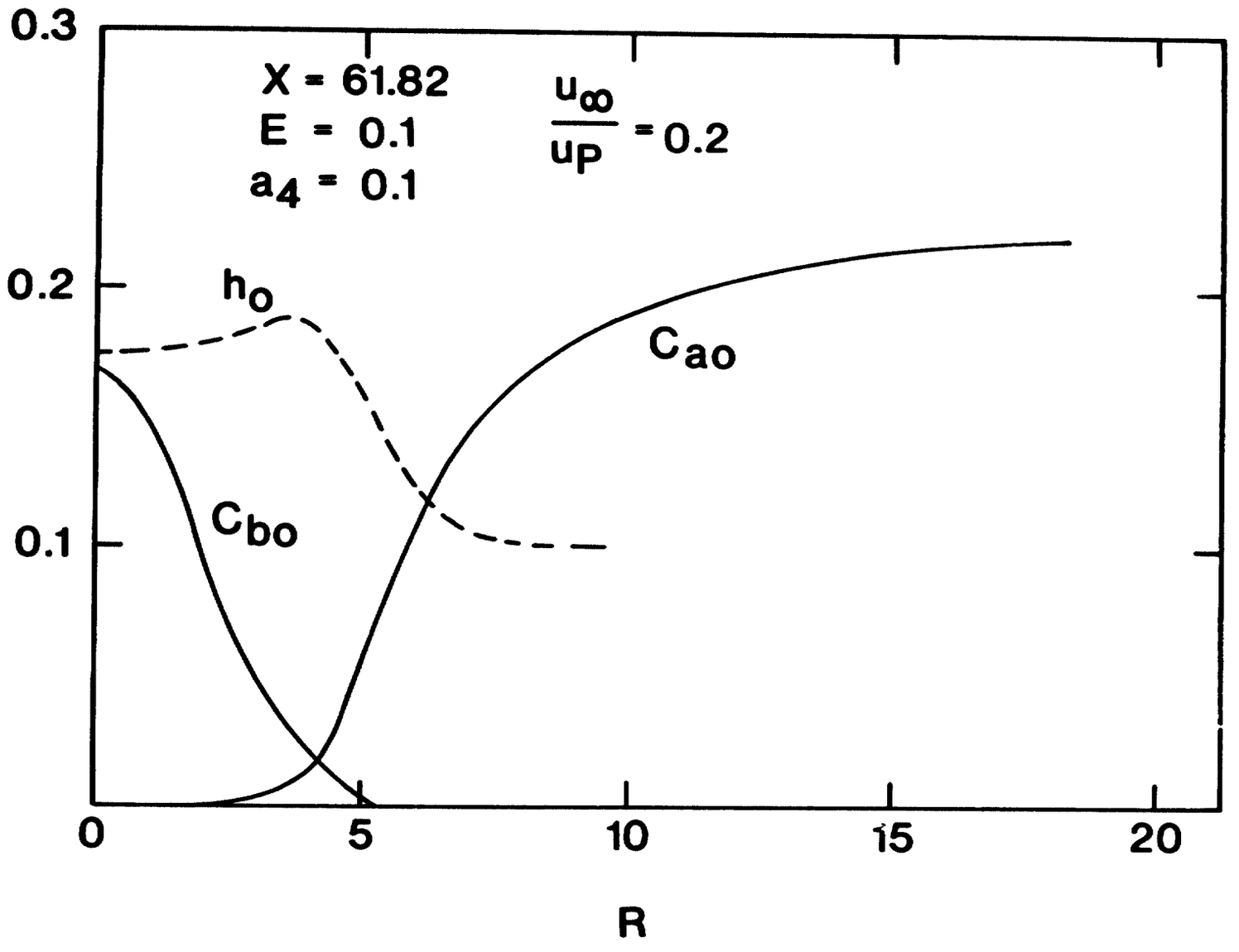
0.3
0.2
0.1
0
5
10
15
20
R
X = 61.82
E = 0.1
a_4 = 0.1
$\frac{u_\infty}{u_P}$ = 0.2
h_o
C_{ao}
C_{bo}

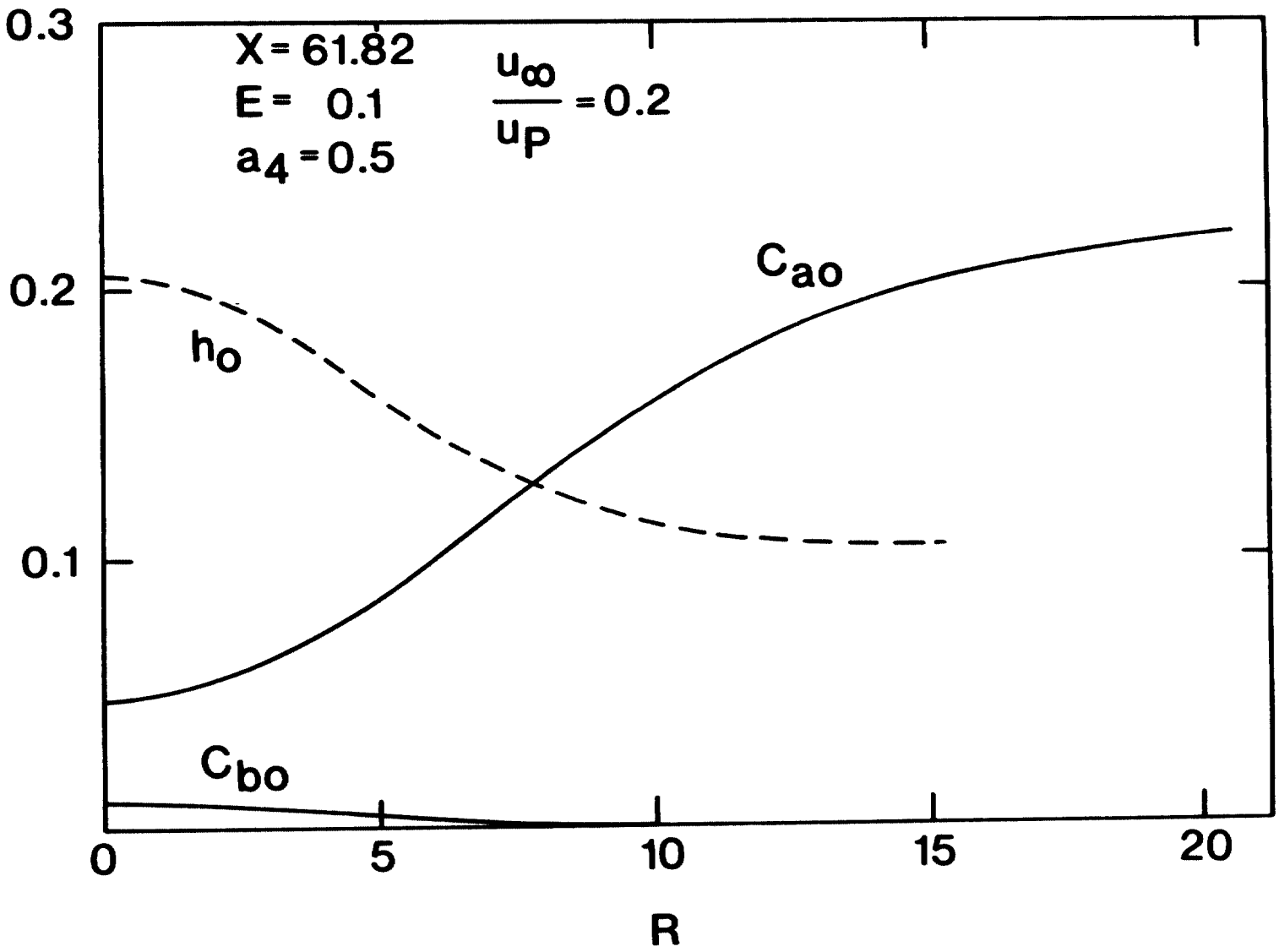
0.3
0.2
0.1
X = 61.82
E = 0.1
a_4 = 0.5
$\frac{u_\infty}{u_P}$ = 0.2
h_o
C_{ao}
C_{bo}
0
5
10
15
20
R

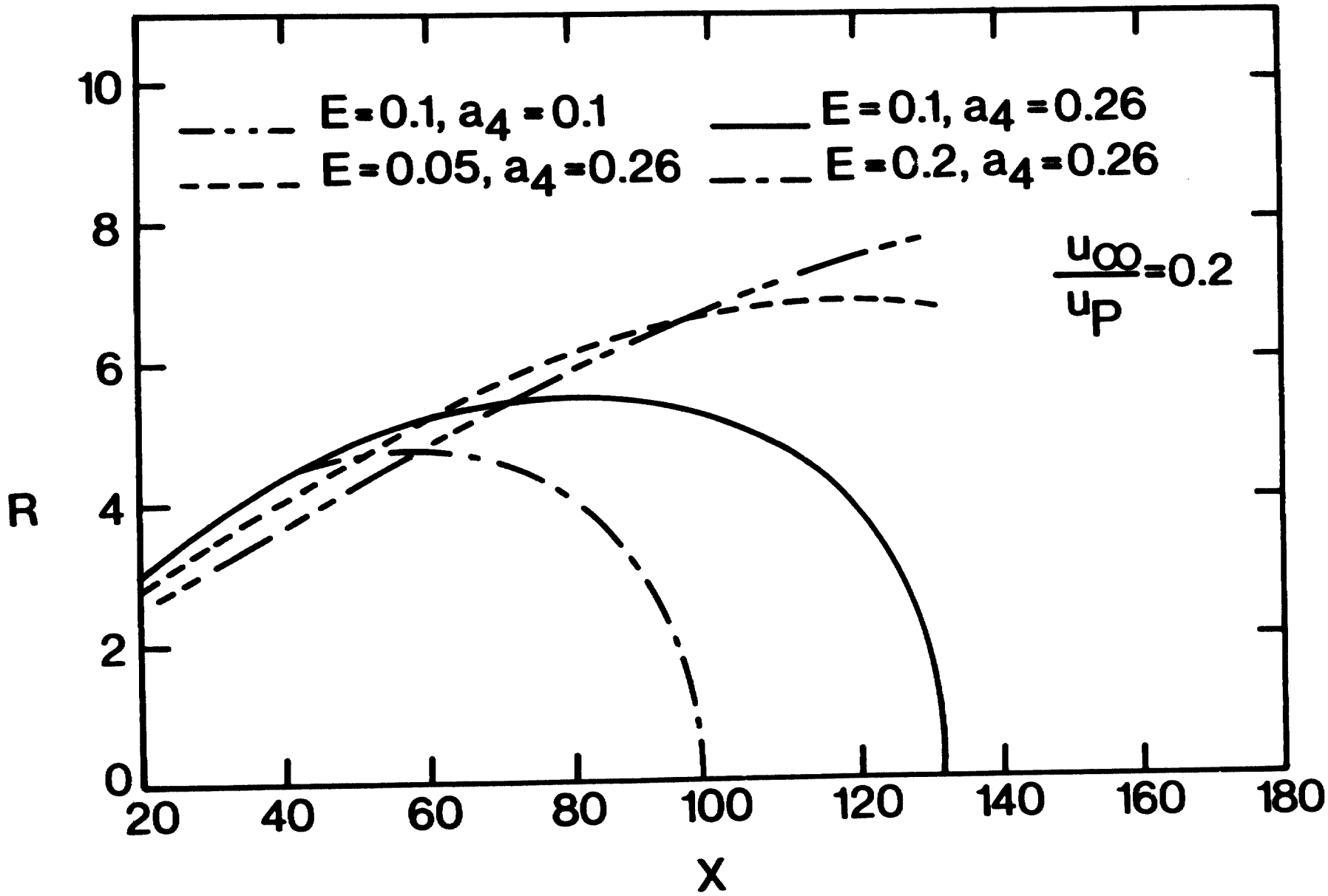
E=0.1, a_4=0.1
E=0.1, a_4=0.26
E=0.05, a_4=0.26
E=0.2, a_4=0.26
$\frac{u_\infty}{u_P}$=0.2
R
X
0
2
4
6
8
10
20
40
60
80
100
120
140
160
180

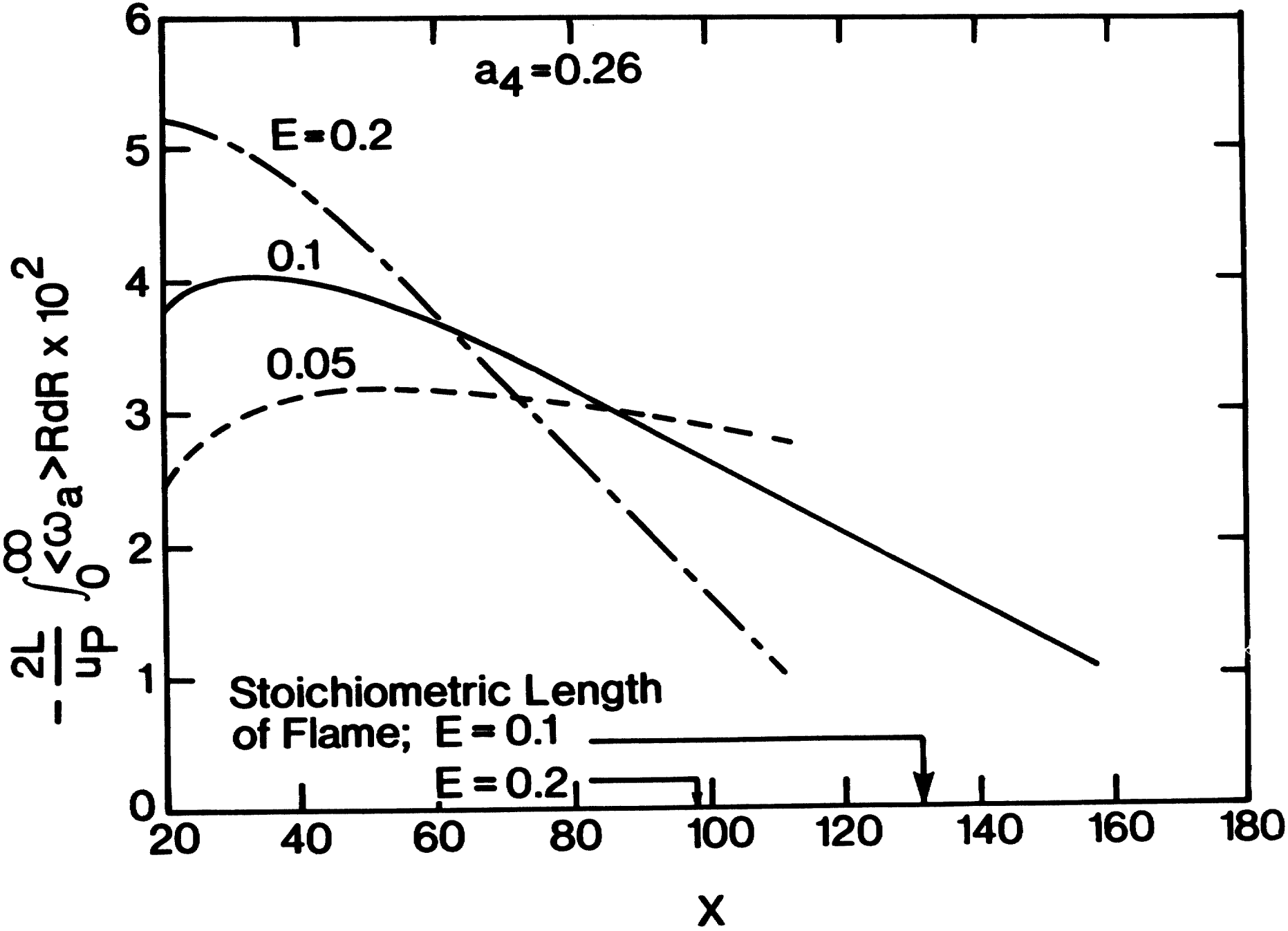
a_4=0.26
E=0.2
0.1
0.05
$-\frac{2L}{u_P}\int_0^\infty <\omega_a> RdR \times 10^2$
Stoichiometric Length
of Flame; E = 0.1
E = 0.2
X
0
1
2
3
4
5
6
20
40
60
80
100
120
140
160
180

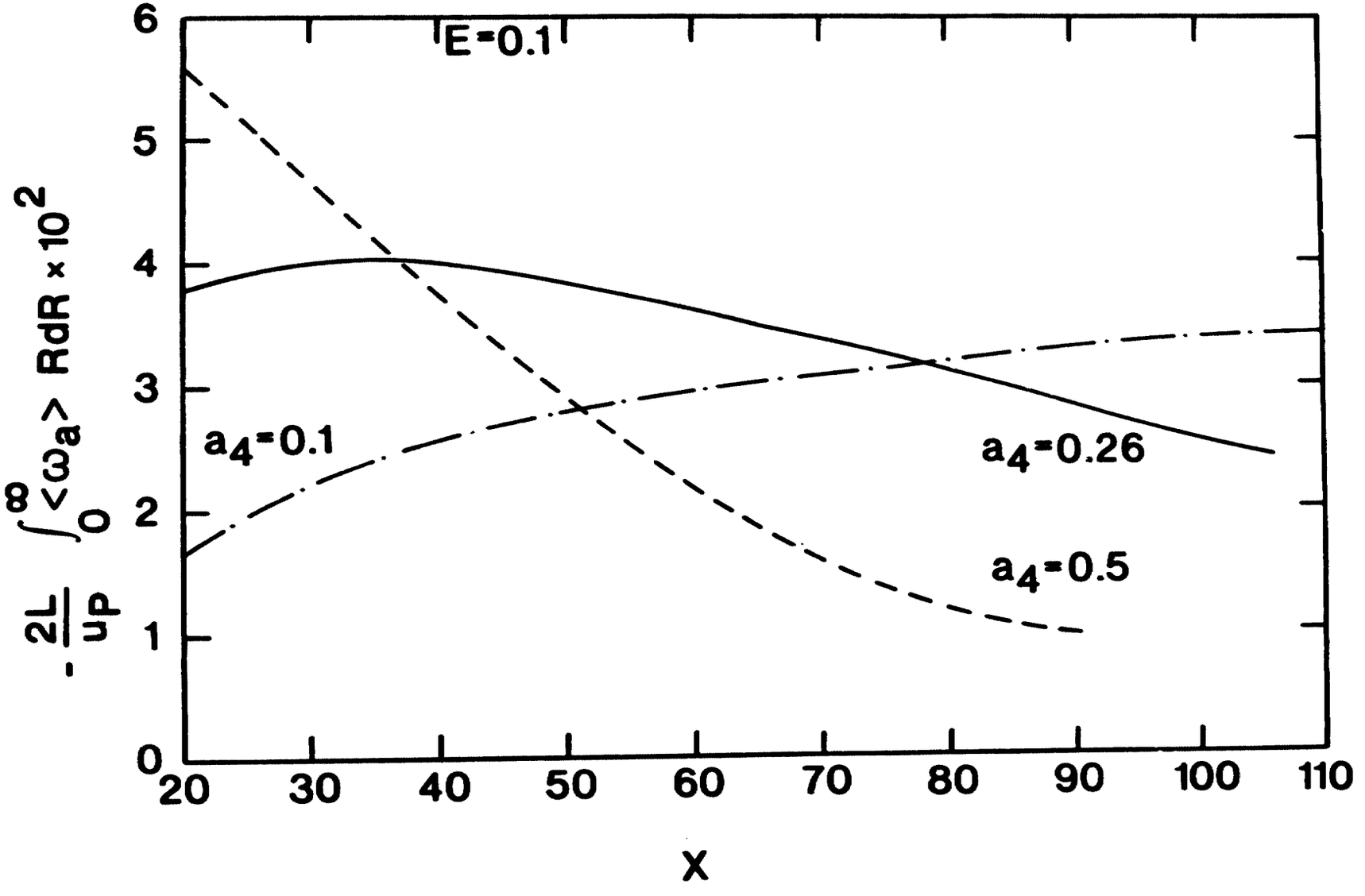
E=0.1
a_4=0.1
a_4=0.26
a_4=0.5
$-\frac{2L}{up}\int_0^8 <\omega_a> RdR \times 10^2$
X
0
1
2
3
4
5
6
20
30
40
50
60
70
80
90
100
110

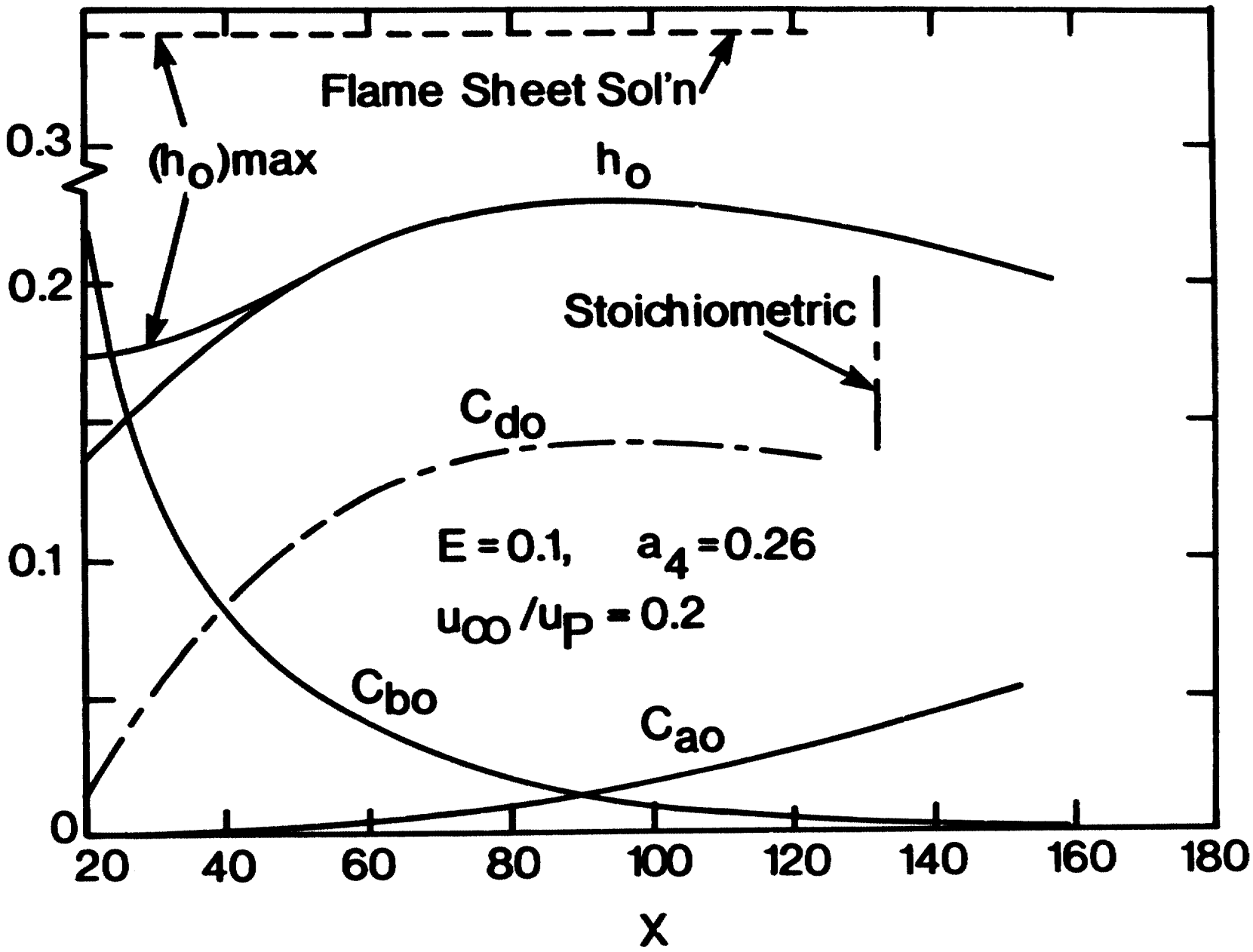
Flame Sheet Sol'n
$(h_o)_{max}$
h_o
Stoichiometric
C_{do}
E = 0.1, a_4 = 0.26
u_∞ / u_P = 0.2
C_{bo}
C_{ao}
0.3
0.2
0.1
0
20
40
60
80
100
120
140
160
180
X

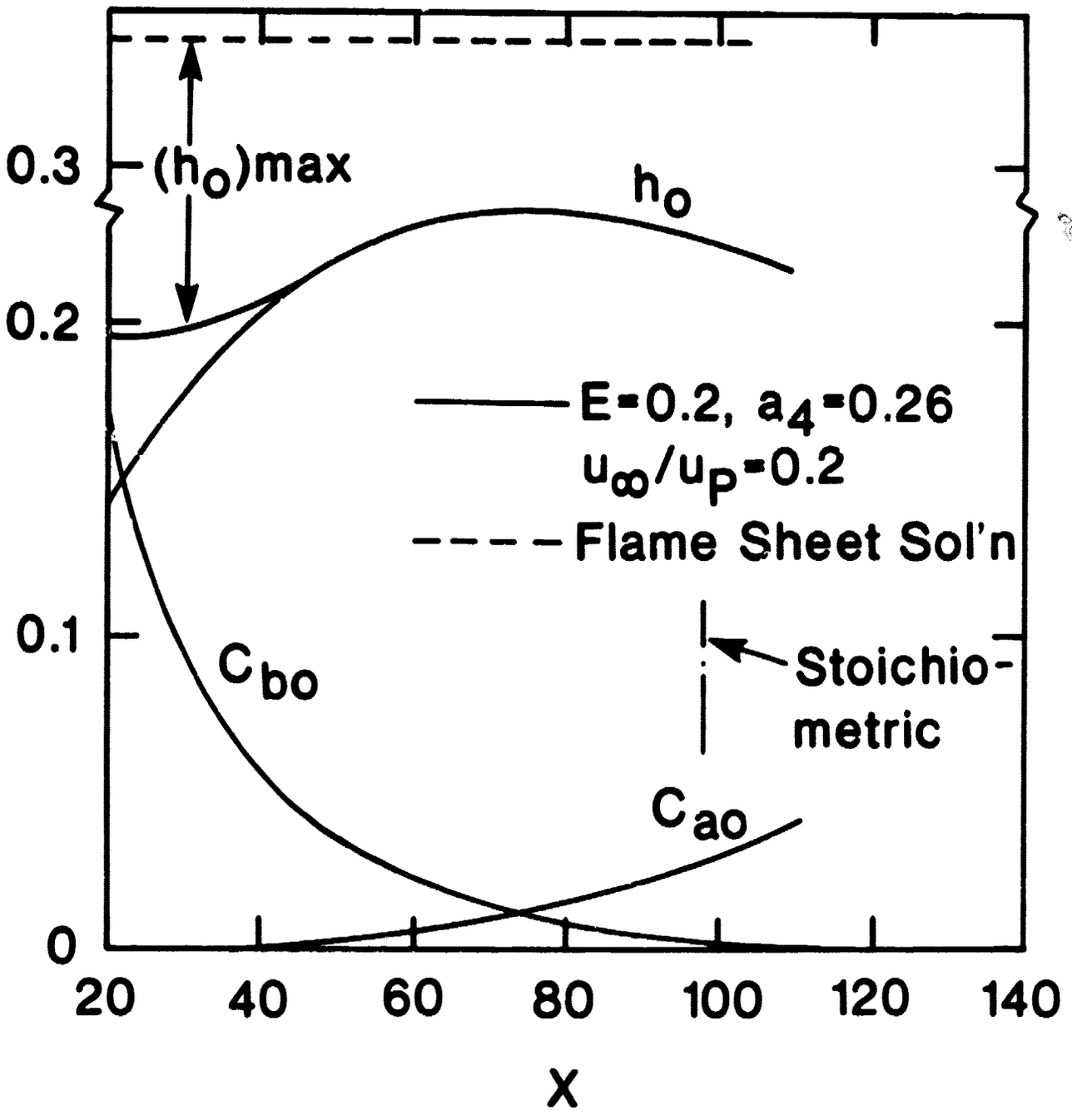
0.3
0.2
0.1
0
$(h_o)max$
h_o
E=0.2, a_4=0.26
u_∞/u_P=0.2
Flame Sheet Sol'n
Stoichio-
metric
C_{bo}
C_{ao}
20
40
60
80
100
120
140
X

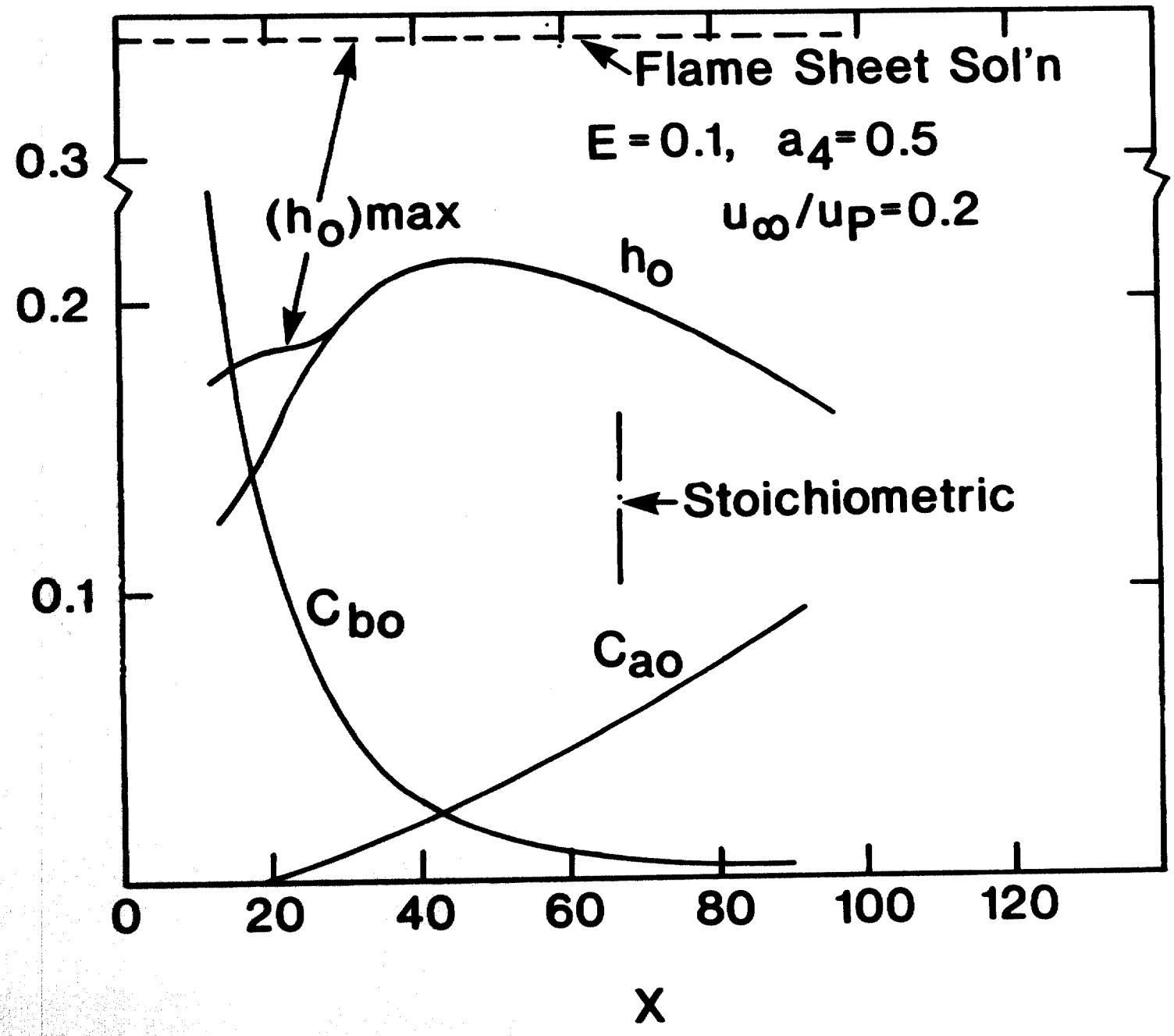
Flame Sheet Sol'n
E = 0.1, a_4 = 0.5
u_∞/u_P = 0.2
$(h_o)_{max}$
h_o
Stoichiometric
C_{bo}
C_{ao}
0.3
0.2
0.1
0
20
40
60
80
100
120
X

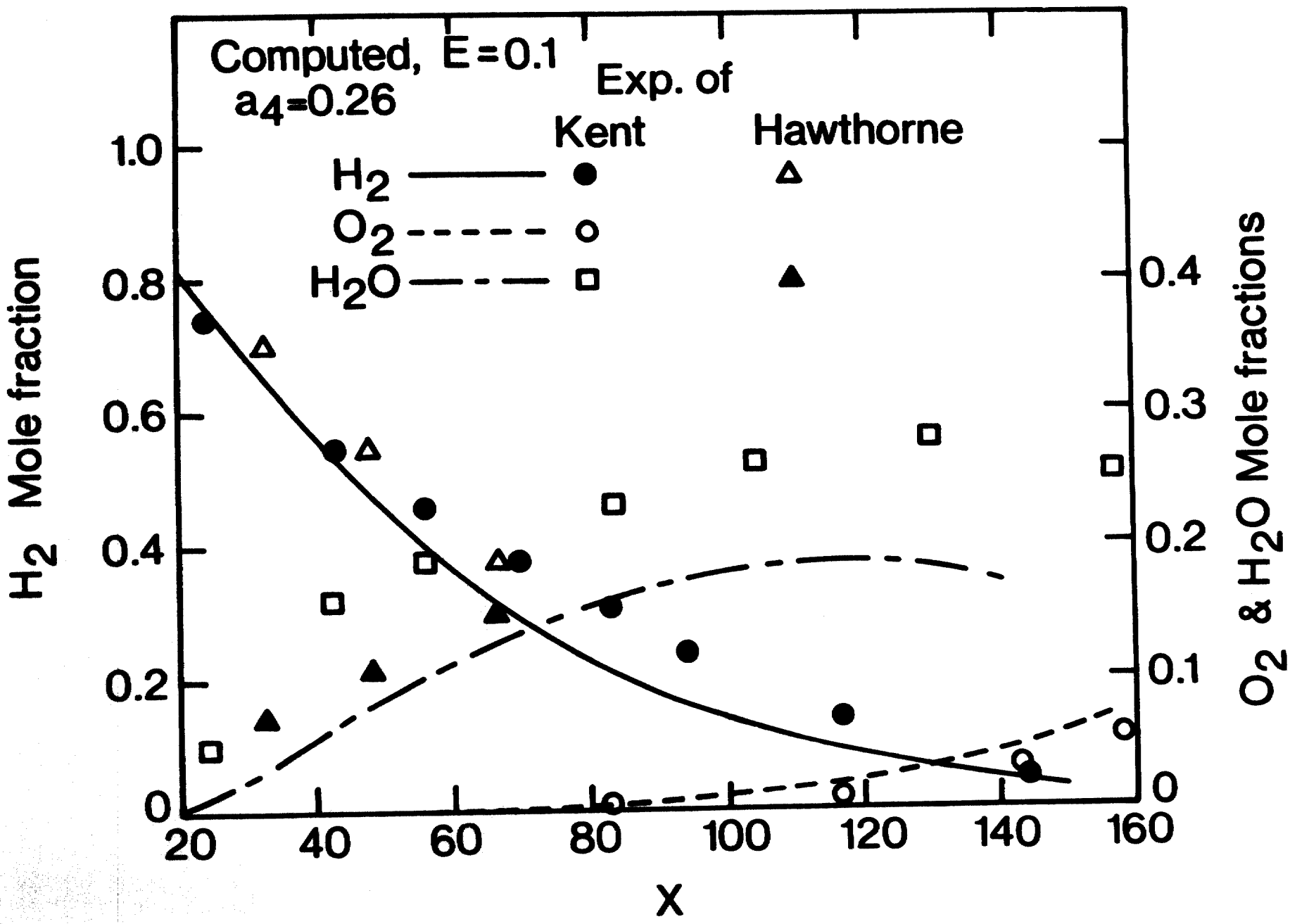
Computed, E=0.1
a_4=0.26
Exp. of
Kent
Hawthorne
H_2
O_2
H_2O
H_2 Mole fraction
O_2 & H_2O Mole fractions
X
0
0.2
0.4
0.6
0.8
1.0
0.1
0.3
20
40
60
80
100
120
140
160

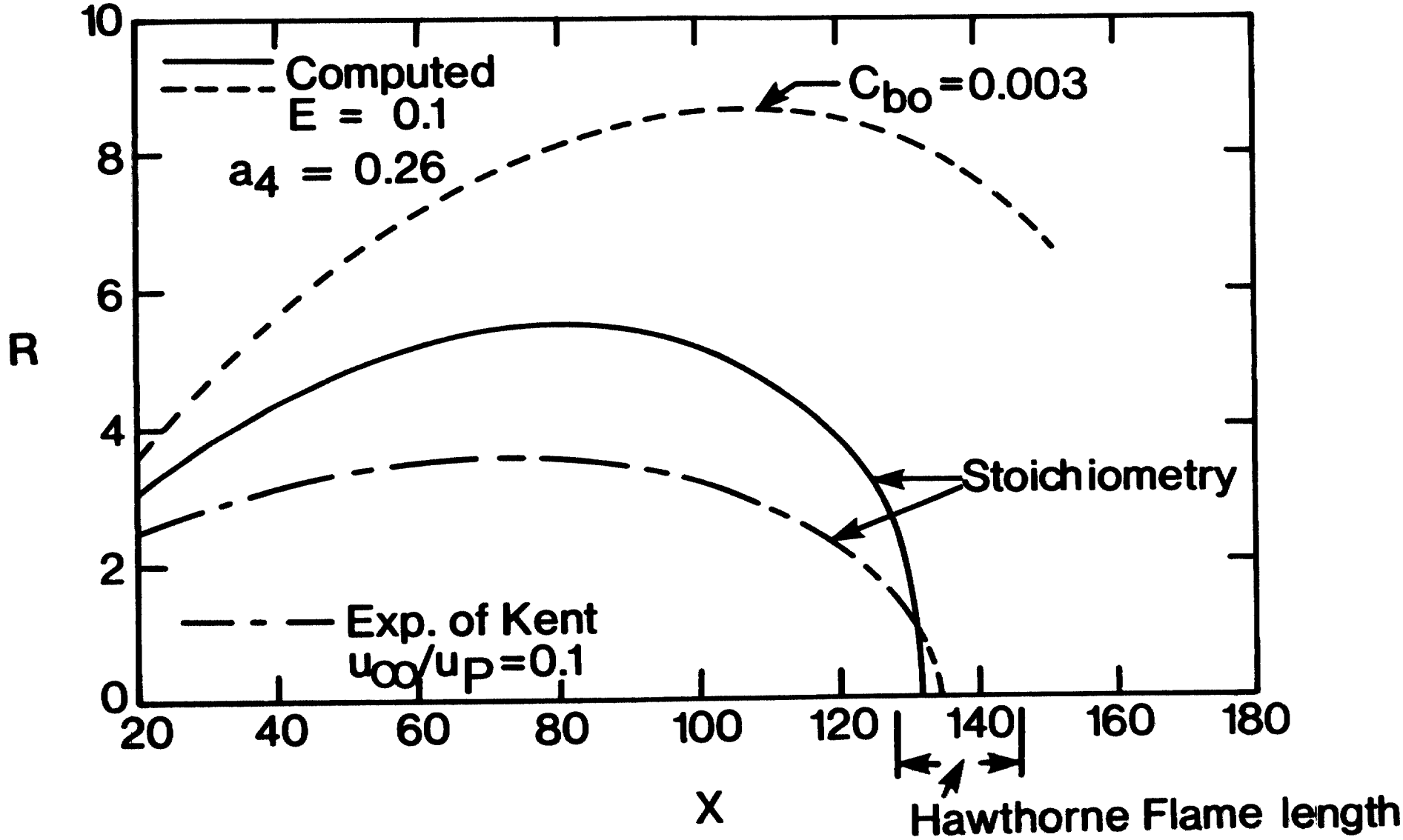
10
8
6
4
2
0
R
Computed
E = 0.1
a_4 = 0.26
C_{bo} = 0.003
Stoichiometry
Exp. of Kent
u_∞/u_P = 0.1
20
40
60
80
100
120
140
160
180
X
Hawthorne Flame length